P-05-34

Oskarshamn site investigation

Interpretation of geophysical borehole measurements and compilation of petrophysical data from KLX01, KLX03, KLX04, HLX21, HLX22, HLX23, HLX24, HLX25, HLX26, HLX27 and HLX28

Håkan Mattsson, Hans Thunehed and Mikael Keisu
GeoVista AB

February 2005

Svensk Kärnbränslehantering AB
Swedish Nuclear Fuel
and Waste Management Co
Box 5864
SE-102 40 Stockholm Sweden
Tel 08-459 84 00
+46 8 459 84 00
Fax 08-661 57 19
+46 8 661 57 19

ISSN 1651-4416
SKB P-05-34

Oskarshamn site investigation

Interpretation of geophysical borehole measurements and compilation of petrophysical data from KLX01, KLX03, KLX04, HLX21, HLX22, HLX23, HLX24, HLX25, HLX26, HLX27 and HLX28

Håkan Mattsson, Hans Thunehed and Mikael Keisu
GeoVista AB

February 2005

Keywords: Borehole, Logging, Geophysics, Geology, Bedrock, Fractures, Density, Porosity, Magnetic susceptibility, Anisotropy, Resistivity, Induced polarization.

Abstract

This report presents the compilation and interpretations of geophysical logging data and petrophysical measurements on rock samples from the cored boreholes KLX01, KLX03 and KLX04, and the percussion drilled boreholes HLX21, HLX22, HLX23, HLX24, HLX25, HLX26, HLX27 and HLX28.

The main objective of these investigations is to use the results as supportive information during the geological core and drill chip mappings and as supportive information during the single-hole interpretations. The petrophysical data are used to perform quality controls of the logging data and constitute supportive information to the rock type classification.

The results show that there are dominant occurrences of rocks with silicate density in the interval 2,730–2,800 kg/m^3 (tonalite composition) in KLX03 and in HLX26–28, located in the southern part of the Laxemar area, within or close to a major quartz monzodiorite rock unit. In KLX01, KLX04 and HLX21–25, in the central part of the Laxemar area, there is a clear dominance of more low density rocks; in KLX01 and KLX04 densities are mainly in the interval 2,680–2,730 kg/m^3 (granodiorite composition) and in the percussion drilled boreholes densities are even lower. These general variations in physical properties of rocks are also indicated in the natural gamma radiation and magnetic susceptibility measurements, where lower radiation levels and higher susceptibilities are identified in KLX03 and HLX26–28 as compared to KLX01, KLX04 and HLX21–25.

Large variations in physical properties of the most abundant rock type in the area, Ävrö granite, are found when comparing logging data from KLX03 with corresponding data from KLX04. The Ävrö granite in KLX03 has higher silicate density and magnetic susceptibility and lower natural gamma radiation than the Ävrö granite in KLX04.

The estimated fracture frequency in KLX01 is generally low or moderate. However, four distinct fracture anomalies are identified that coincide with increased porosity and anomalies in the fluid temperature gradient log, which suggest that they are water bearing. In KLX03, increased fracture frequencies (possible deformation zones) are indicated in the sections c 260–320 m, 615–630 m, 655–685 m and 725–780 m. However, the three uppermost sections are mainly characterized by low resistivity anomalies and only partly decreased P-wave velocity, which indicates that the suggested deformation zones are dominated by sealed fractures and/or alteration, and that open fractures are less common. Along the section c 720–780 m the geophysical measurements indicate high frequency of water bearing fractures. In KLX04 there are indications of strongly increased fracturing (several possible deformation zones) along major parts of the sections 100–450 m and 870–970 m.

The petrophysical data compiled from KLX01 and KLX03 generally agrees well with corresponding data from samples collected on the surface. However, the density of the Ävrö granite constitutes an exception with a clear indication that the mineral composition of the Ävrö granite in the vicinity of KLX01 and KLX03 differs from the general distribution from samples taken on bedrock outcrops on the surface.

Sammanfattning

Föreliggande rapport presenterar en sammanställning och tolkning av geofysiska borrhålsmätningar och petrofysiska data från kärnborrhålen KLX01, KLX03 och KLX04, samt hammarborrhålen HLX21, HLX22, HLX23, HLX24, HLX25, HLX26, HLX27 och HLX28.

Syftet med denna undersökning är framförallt att ta fram ett material som på ett förenklat sätt åskådliggör resultaten av de geofysiska loggningarna, s k generaliserade geofysiska loggar. Materialet används dels som stödjande data vid borrkärnekarteringen samt som underlag vid enhålstolkningen för respektive borrhål. Petrofysikdata används främst för att kontrollera kvaliteten på vissa geofysiska loggar.

Resultaten av undersökningarna visar att bergrunden i närheten av borrhålen KLX03 och HLX26–28, vilka ligger i den södra delen av Laxemarområdet nära eller inuti en större enhet med kvartsmonzodiorit, domineras av bergarter med en silikatdensitet i intervallet 2 730–2 800 kg/m^3 (motsvarande tonalitisk mineralsammansättning). I KLX01, KLX04 och HLX21–25, vilka ligger mer centralt i Laxemarområdet, finns en tydlig dominans av bergarter med lägre densitet; i KLX01 och KLX04 främst i intervallet 2 680–2 730 kg/m^3, och i de hammarborrade borrhålen förekommer långa sektioner med ännu lägre densitet. Dessa generella skillnader i fysikaliska egenskaper mellan KLX03 och HLX26–28 i söder och KLX01, KLX04 samt HLX21–25 längre norrut, framträder även tydligt i den naturliga gammastrålningen och magnetiska susceptibiliteten. Dessa två parametrar är lägre respektive högre i framförallt KLX03 jämfört med KLX01 och KLX04.

Den vanligast förekommande bergarten i området, s k Ävrögranit, uppvisar stor heterogenitet i fysikaliska egenskaper vid en jämförelse mellan KLX03 och KLX04. Ävrögraniten i KLX03 har betydligt högre densitet, högre magnetisk susceptibilitet och lägre naturlig gammastrålning än Ävrögraniten i KLX04.

Den geofysiskt beräknade sprickfrekvensen är generellt låg till moderat i KLX01. Fyra stycken större sprickanomalier kan dock identifieras i loggdata, vilka alla sammanfaller med hög porositet och temperaturgradientanomalier, vilket indikerar att sprickorna är vattenförande. I KLX03 kan fyra möjliga deformationszoner identifieras längs sektionerna 260–320 m, 615–630 m, 655–685 m och 725–780 m. De tre översta sektionerna karakteriseras dock främst av låg resistivitet, och uppvisar ingen större sänkning i P-vågshastighet, vilket indikerar att dessa främst utgörs av läkta sprickor och/eller omvandlingszoner. Längs den nedersta sektionen (725–780 m) finns dock flera tydliga indikationer på vattenförande sprickor. KLX04 har en relativt hög indikerad sprickfrekvens och ett flertal möjliga deformationszoner kan identifieras längs sektionerna 100–450 m och 870–970 m.

En sammanställning av petrofysiska egenskaper på borrkärneprov från KLX01 och KLX03 visar på en god samstämmighet med motsvarande egenskaper uppmätta på prover från markytan. Densiteten hos Ävrögraniten i KLX01 och KLX03 utgör dock ett undantag, med betydligt högre värden i de två borrhålen än medelvärdet hos proverna tagna på hällar på markytan.

Contents

1 Introduction

SKB performs site investigations for localization of a deep repository for high level radioactive waste. The site investigations are performed at two sites, Forsmark and Simpevarp. This document reports the results gained from the interpretation of geophysical borehole logging data from the cored boreholes KLX01, KLX03 and KLX04, and the percussion drilled boreholes HLX21, HLX22, HLX23, HLX24, HLX25, HLX26, HLX27 and HLX28 (Figure 1-1). A compilation of petrophysical data from measurements on 11 core samples from KLX03 and 90 core samples from KLX01 is also presented.

Generalized geophysical loggings related to lithological variations are presented together with indicated fracture loggings, including estimated fracture frequency. Calculations of the vertical temperature gradient, salinity and apparent porosity are presented for the cored boreholes. The logging measurements in KLX03, KLX04 and HLX21–28 were conducted in 2004 by Rambøll, and the measurements in KLX01 were conducted by Malå GeoScience in 1988.

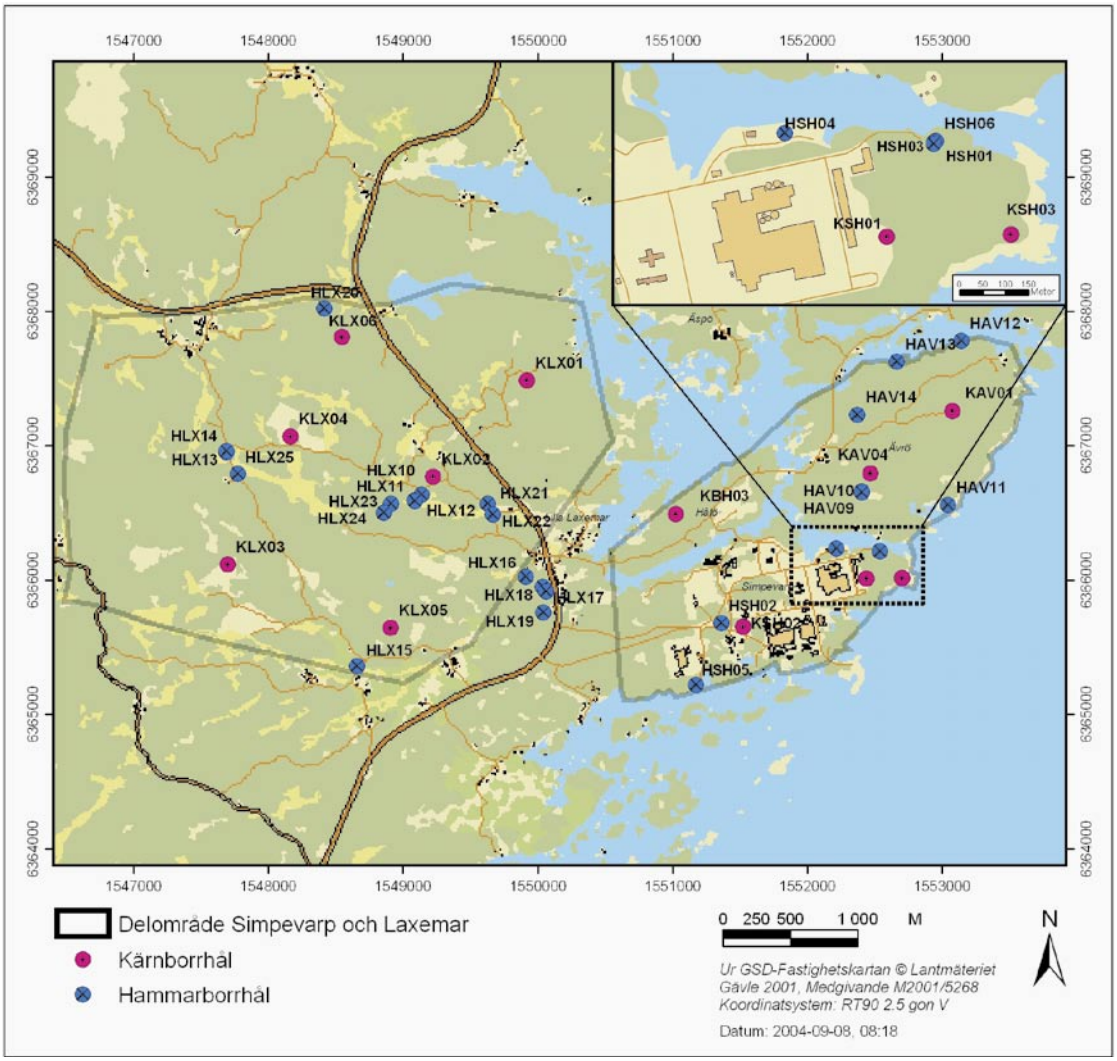

Figur 1-1. *Location of the cored boreholes KLX01, KLX03 and KLX04, and the percussion drilled boreholes HLX21, HLX22, HLX23, HLX24, HLX25, HLX26, HLX27 and HLX28.*

The petrophysical determinations of KLX03 include magnetic susceptibility, wet and dry density, porosity, anisotropy of magnetic susceptibility, electric resistivity and induced polarization. The measurements were performed at the laboratory of the Division of Applied Geophysics, Luleå University of Technology. The petrophysical data from KLX01 originate from a study previously reported by Nisca in 1988 /1/ and are here reinterpreted and presented according to the updated rock type nomenclature.

The interpretation presented in this report is performed by GeoVista AB in accordance with the instructions and guidelines from SKB (activity plans AP PS 400-04-094 and AP PS 400-04-100, and method descriptions MD 221.003, MD 230.001 and MD 160.002e, SKB internal controlling documents, Table 1-1).

The original results are stored in the primary data base (SICADA) and the data are traceable by the activity plan numbers.

Table 1-1. Controlling documents for the performance of the activity.

Activity plan	**Number**	**Version**
Tolkning av borrhålsgeofysiska data från KLX01, KLX03, KLX04, HLX21, HLX22, HLX23, HLX24 och HLX25	AP PS 400-04-094	1.0
Tolkning av borrhålsgeofysiska data från HLX26, HLX27 och HLX28	AP PS 400-04-100	1.0
Method descriptions	**Number**	**Version**
Metodbeskrivning för tolkning av geofysiska borrhålsdata	SKB MD 221.003	2.0
Metodbeskrivning för mätning av bergarters petrofysiska egenskaper	SKB MD 230.001	1.0
Determining density and porosity of intact rock	SKB MD160.002e	1.0

2 Objective and scope

The purpose of geophysical measurements in boreholes is to gain knowledge of the physical properties of the bedrock in the vicinity of the borehole. A combined interpretation of the "lithological" logging data (silicate density, magnetic susceptibility and natural gamma radiation) together with petrophysical data makes it possible to estimate the physical signature of different rock types. The three loggings are generalized and are then presented in a simplified way. The location of major fractures and an estimation of the fracture frequency along the borehole are calculated by interpreting data from the resistivity loggings, the single point resistance (SPR), caliper and sonic loggings.

The vertical temperature gradient, an estimation of the salinity and the apparent porosity are presented for the cored boreholes. These parameters indicate the presence of water bearing fractures, saline water and the transportation properties of the rock volume in the vicinity of the borehole.

The main objective of these investigations is to use the results as supportive information during the geological core mappings and as supportive information during the so called "single-hole interpretation", which is a combined borehole interpretation of core logging (Boremap) data, geophysical data and radar data.

The petrophysical data are used to perform quality controls of the logging data and constitute supportive information to the rock type classification.

3 Equipment

3.1 Description of equipment for petrophysical measurements

The measurements of magnetic remanence were performed with a cryogenic DC-SQUID magnetometer from 2G Enterprises and the anisotropy of magnetic susceptibility (AMS), including the magnetic volume susceptibility, was measured with a KLY-3 Kappabridge from Geofyzika Brno. Masses for the density and porosity determinations were measured with a digital Mettler Toledo PG 5002. The electric resistivity and induced polarization measurements were performed by use of a two-electrode in-house equipment (Luleå University of Technology) /2/.

3.2 Description of equipment for analyses of logging data

The software used for the interpretation are WellCad v3.2 (ALT) and Strater 1.00.24 (Golden Software), which are mainly used for plotting, Grapher v4 (Golden Software), mainly used for plotting and some statistical analyses, and a number of in-house software developed by GeoVista AB on behalf of SKB.

4 Execution

4.1 Interpretation of the logging data

The execution of the interpretation can be summarized in the following four steps:

1. Preparations of the logging data (calculations of noise levels, median filtering, error estimations, re-sampling, drift correction, length adjustment).

The loggings are median filtered (generally 5 point filters for the resistivity loggings and 3 point filters for other loggings) and re-sampled to common depth co-ordinates (0.1 m point distance).

The density and magnetic susceptibility logging data are calibrated with respect to petrophysical data. Petrophysical data from KLX03 were used to calibrate the loggings from KLX03, petrophysical data from KLX01 /1/ were used to calibrate the loggings from KLX01 and the logging data of KLX04 and HLX21–28 were calibrated by use of a combination of petrophysical data from the boreholes KSH01A, KSH02, KSH03A and KAV04A, see /3, 4, 5 and 6/.

2. Interpretation rock types (generalization of the silicate density, magnetic susceptibility and natural gamma radiation loggings).

The silicate density is calculated with reference to /7/ and the data are then divided into 5 sections indicating a mineral composition corresponding to granite, granodiorite, tonalite, diorite and gabbro rocks, according to /8/. The sections are bounded by the threshold values

granite < 2,680 kg/m^3
2,680 kg/m^3 < granodiorite < 2,730 kg/m^3
2,730 kg/m^3 < tonalite < 2,800 kg/m^3
2,800 kg/m^3 < diorite < 2,890 kg/m^3
2,890 kg/m^3 < gabbro.

The magnetic susceptibility logging is subdivided into steps of decades and the natural gamma radiation is divided into steps of “low” (< 10µR/h), “medium” (10 µR/h < gamma < 20 µR/h), “high” (20 µR/h < gamma < 30 µR/h) and “very high” (> 30 µR/h).

3. For the cored boreholes the normal resistivity loggings are corrected for the influence of the borehole diameter and the borehole fluid resistivity. The apparent porosity is calculated during the correction of the resistivity loggings. The calculation is based on Archie’s law /9/; $\sigma = a\ \sigma_w\ \varphi^m + \sigma_s$ where σ = bulk conductivity (S/m), σ_w = pore water conductivity (S/m), φ = volume fraction of pore space, σ_s = surface conductivity (S/m) and “a” and “m” are constants. Since “a” and “m” vary significantly with variations in the borehole fluid resistivity, estimations of the constants are performed with reference to the actual fluid resistivity in each borehole respectively. The constants used in this investigation are presented in Table 4-1.

Table 4-1. Values of the constants a and m in Archie's law used in the calculation of the apparent porosity.

Borehole	Average fluid resistivity (Ωm)	a	m
KLX01	21.8	17.5	1.715
KLX03	4.4	17.5	1.715
KLX04	21.3	17.5	1.715

The vertical temperature gradient (in °C/km) is calculated from the fluid temperature logging for 9 metre sections according to the following equation /10/:

$$TempGrad = \frac{1000\left[9\sum zt - \sum z \sum t\right]\sin\varphi}{9\sum z^2 - \left(\sum z\right)^2}$$

where z = depth co-ordinate (m), t = fluid temperature (°C) and φ = borehole inclination (°). The vertical temperature gradient is only calculated for cored boreholes.

4. Interpretation of the position of large fractures and estimated fracture frequency (classification to fracture logging and calculation of the estimated fracture frequency logging are based on analyses of the short and long normal resistivity, caliper mean, single point resistance (SPR), focused resistivity (140 and 300 cm) and sonic.

The position of large fractures is estimated by applying a second derivative filter to the logging data and then locating maxima (or minima depending on the logging method) in the filtered logging. Maxima (or minima) above (below) a certain threshold value (Table 4-2) are selected as probable fractures. The result is presented as a column diagram where column height 0 = no fracture, column height 1 = fracture indicated by all logging methods.

The estimated fracture frequency is calculated by applying a power function to the weighted sum of the maxima (minima) derivative logging for each method respectively, and then calculating the total sum of all power functions. Parameters for the power functions were estimated by correlating the total weighted sum to the mapped fracture frequency in the cored boreholes KLX03 and KLX04. The powers and linear coefficients (weights) used are presented in Table 4-2.

5. Report evaluating the results.

Table 4-2. Threshold values, powers and weights used for estimating position of fractures and calculate estimated fracture frequency, respectively.

	Borehole	Sonic	Focused res. 140	Focused res. 300	Caliper	SPR	Normal res. 64	Normal res. 16	Lateral res.
Threshold	KLX01	1.4	–	–	–	0.6;0.9*	5.0	–	2.0
Power	KLX01	1.0	–	–	–	0.5	0.5	–	0.6
Weight	KLX01	1.0	–	–	–	5.0	2.9	–	3.3
Threshold	KLX03	1.8	2.0	2.0	–	4.0	7.0	7.0	–
Power	KLX03	1.0	1.0	1.6	–	0.5	0.5	0.6	–
Weight	KLX03	1.0	7.1	6.7	–	5.0	2.9	5.0	–
Threshold	KLX04	1.8	2.0	2.0	0.5	4.0	7.0	7.0	–
Power	KLX04	1.0	1.0	1.6	–	0.5	0.5	0.6	–
Weight	KLX04	1.0	7.1	6.7	–	5.0	5.0	2.9	–
Threshold	HLX21	1.0	1.0	1.2	0.35	1.0	2.5	2.5	1.2
Power	HLX21	–	1.0	1.6	1.0	0.5	0.5	0.6	–
Weight	HLX21	–	7.1	6.7	1.0	5.0	5.0	2.9	–
Threshold	HLX22	1.0	1.2	1.2	0.35	1.0	2.5	2.5	1.3
Power	HLX22	1.0	1.0	1.6	1.0	0.5	0.5	0.6	–
Weight	HLX22	1.0	7.1	6.7	1.0	5.0	5.0	2.9	–
Threshold	HLX23	1.0	1.2	1.2	0.35	1.0	2.5	2.5	1.0
Power	HLX23	1.0	1.0	1.6	1.0	0.5	0.5	0.6	–
Weight	HLX23	1.0	7.1	6.7	1.0	5.0	5.0	2.9	–
Threshold	HLX24	0.9	1.0	1.1	0.35	1.0	3.8	4.0	1.2
Power	HLX24	1.0	1.0	1.6	1.0	0.5	0.5	0.6	–
Weight	HLX24	1.0	7.1	6.7	1.0	5.0	5.0	2.9	–
Threshold	HLX25	–	1.2	1.2	0.35	1.0	2.5	2.5	1.0
Power	HLX25	1.0	1.0	1.6	1.0	0.5	0.5	0.6	–
Weight	HLX25	1.0	7.1	6.7	1.0	5.0	5.0	2.9	–
Threshold	HLX26	1.0	1.2	1.2	0.35	1.0	3.0	2.5	0.7
Power	HLX26	1.0	1.0	1.6	1.0	0.5	0.5	0.6	–
Weight	HLX26	1.0	7.1	6.7	1.0	5.0	5.0	2.9	–
Threshold	HLX27	1.0	1.0	1.2	0.35	1.0	2.5	2.5	1.2
Power	HLX27	1.0	1.0	1.6	1.0	0.5	0.5	0.6	–
Weight	HLX27	1.0	7.1	6.7	1.0	5.0	5.0	2.9	–
Threshold	HLX28	1.0	1.2	1.2	0.35	1.0	2.5	2.5	1.0
Power	HLX28	1.0	1.0	1.6	1.0	0.5	0.5	0.6	–
Weight	HLX28	1.0	7.1	6.7	1.0	5.0	5.0	2.9	–

*the lower value was used for the section 0–100 m, and the higher for 100–700 m.

4.2 Preparations

11 samples were collected in KLX03 by Thomas Kisiel (SKB) for petrophysical analyses (Table 4-3). Each petrophysical sample is a c 100 mm long core with a diameter of c 50 mm. The samples were assigned an identity code comprising “Borehole identity”, “section up” and “section low”. The electric resistivity measurements were performed on the full core samples. Four 22 mm long specimens were then drilled from each of the original core samples, parallel to the core axis. Each specimen was given a specimen number, to separate them from each other. The magnetic measurements were performed on single specimens. All specimens plus, if possible, the remains of the core sample, were

then assembled and the density (wet and dry) and porosity measurements were performed. Measurement techniques and sample handling are described in more detail in /2/.

The samples are not oriented with reference to any co-ordinate system, there is only a mark indicating section up and section low. The orientation of the remanence vectors and the principal anisotropy axes are therefore only made with reference to the core axis. Declination data of these parameters are consequently meaningless but inclination variations may be possible to interpret if the borehole is sub-vertical. The dip of KLX03 is c 75° and this is steep enough to allow a meaningful interpretation of inclination variations of the remanence vector and the principal anisotropy directions, with an accuracy of c ± 15°.

Table 4-3. Sample information for KLX03.

Section up (m)	section low (m)	rock type (preli.classification)
126.04	126.14	Fine-grained diorite to gabbro
240.45	240.55	Ävrö granite
298.52	298.62	Ävrö granite
311.00	311.10	Ävrö granite
340.92	341.02	Ävrö granite
431.60	431.70	Diorite to gabbro
511.18	511.28	Ävrö granite
572.02	572.12	Ävrö granite
782.42	782.52	Quartz monzodiorite (altered)
865.51	865.61	Quartz monzodiorite
990.19	990.29	Quartz monzodiorite (foliated)

4.3 Data handling

The laboratory measurements of petrophysical parameters produce raw-data files in ascii, binary or Microsoft Excel formats. All data files were delivered via email from the laboratory at the Luleå University of Technology to GeoVista AB. The data were then rearranged and placed in Microsoft Excel files. Back-up files of all raw-data are stored both at GeoVista AB and at the laboratory.

The logging data from KLX03, KLX04 and HLX21–28 were delivered as a Microsoft Excel file via email from Rambøll. The data used for interpretation are:

- Density (gamma-gamma).
- Magnetic susceptibility.
- Natural gamma radiation.
- Focused resistivity (300 cm).
- Focused resistivity (140 cm).
- Sonic (P-wave).
- Caliper mean.
- SPR.
- Short normal resistivity (16 inch).

- Long normal resistivity (64 inch).
- Lateral resistivity.
- Fluid resistivity.
- Fluid temperature.

Data from KLX01 were downloaded from the SICADA database, and the loggings used for interpretation are:

- Density (gamma-gamma).
- Magnetic susceptibility.
- Natural gamma radiation.
- Sonic (P-wave).
- Caliper 1D.
- SPR.
- Lateral resistivity.
- Long normal resistivity (64 inch).
- Fluid resistivity.
- Fluid temperature.

4.4 Analyses and interpretations

4.4.1 Logging data

The analyses of the logging data are made with respect to identifying major variations in physical properties with depth as indicated by the silicate density, the natural gamma radiation and the magnetic susceptibility. Since these properties are related to the mineral composition of the rocks in the vicinity of the borehole they correspond to variations in lithology and in thermal properties.

The resistivity, sonic and caliper loggings are mainly used for identifying sections with increased fracturing and alteration. The interpretation products vertical temperature gradient, salinity and apparent porosity help to identify water bearing fractures, saline ground water and porous rocks.

4.4.2 Density and magnetic properties of rock samples

The density and the magnetic properties of the core samples are used partly for calibrating the density and susceptibility logging data and partly for supporting the core mapping since these parameters relate to the mineral composition /7 and 8/.

4.4.3 Anisotropy of magnetic susceptibility (AMS) on rock samples

The magnetic anisotropy of rock forming minerals basically originates from two sources, the grain shape and the crystallographic structure. The orientation of the anisotropy of magnetic susceptibility (AMS) coincides with the crystallographic axes for most rock forming minerals, and it is therefore possible to directly transfer “magnetic directions” to “tectonic directions” (foliation and lineation) measured in the field. AMS is very sensitive

and can detect even small amounts of strain. Parameters related to the length of the three orthogonal principal AMS axes indicate if the rock has suffered from deformation and if so, what type of deformation and in some cases the degree of strain. The method is commonly used for tectonic reconstructions, and to characterise ancient stress fields and magmatic flow directions. For further descriptions of AMS see e.g. /11/.

4.4.4 Resistivity and induced polarisation of rock samples

The electric resistivity and induced polarization is measured with the sample soaked in both tap water and in saline water (2.5% NaCl by weight). The contrast in resistivity (ρ) between silicate minerals and more conducting media like water or sulphides/graphite is extremely high. The bulk resistivity of a rock is therefore more or less independent of the type of silicate minerals that it contains. Electric conduction will be almost purely electrolytic if the rock is not mineralised. Archie's law /9/ is frequently used to calculate the conductivity ($1/\rho$) of sedimentary rocks.

Archie's law has proved to work well for rocks with a porosity of a few percent or more. Old crystalline rocks usually have a porosity of 0.1 to 2 % and sometimes even less. With such low porosity the interaction between the electrolyte and the solid minerals becomes relevant. Some solids, especially clay minerals, have a capacity to adsorb ions and retain them in an exchangeable state /12/. This property makes clays electrically conductive but the same property can to some degree be found for most minerals. The resulting effect, surface conductivity, can be accounted for by the parameter a in Archie's law. The relative effect of surface conductivity will be greatly reduced if the pore water is saline. The amount of surface conductivity is dependent upon the grain size and texture of the rock. Fine grained and/or mica- or chlorite-rich, foliated rocks are expected to have a large relative portion of thin membrane pore spaces that contribute to surface conductivity.

The induced polarisation (IP) effect can be caused by different mechanisms of which two are the most important. When the electric current passes through an interface between electronic and electrolytic conduction there is an accumulation of charges at the interface due to the kinetics of the electrochemical processes involved. This will occur at the surface of sulphide, oxide or graphite grains in a rock matrix with water filled pores. The second mechanism is related to electric conduction through thin membrane pore spaces. In this case an accumulation of charges will occur at the beginning and end of the membrane. The membrane polarisation is thus closely related to the surface conduction effect mentioned above for electric resistivity. Fine grained and/or mica- or chlorite-rich, foliated rocks are therefore expected to show membrane polarisation. Also, the effect of membrane polarisation is greatly reduced in saline water in the same way as surface conductivity.

4.5 Nonconformities

Apparent porosity calculations and corrections for the borehole diameter and fluid resistivity are not presented for the long normal resistivity loggings of KLX03 and KLX04 since the calculation show unrealistic values. In the petrophysical data from KLX01 retrieved from SICADA it was discovered that the magnetic susceptibility and the NRM intensity incorrectly were given in cgs units, and not in the SI-system. To correct for this the susceptibility was multiplied by the factor 4π and the NRM intensity was multiplied by the factor 1,000. Apart from this, no nonconformities are reported.

5 Results

The original results are stored in the primary data base (SICADA). For further interpretation and modelling the data in SICADA must be used. The data is traceable in SICADA by the Activity Plan numbers (AP PS 400-04-094 and AP PS 400-04-100 respectively).

5.1 Petrophysical properties of KLX01

The analyses cover 90 samples from KLX01 and the data have previously been presented by Nisca /1/. The old rock type classification of the samples was updated by use of the new rock type classification data of the drill core (see Appendix 1). Each rock type group conforms to the SKB standard.

5.1.1 Density and magnetic properties

The rock type classifications diagram in Figure 5-1 shows the distribution of the magnetic susceptibility versus density for each sample group. Rock type distributions of petrophysical data from the surface sampling on bedrock outcrops in 2002–2004 /13/ are shown as colored areas in the figure.

The density of the primary Ävrö granite in KLX01 is high compared to the surface data, with an average in KLX01 of 2,740 ± 37 kg/m^3, and a majority of the samples plot between the granodiorite and tonalite classification curves. The average density of the Ävrö granite on the surface is 2,690 ± 24 kg/m^3. Several of the altered Ävrö granite samples have markedly lower density and/or lower susceptibility compared to the primary rock, which shows that the alteration has had a significant effect on the physical properties of the rocks. The fine-grained granite samples overlap nicely with the surface data, and their average density is 2,630 ± 10 kg/m^3. The diorite to gabbro rock samples (including the fine-grained diorite to gabbro) appears to have slightly lower susceptibility compared to the surface data, but they generally overlap in density. It must be noted that the area of distribution of the diorite to gabbro rocks indicated by the surface data is only based on 5 samples, and this makes the area of distribution uncertain.

The natural remanent magnetization (NRM) intensity is plotted versus magnetic susceptibility in Figure 5-2. All Q-values are below 1.0. The Q-values of different rock types and the general distribution of the data, coincides well with the distribution of the surface data /13/. However, the average magnetic susceptibility of the Ävrö granite samples of KLX01 (average susc. = 0.034 SI) is twice as high as for the surface data (average susc. = 0.017 SI), which indicates that the amount of magnetite is higher in the Ävrö granite rock in the vicinity of KLX01 compared to the general distribution on the surface.

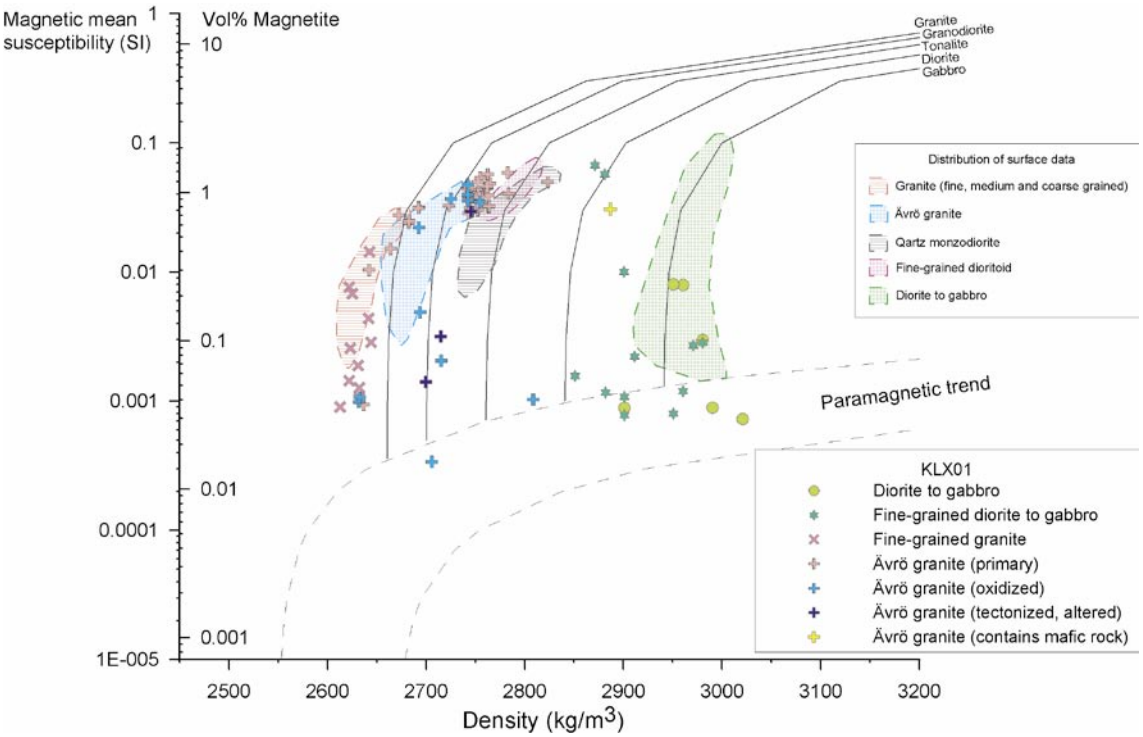

Figure 5-1. *Density-susceptibility rock classification diagram for KLX01. See the text for explanation.*

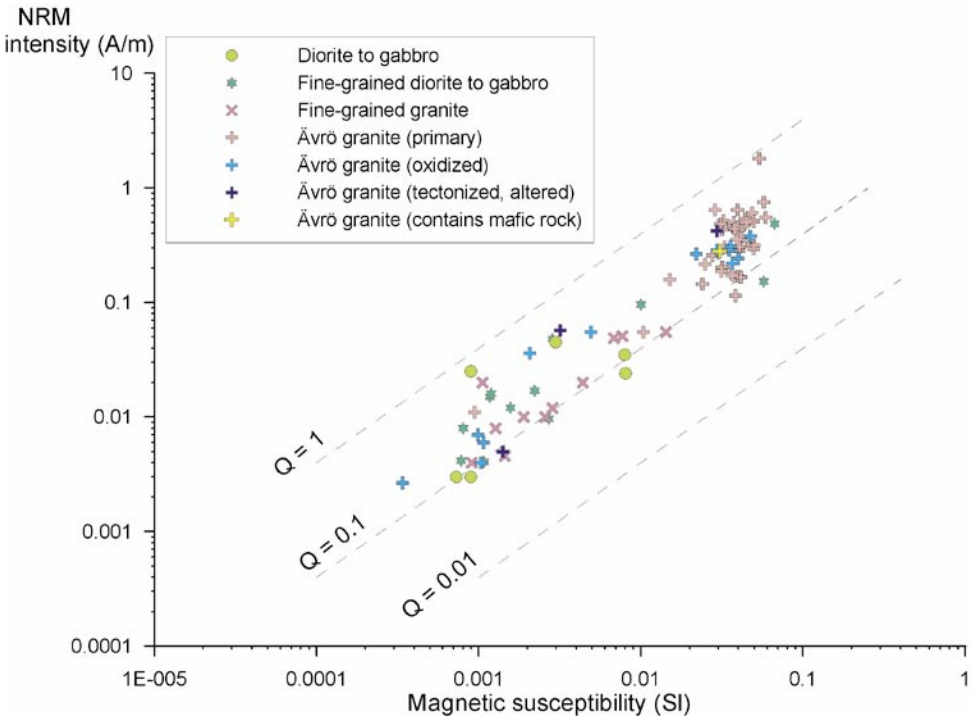

Figure 5-2. *Natural remanence intensity versus magnetic susceptibility for KLX01. See the text for explanation.*

5.1.2 Resistivity, induced polarisation and porosity

The resistivity and IP data for the KLX01 samples can be seen in Figure 5-3. The IP has been measured in the time domain and those data are therefore not directly comparable with the IP data from e.g. surface petrophysical sampling during 2002 and 2004 or sampling of KLX03. The resistivity of the soaking water was not recorded but a reasonable assumption of the resistivity of the used tap water might be around 30 Ωm.

No overall correlation between resistivity and IP can be seen. Different rock types do however show different properties. Tectonized Ävrö granite has very low resistivity and also IP below average, whereas primary and oxidized Ävrö granite has resistivity and IP values that can be considered as normal for crystalline rocks in Sweden. The diorite to gabbro and fine-grained diorite to gabbro samples have high resistivity but normal IP values. The fine-grained granite samples have fairly high resistivity and low IP. The results are consistent with the results from the surface sampling.

Resistivity as a function of porosity is plotted in Figure 5-4. The porosity values cluster around 0.3 % for the primary and oxidized Ävrö granite samples. This level is lower than the porosity measured for the surface sampling. The absolute accuracy of porosity measurements is only about 0.1 % since excess water has to be dried off the surface of the samples without removing pore water. The relative accuracy of porosity measurements is usually better as long as the same person performs the measurements. This probably explains, at least partly, the difference in results of the KLX01 samples compared to more recent measurements. The diorite to gabbro and fine-grained diorite to gabbro samples have low porosity whereas high porosity can be seen for the tectonized Ävrö granite samples.

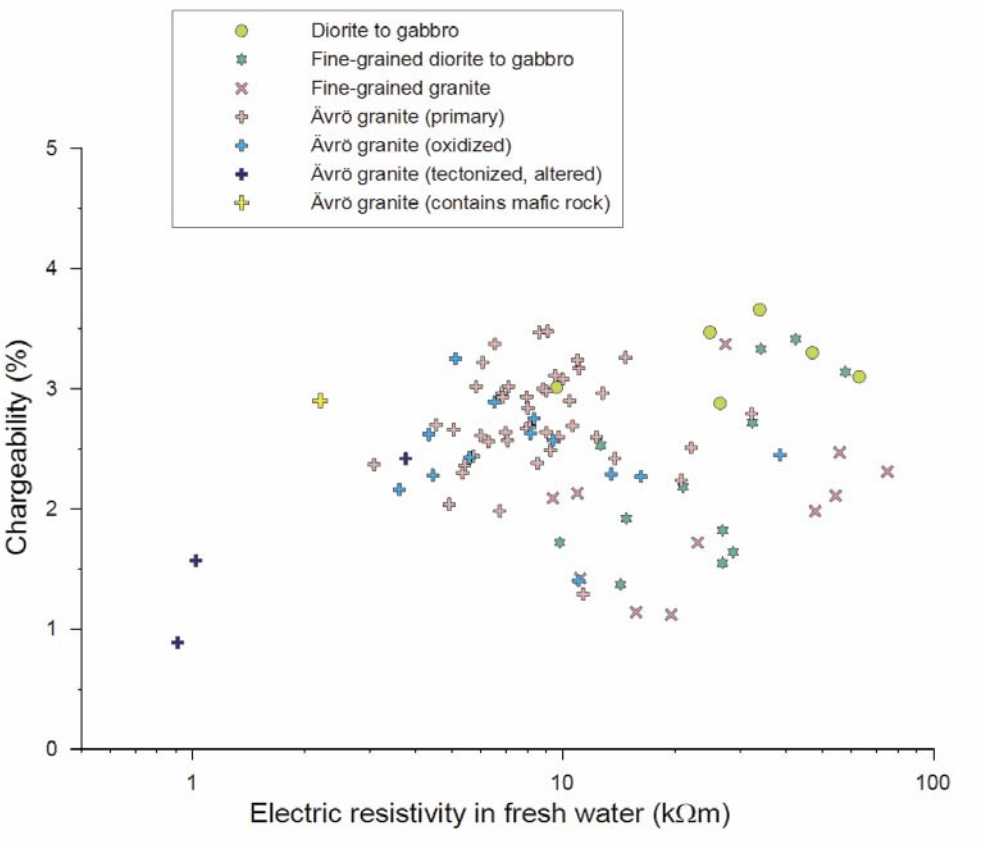

Figure 5-3. *Chargeability (IP) versus resistivity for the KLX01 samples.*

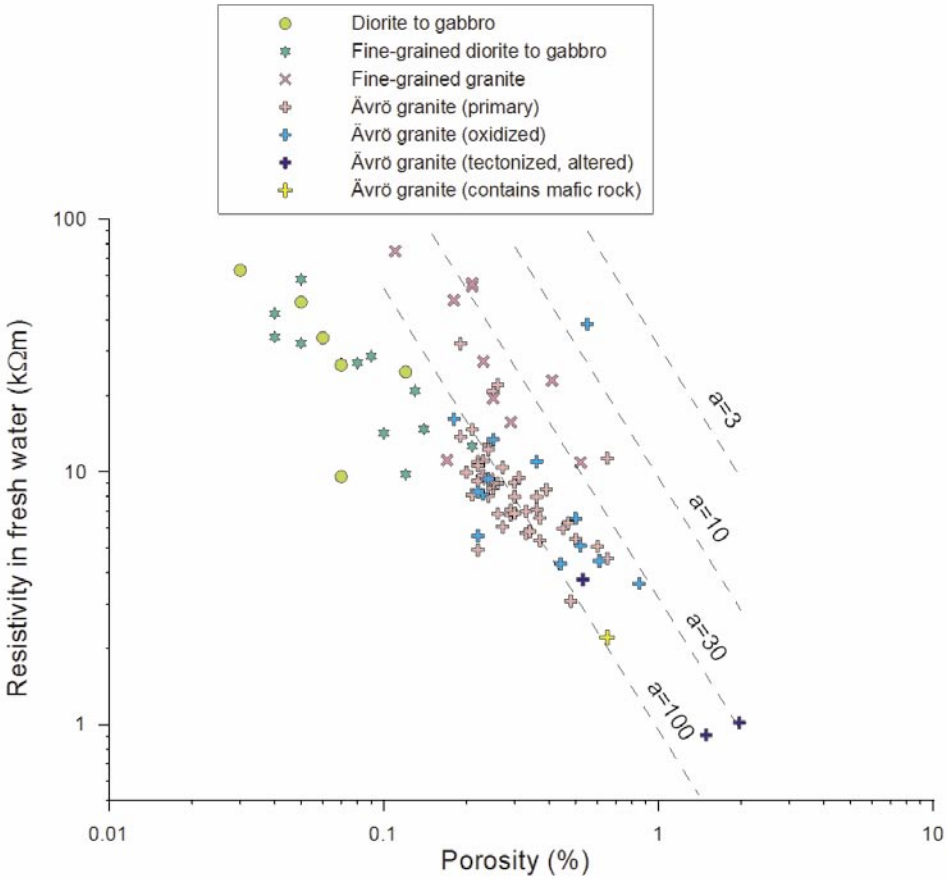

Figure 5-4. *Resistivity versus porosity for the KLX01 samples. The straight dashed lines corresponds to Archie's law, m = 1.75 and different values for a (see text for explanation).*

The electric conductivity (reciprocal to resistivity) of porous rock samples as a function of porosity can be modelled with Archie's law:

$$\sigma = a \cdot \sigma_w \cdot \varphi^m \cdot s^n$$

where
σ = bulk conductivity (= 1/ρ, S/m),
σ_w = pore water conductivity (S/m),
φ = volume fraction of pore space,
s = fraction of pore space that is water saturated,
a, m, n = dimensionless numbers, m ≈ 1.5 to 2.2.

Even if Archie's law is not valid for low-porosity crystalline rock, it can still be used as a starting point to analyze the results. Straight lines corresponding to Archie's law with 1.75 assigned for the exponent m and different values for a are plotted in Figure 5-4. A fairly good correlation between porosity and resistivity can be seen in the data, if the fine-grained granite samples are excluded. The slope of this trend is however more gentle than the lines corresponding to Archie's law. A very low value of the exponent m is unrealistic and this means that the low-porosity samples must be modeled with higher values for a. This coefficient attributes for the surface conductivity, i.e. the apparently high electric conductivity seen at the interface between mineral grains and the electrolyte in pore-spaces. It thus seems as if the electric conductivity of low-porosity samples is more affected by

surface conductivity than the ones with higher porosity. Fine-grained granite shows less surface conductivity than other rock types. This is not surprising since surface conductivity becomes large in samples containing e.g. chlorite, sericite or clay minerals.

Porosity, resistivity and IP as a function of depth along the hole is plotted in Figure 5-5. A spatial correlation between porosity and resistivity values can be seen for some of the rock types. High porosity and low resistivity can e.g. be seen for Ävrö granite samples between 100 and 200 metres depth. Fine-grained diorite to gabbro samples above 120 metres depth have higher porosity, lower resistivity and IP than samples from greater depth.

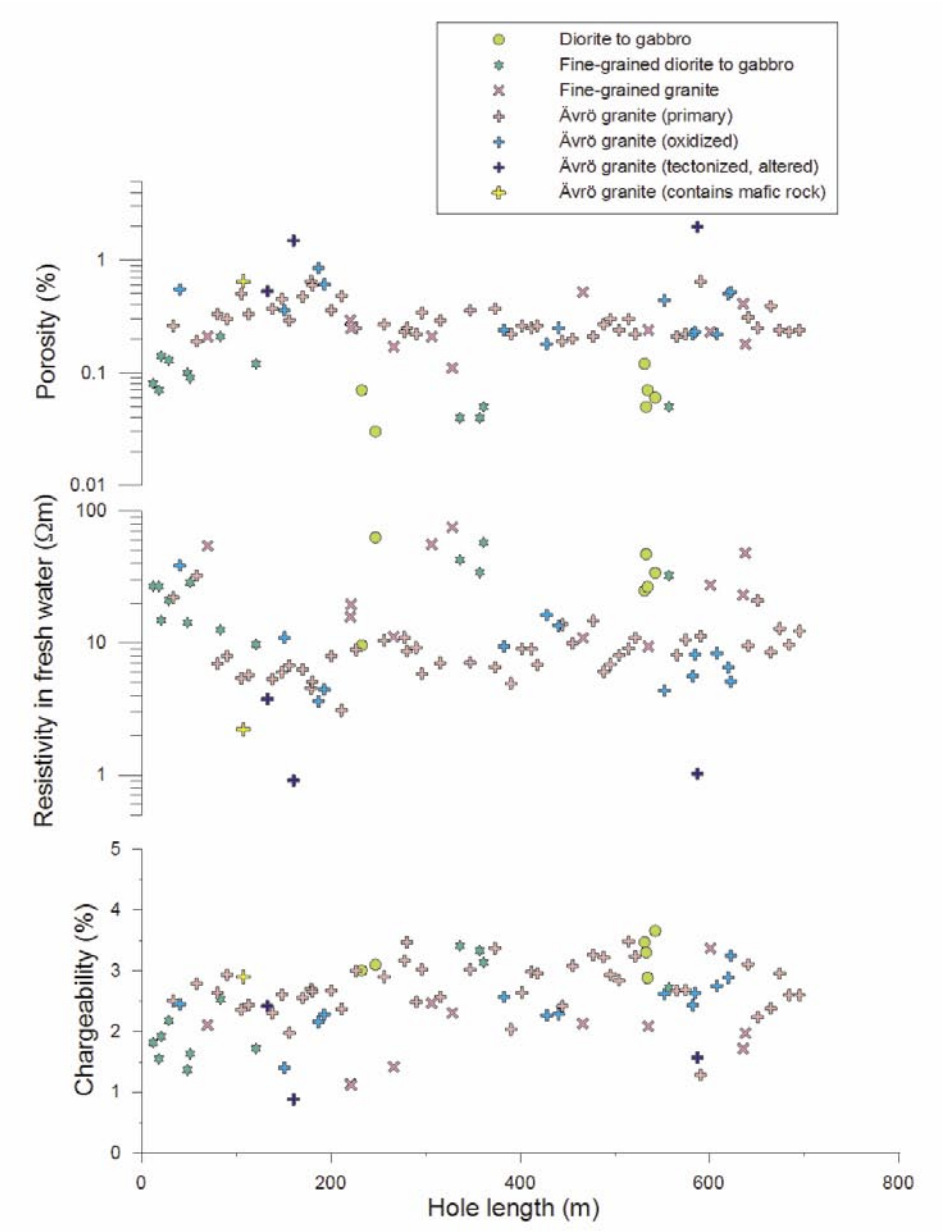

Figure 5-5. *Porosity, resistivity and chargeability (IP) versus depth along the hole for the KLX01 samples.*

5.2 Petrophysical properties of KLX03

The sampling covers 11 samples from KLX03 (Table 4-3, section 4.2), collected and preliminary classified by Thomas Kisiel (SKB). The rock type classification was later updated by use of the Boremap classification data. Each rock type group conforms to the SKB standard.

5.2.1 Density and magnetic properties

The rock type classifications diagram in Figure 5-6 shows the distribution of the magnetic susceptibility versus density for each sample group. Rock type distributions of petrophysical data from the surface sampling on bedrock outcrops in 2002–2004 /13/ are shown as colored areas in the figure. The magnetic susceptibility of the diorite to gabbro sample at 431.65 m depth was too high to be measured by the instrument; consequently this sample is missing in Figure 5-6.

The 6 Ävrö granite samples have an average density of 2,756 ± 16 kg/m^3, which is fairly high and they plot close to, or outside, of the upper boundary of the Ävrö granite distribution indicated by the surface data. Their indicated mineral composition corresponds to that of granodiorite to tonalite rocks. Two quartz monzodiorite samples fall between the tonalite and diorite curves, fairly close but outside of the area of distribution of the surface

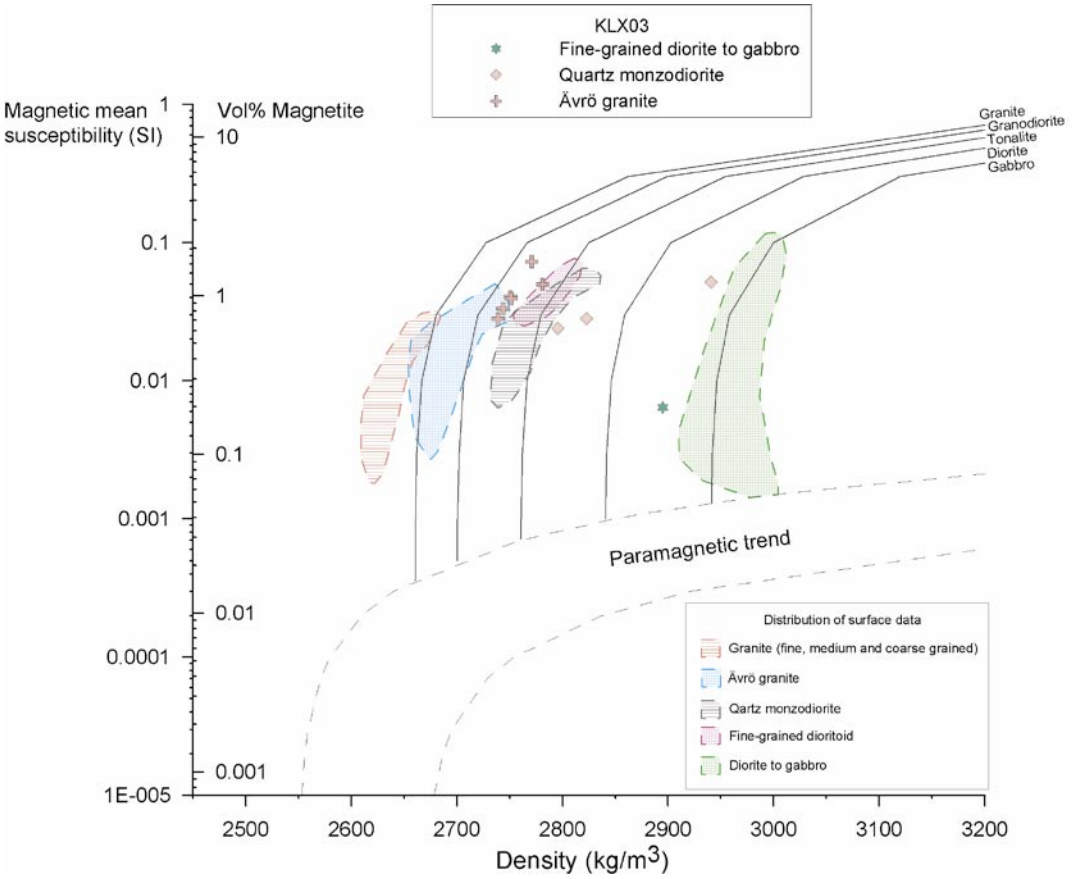

Figure 5-6. *Density-susceptibility rock classification diagram for KLX03. See the text for explanation.*

data. The third quartz monzodiorite sample (depth = 782.47 m) has a density of 2,941 kg/m^3 and appears to have been incorrectly classified. The rock should most likely belong to the diorite to gabbro rock type group. The single fine-grained diorite to gabbro sample plots in the middle of the diorite and gabbro classification curves.

It must be noted that the rock types used in the rock classification diagram do not conform perfectly to the geology of the Simpevarp area. There is for example no corresponding rock type curve for fine-grained dioritoid, a rock type that occurs frequently in the area. We therefore suggest that the data in rock classification diagram such as shown in Figure 5-6 should be used as indicators of the compositional variation between and within different rock types (or groups of rocks).

The natural remanent magnetization (NRM) intensity is plotted versus magnetic susceptibility in Figure 5-7. Q-values are moderate to low and the distribution of the data coincides well to the distribution of the surface data /13/. Two samples, 126.09 m and 865.56 m depth (fine-grained diorite to gabbro and quartz monzodiorite respectively) have negative, or upward, directed remanence vectors, which is an indication that these rocks have been affected by some kind of alteration or reheating after their emplacement. The diorite to gabbro sample from 431.65 m depth has a remanence intensity of 1.068 A/m, which is high and most likely corresponds to a high content of magnetite.

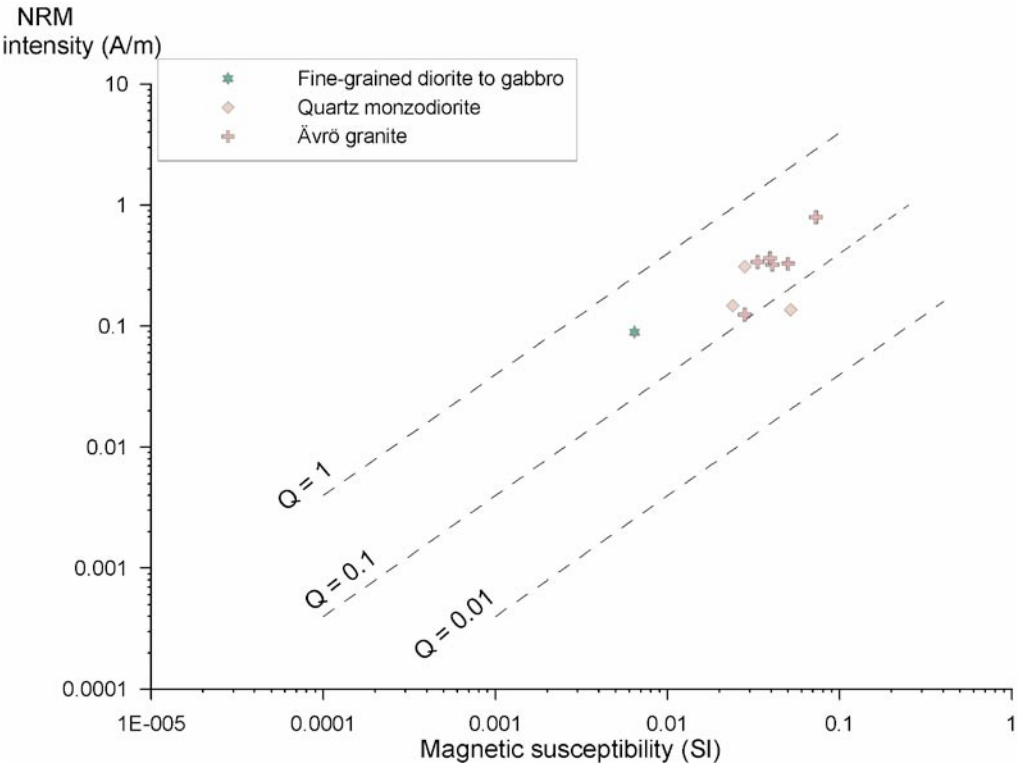

Figure 5-7. *Natural remanence intensity versus magnetic susceptibility for KLX03. See the text for explanation.*

5.2.2 Resistivity, induced polarisation and porosity

Resistivity and IP data for the KLX03 samples soaked in tap water can be seen in Figure 5-8. The resistivity values are typical for crystalline rocks in Sweden and similar to e.g. those obtained with surface samples. The IP values are however higher than surface data by approximately a factor of 2.

The IP data are plotted against magnetic susceptibility in Figure 5-9. No correlation can be seen for the 0.1 Hz phase angles. However, the 4 Hz phase angle show a positive correlation with magnetic susceptibility. The number of samples is small but it seems like the IP effect in the samples is a combined effect of polarization at the surface of magnetite grains and membrane polarization; the former effect dominating at high frequencies and the latter at low frequencies.

The relation between resistivity and porosity can be seen in Figure 5-10. Porosity values are consistent with those obtained for surface samples but higher than the samples from KLX01 (see section 5.1.2). The lowest porosities are seen for the mafic rock types.

The relative effect of surface conductivity becomes smaller in saline water (0.28 Ωm). Straight lines corresponding to Archie's law (section 5.1.2) and a constant low value for the coefficient a of 4 can be seen in the left graph in Figure 5-10. If this assumption is valid, apparent values for the exponent m in Archie's law can be found for the samples. The samples show apparent m-values in the interval 1.68 to 1.97, which can be considered as quite normal. The exponent m models pore-space efficiency to conduct electric current. High values occur for rocks with vugs, pore constrictions and dead-end pores.

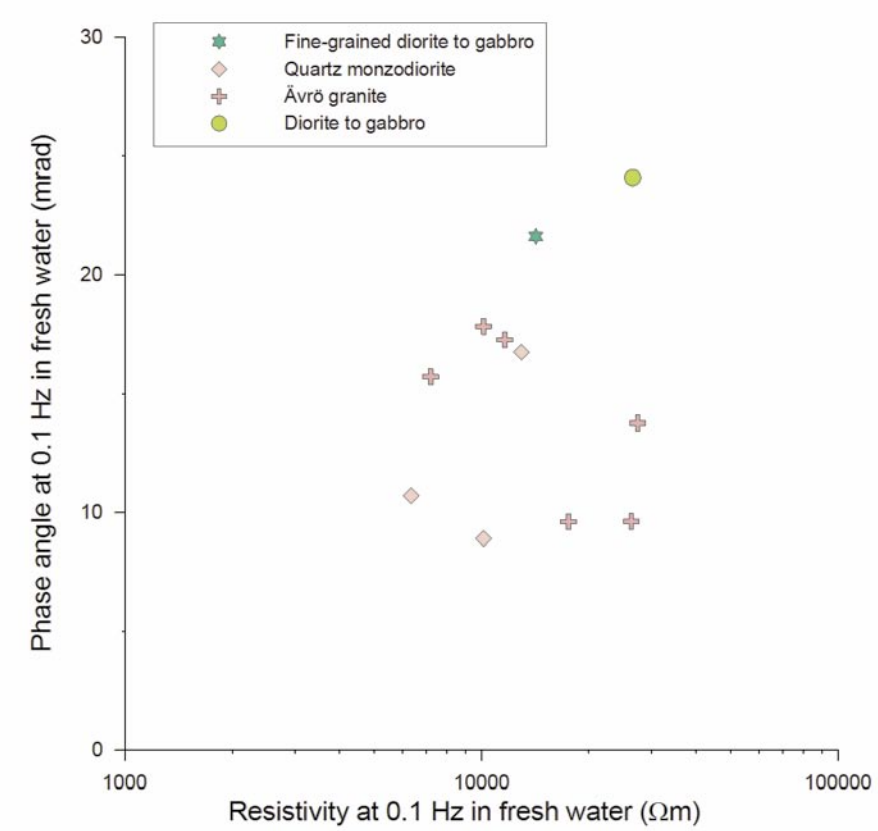

Figure 5-8. *Phase angle (IP) versus resistivity in fresh water for the KLX03 samples.*

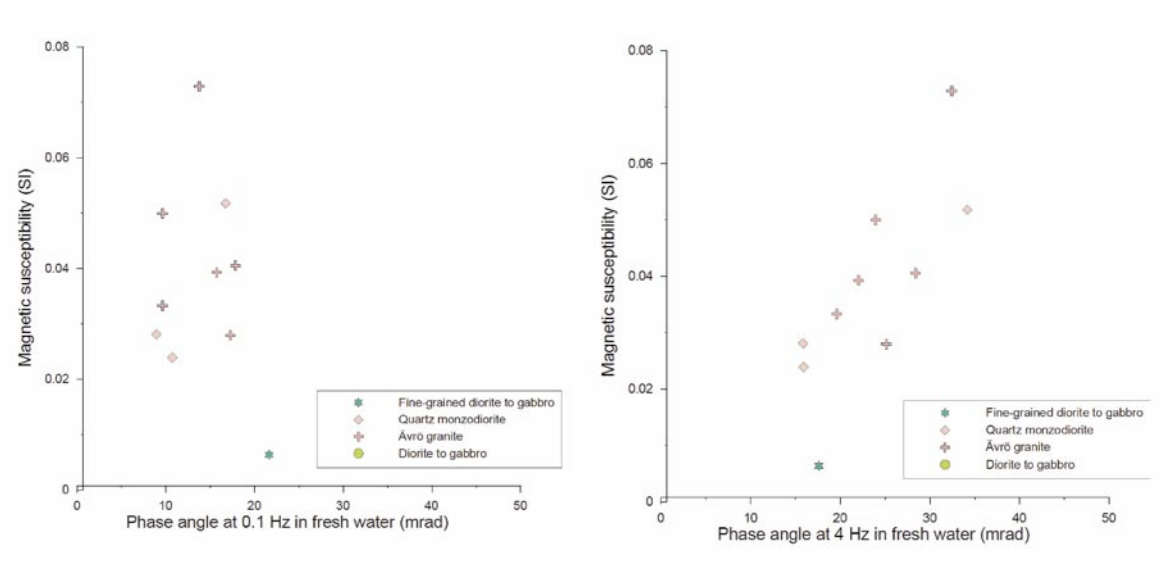

Figure 5-9. *Magnetic susceptibility versus phase angle (IP) in fresh water at 0.1 Hz (left graph) and 4.0 Hz (right graph) for the KLX03 samples.*

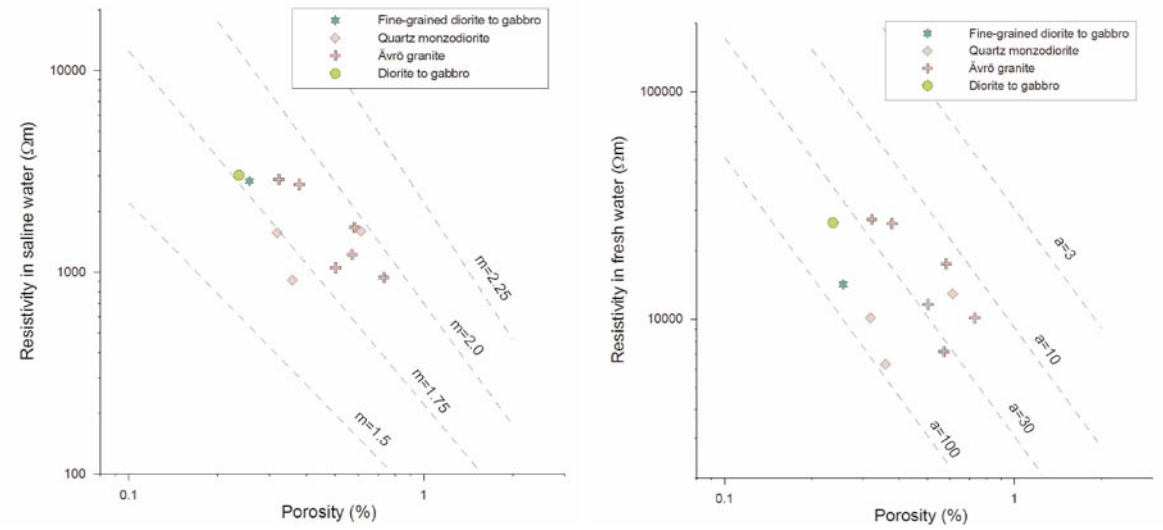

Figure 5-10. *Resistivity in saline water (left graph) and fresh water (right graph) versus porosity. The straight dashed lines in the left graph corresponds to Archie's law and a = 4 for different values of m. The straight dashed lines in the right graph corresponds to Archie's law and m = 1.75 and different values of a (see text for explanation).*

The right graph in Figure 5-10 shows resistivity data for samples soaked in tap water (29.5 Ωm). Dashed lines according to Archie's law with a constant value of m = 1.75 and different values of a. Apparent a-values for the samples range from around 40 to 85 if apparent m-values from the left graph are used for each sample. The highest values are seen for the low-porosity samples. Surface conductivity is thus the completely dominating mechanism for electric conduction through the samples in fresh water conditions.

The electric conductivity of a crystalline rock can be written as:

$\sigma = \sigma_p + \sigma_s + \sigma_m$

Where σ_p corresponds to pure electrolyte conduction in pore spaces, σ_s corresponds to surface conduction and σ_m to conduction through mineral grains. The last term may be neglected in unmineralized rocks. Electrolyte conduction is purely real whereas surface conduction is complex:

$$\sigma = (\sigma_p + \sigma_s) \cdot e^{i\varphi}$$

$$Im(\sigma) = Im(\sigma_s) = \sigma \cdot sin\varphi \approx \sigma \cdot \varphi$$

Where φ is the phase angle. The imaginary conductivity of the samples has been calculated for both tap water and saline water conditions and they are plotted in Figure 5-11. There is a very nice correlation between the two parameters. The imaginary conductivity is however significantly higher in saline water. This can be explained in two ways. The phase of surface conductivity increases with increasing pore-water salinity or the surface conductivity increases with increasing salinity. The latter explanation seems more likely.

5.2.3 Anisotropy of magnetic susceptibility (AMS)

The degree of anisotropy (P) and the dip of the plane of foliation are shown in Figure 5-12 below. Due to an extremely high magnetization of the rock there are no AMS data from the sample at depth 431.65 m. There is no correlation between the degree of anisotropy "P" and the volume susceptibility, and this is an indication that the P-parameter can be used as an indicator of the degree of tectonic strain. The degree of anisotropy is moderate or low for a majority of the sampled rocks. Two samples, 126.09 m and 341.02 m depth, show increased degree of anisotropy, possibly indicating that these rocks have been affected by deformation. The foliation generally dips moderate to steep. For the two samples located at 340.97 m and 990.24 m depth the foliation planes dip shallow.

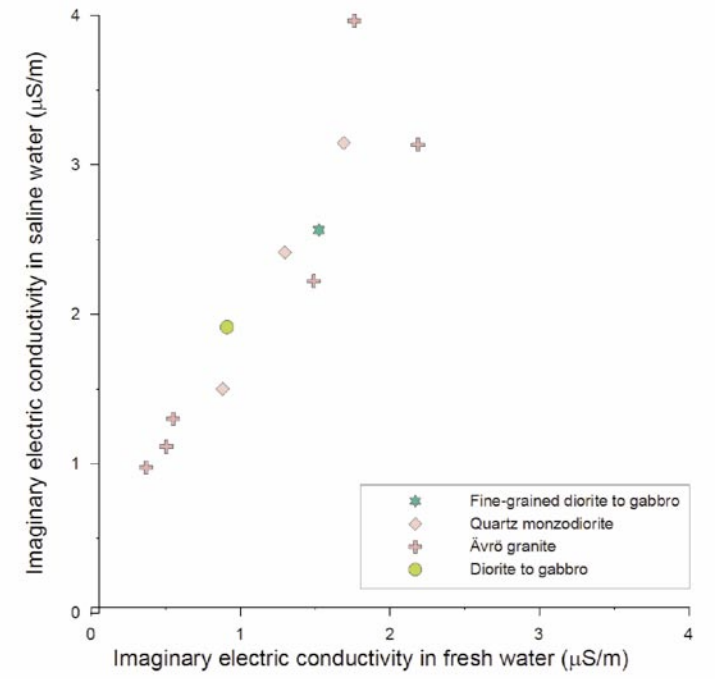

Figure 5-11. *Relation between imaginary electric conductivity in fresh and saline water for the KLX03 samples.*

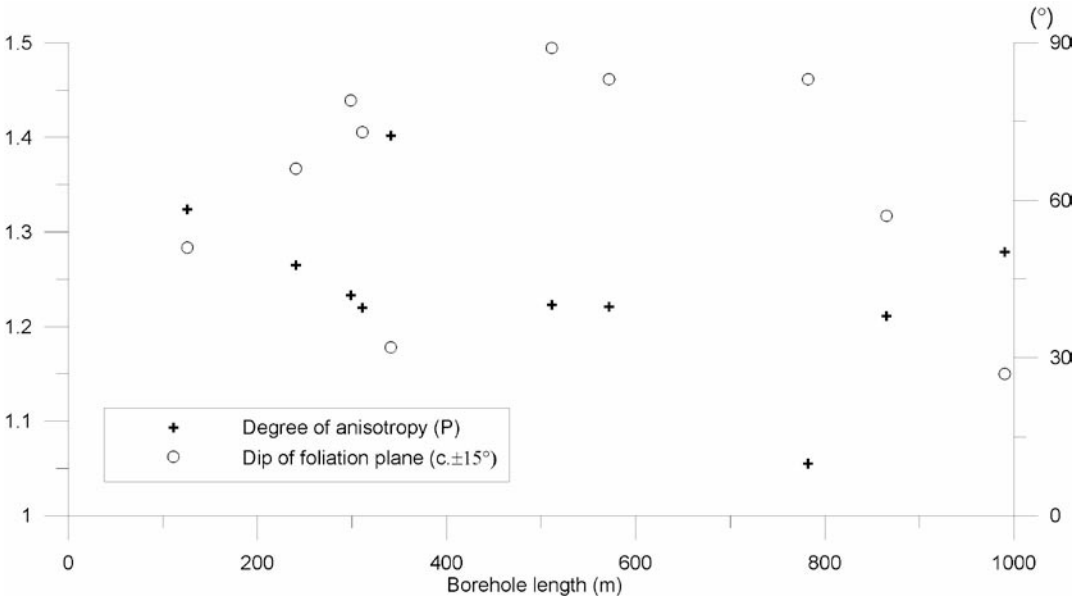

Figure 5-12. *Degree of magnetic anisotropy (P) and dip of the magnetic foliation plane plotted with respect to the depth of the sample.*

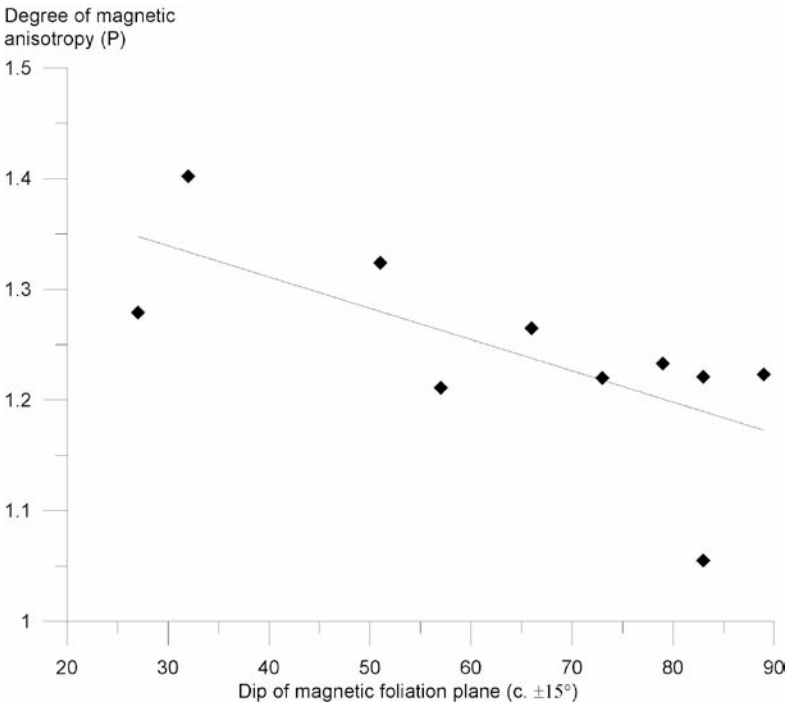

Figure 5-13. *Cross plot of the degree of magnetic anisotropy (P) and dip of the magnetic foliation plane.*

An interesting observation of the AMS data is that there is a clear negative correlation between the degree of anisotropy and the dip of the magnetic foliation (Figure 5-13). This indicates that the rock fabric turns from subvertical to subhorizontal with increasing degree of strain.

5.3 Quality controll of the logging data

5.3.1 Noise levels

Noise levels of the raw data for each logging method are presented in Table 5-1. Noise levels are above the recommended levels for all density logs, except the log from KLX01, and for the percussion drilled boreholes HLX22–28 the noise of the density logs greatly exceed the recommended level. Also several of the sonic and natural gamma radiation logs have high noise levels, but these are most likely low enough to allow a meaningful interpretation of the data. To reduce the influence of the noise, all logs were average or median filtered prior to the interpretation. However, the very high noise levels of the density data of the above noted boreholes may have a significant affect on the quality of the interpretation of these boreholes, especially regarding the possibility of resolving anomalies produced by thin veins or dykes.

A qualitative inspection was performed on the loggings. The data were checked for spikes and/or other obvious incorrect data points. Erroneous data were replaced by null values (–999) by the contractor Rambøll prior to the delivery of the data, and all null values were disregarded in the interpretation. The 3D caliper of KLX03 seems to indicate unrealistic variations and a periodic noise probably related to measurement error.

5.3.2 Comparsion between logging and petrophysical data for KLX01

A quality control of the gamma-gamma and the magnetic susceptibility loggings is performed by comparing the logging data to the petrophysical data at the corresponding depths. In Figure 5-14 the gamma-gamma (density) logging data (after 3 point average filtering) is plotted versus wet density sample measurements. The correlation is fair for the linear fit. A few possible outliers occur in the data, but they were not removed. The logging density data of KLX01 were calibrated by use of linear fit.

A cross plot between the susceptibility log data and susceptibility measured on core samples is shown in Figure 5-15. There is a fairly good correlation between logging and petrophysical data. The slope of the fitted line (through the origin) is 0.224, which indicates that the logging measurements greatly underestimate the true magnetic susceptibility. A large number of data point at low susceptibility values lay above the fitted line. A linear fit would however overcompensate for this problem, therefore the logging data were calibrated by use of a straight fitted line through the origin.

5.3.4 Comparsion between logging and petrophysical data for KLX03

A quality control of the gamma-gamma and the magnetic susceptibility loggings is performed by comparing the logging data to the petrophysical data at the corresponding depths. In Figure 5-16 the gamma-gamma (density) logging data (after 3 point average filtering) is plotted versus wet density sample measurements. The correlation is fair for the linear fit. The sample at c 341 m depth deviates significantly compared to the logging data at the corresponding depth position. The logging density data were calibrated by use of the linear fit, with the outlying data point excluded.

A cross plot between the susceptibility log data and susceptibility measured on core samples is shown in Figure 5-17. There is a fairly good correlation between logging and petrophysical data. The data point at 782.5 m depth deviate significantly from the rest of the data set, and this outlier was removed before calibrating the logging susceptibility measurement. The slope of the fitted line (disregarding the outlier) is 0.628, which indicates that the logging measurements underestimate the true magnetic susceptibility.

Table 5-1. Noise levels in the investigated geophysical logging data.

Logging method	KLX01	KLX03	KLX04	HLX21	HLX22	HLX23	HLX24	HLX25	HLX26	HLX27	HLX28	Recommended max noise level
Density (kg/m^3)	3	23	21	20	29	35	35	40	31	30	38	3–5
Magnetic susceptibility (SI)	$1*10^{-4}$	$5*10^{-4}$	$4*10^{-4}$	$1*10^{-4}$	$2*10^{-4}$	$5*10^{-4}$	$5*10^{-4}$	$3*10^{-4}$	$3*10^{-4}$	$2*10^{-4}$	$5*10^{-4}$	$1*10^{-4}$
Natural gamma radiation (µR/h)	0.4	0.6	0.7	0.8	1.2	1.3	1.2	1.1	1.1	0.9	1.3	0.3
Long normal resistivity (%)	0.1	0.2	0.8	0.4	0.2	0.2	0.3	0.3	0.4	0.2	0.1	2.0
Short normal resistivity (%)	No data	0.1	0.7	0.3	0.2	0.2	0.3	0.3	0.1	0.1	0.1	2.0
Fluid resistivity (%)	0.003	0.2	0.01	Not used	Not used	Not used	Not used	Not used	Not used	Not used	Not used	2
Fluid temperature (°C)	0.0004	0.002	0.002	Not used	Not used	Not used	Not used	Not used	Not used	Not used	Not used	0.01
Lateral resistivity (%)	0.9	Not used	Not used	0.4	0.3	0.2	0.3	0.4	0.1	0.1	0.1	2
Single point resistance (%)	0.1	0.1	0.5	0.4	0.2	0.2	0.3	0.3	0.1	0.1	0.1	No data
Caliper (metre)	$4*10^{-6}$	$8*10^{-5}$	$1*10^{-5}$	$4*10^{-4}$	$2*10^{-4}$	$2*10^{-4}$	$2*10^{-4}$	$2*10^{-4}$	$2*10^{-4}$	$2*10^{-4}$	$1*10^{-4}$	0.0005
Focused resistivity 300 (%)	No data	9.6	10.2	14.5	15.6	11.7	14.0	14.2	12.0	16.9	8.1	No data
Focused resistivity 140 (%)	No data	4.8	9.7	11.4	12.5	8.4	10.7	11.5	3.9	7.8	5.8	No data
Sonic (m/s)	3	17	15	35	46	38	62	68	24	52	31	20

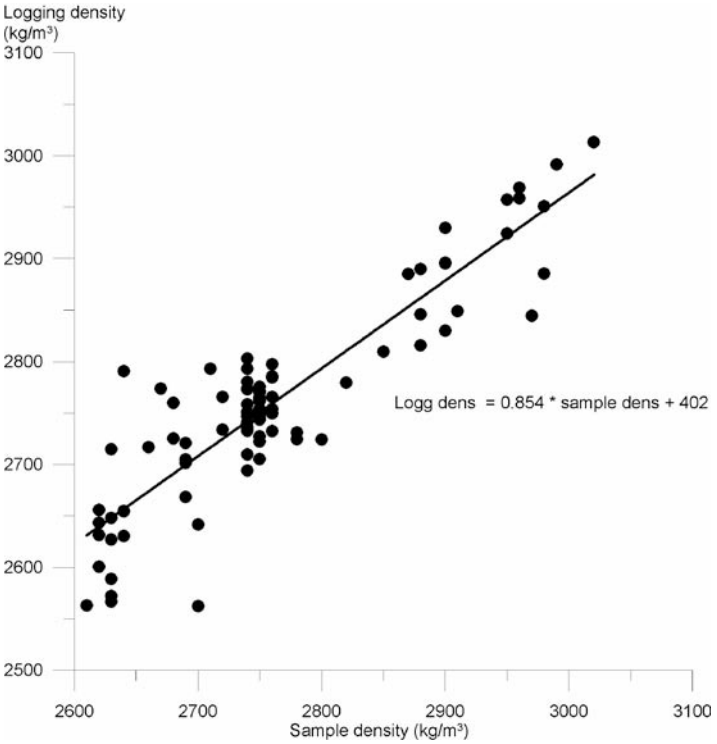

Figure 5-14. *Cross plot of density logging data versus density data from core samples.*

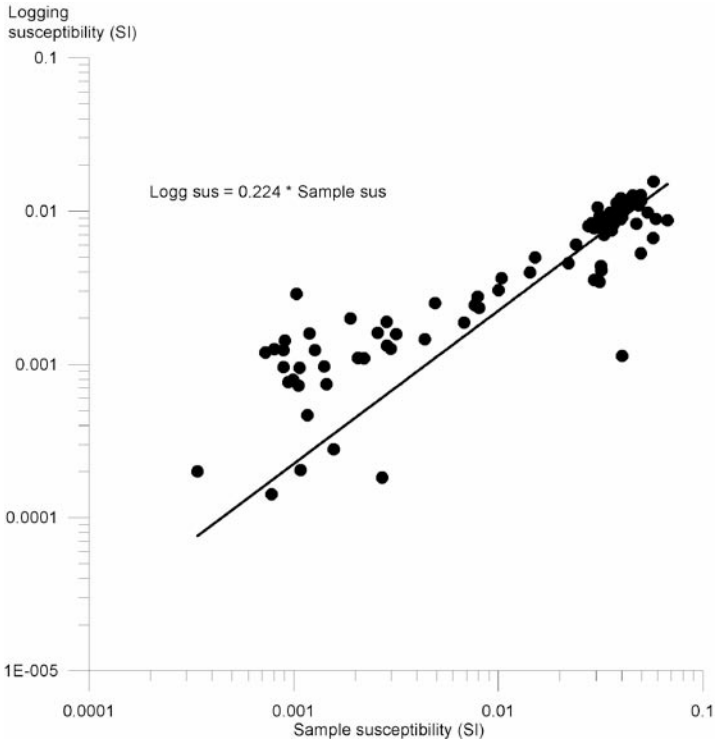

Figure 5-15. *Cross plot of magnetic susceptibility logging data versus susceptibility data from core samples.*

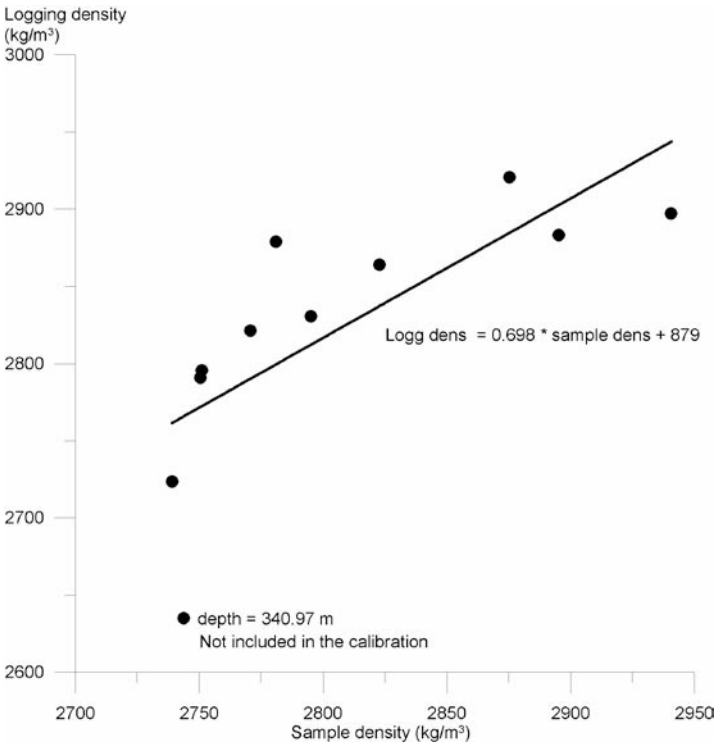

Figure 5-16. *Cross plot of density logging data versus density data from core samples.*

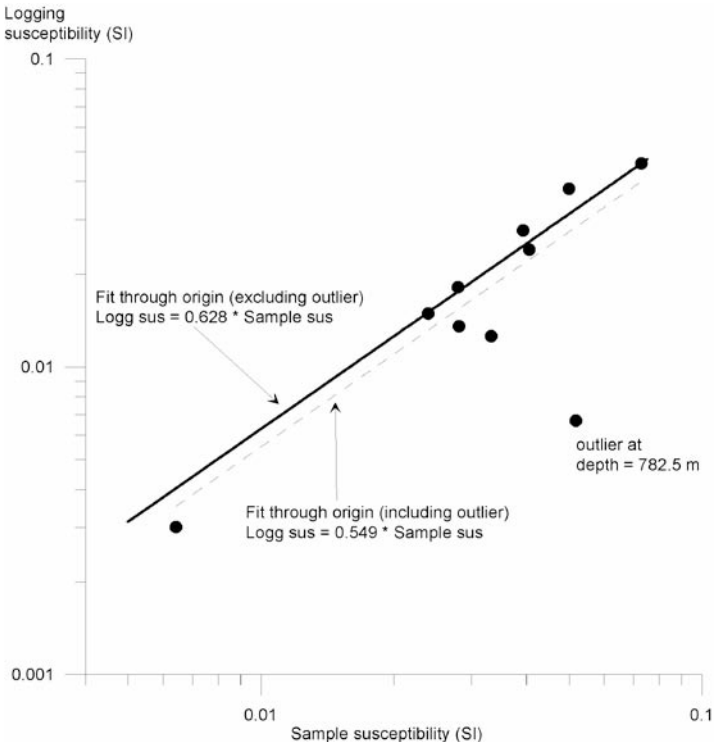

Figure 5-17. *Cross plot of magnetic susceptibility logging data versus susceptibility data from core samples.*

5.4 Interpretation of the logging data

The presentation of interpretation products presented below, in chapters 5.4.1 to 5.4.11, includes:

- Classification of silicate density.
- Classification of natural gamma radiation.
- Classification of magnetic susceptibility.
- Position of inferred fractures (0 = no method, 1 = all methods).
- Estimated fracture frequency in 5 metre sections.
- Classification of estimated fracture frequency (0 to 3, 3 to 6 and > 6 fractures/m).

5.4.1 Interpretation of KLX01

The results of the generalized logging data and fracture estimations of KLX01 are presented in Figure 5-18 below, and in a more detailed scale in Appendix 2.

The rocks in the vicinity of KLX01 are dominated by silicate densities in the intervals 2,680–2,730 kg/m^3 and 2,730–2,800 kg/m^3, which indicate a mineral composition that corresponds to granodiorite and tonalite rocks respectively (Table 5-2). These two silicate density intervals together occur at c 74% of the entire borehole length. Three fairly long sections of high density rocks are indicated at borehole lengths c 30 m, c 240 m and c 540 m. All three sections show correspondingly low values of the natural gamma radiation and the magnetic susceptibility, which is typical for fine-grained diorite to gabbro rocks. The density is generally higher along the uppermost 150 m and lowermost c 200 m (section 500–700 m) of the borehole compared to the intermediate c 150–500 m section. The natural gamma radiation mainly lay in the interval 10–20 µR/h, except for the lowest section 570–690 m, which is dominated by higher radiation levels. Several short positive natural gamma radiation anomalies occur along the entire borehole, and these correspond most likely to fine-grained granite or pegmatite dykes. Many of these occur close to high density anomalies (probable indications of diorite to gabbro rocks), which suggests that felsic and mafic rocks often are spatially related.

The estimated fracture frequency logs indicate a general low level of fracturing along the entire investigated borehole length. Four short, but very distinct fracture anomalies occur at borehole length coordinates c 160 m, 185 m, 460 m and 590 m. In Figure 5-19 below diagrams showing estimated salinity, apparent porosity, porosity measured on core samples, vertical temperature gradient and estimated fracture frequency of KLX01 are displayed. There is a well defined co-variation between the apparent porosity log (based on the short normal resistivity log data) and the sample measurements. The rock porosity averages at c 0.4%. There are several peaks close to indicated fractures, and all of the four probable large fractures mentioned above show up as high porosity anomalies in the porosity log as well as in the sample data. In the fluid temperature gradient log there are distinct anomalies at length coordinates c 185 m, 420 m and 460 m, indicating the presence of water bearing fractures. The salinity shows an increase from c 200 ppm NaCl to c 600 ppm NaCl at c 500 m depth.

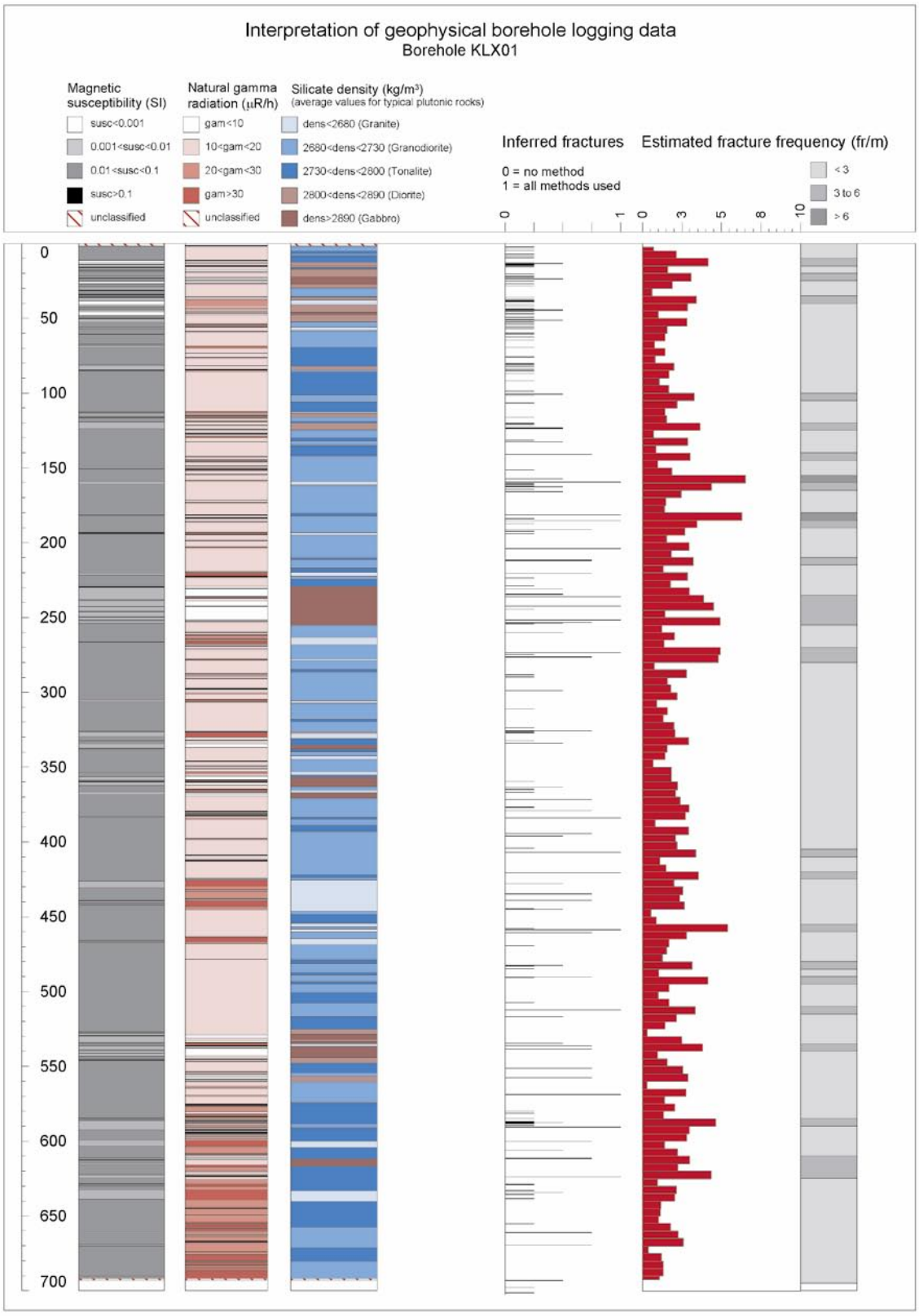

Figure 5-18. *Generalized geophysical logs of KLX01.*

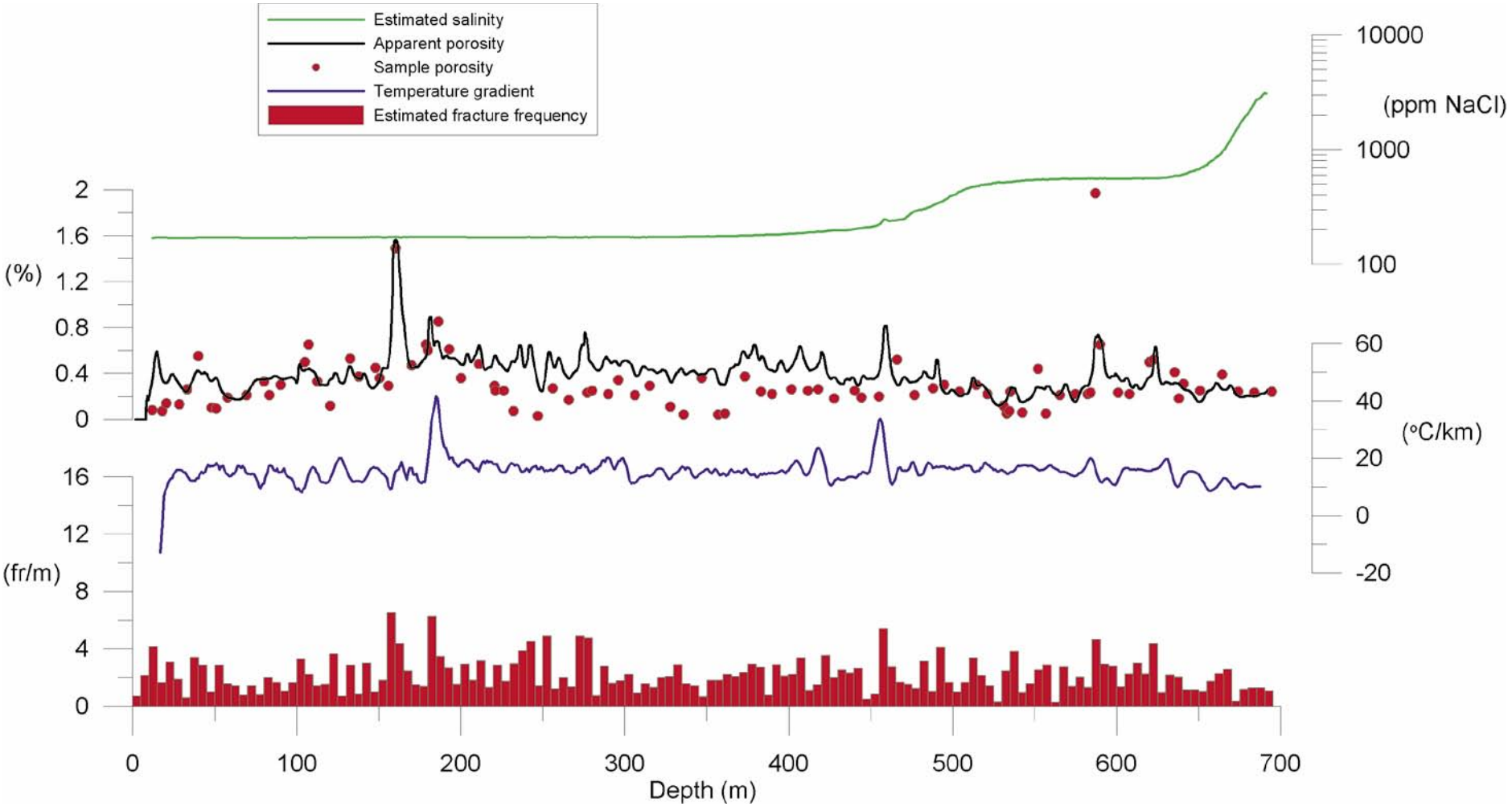

Figure 5-19. *Estimated salinity, apparent porosity, sample porosity, vertical temperature gradient and estimated fracture frequency of KLX01.*

Table 5-2. Distribution of silicate density classes with borehole length of KLX01.

Silicate density interval (kg/m^3)	Borehole length (m)	Relative borehole length (%)
dens < 2,680 (granite)	78	11
2,680 < dens < 2,730 (granodiorite)	314	45
2,730 < dens < 2,800 (tonalite)	200	29
2,800 < dens < 2,890 (diorite)	46	7
dens>2,890 (gabbro)	54	8

5.4.2 Interpretation of KLX03

The results of the generalized logging data and fracture estimations of KLX03 are presented in Figure 5-20 below, and in a more detailed scale in Appendix 3.

The silicate density distribution of KLX03 is in general very variable, which indicates a heterogeneous mineral composition. The section c 100–285 m are dominated by a silicate density in the interval 2,680–2,730 kg/m^3, corresponding to granodiorite mineral composition, with subordinate intervals of slightly higher density. The natural gamma radiation is moderate and the magnetic susceptibility is constant at a fairly high level. The section c 285–325 m contains rocks that are denser, with silicate densities in the interval of 2,730–2,800 kg/m^3, which indicates a mineral composition that corresponds to tonalite. Along the corresponding section the natural gamma radiation is low and the magnetic susceptibility is significantly higher (however, the latter is not visible in the generalized log due to the large classification interval of the susceptibility). From 325 m depth down to c 420 m the silicate density is lower compared to the previous section, but large parts still classify as rock with a mineral composition corresponding to tonalite. However, the natural gamma radiation is above10 µR/h and the magnetic susceptibility corresponds to that of the previously described section. The interval 420–520 m is dominated by a general increase in the natural gamma radiation, but also contains short sections with high density, high magnetic susceptibility and low natural gamma radiation, that most likely correspond to more mafic rocks (e.g. diorite to gabbro). At c 620 m borehole length there is a major change in the magnetic susceptibility log, with a general level decrease and high frequency variations, accompanied by an increase in the occurrence of high density anomalies. This pattern of the physical properties of the rocks continues through out the remaining part of the borehole. One major low density, low susceptibility and high radiation anomaly worth noting occurs at c 900 m borehole length. About 415 m, or almost 50%, of the investigated borehole length (c 900 m) is dominated by silicate density that indicates a mineral composition that correspond to tonalite rock (Table 5-3).

The estimated fracture frequency of KLX03 is generally low or moderate. Increased fracture frequencies (possible deformation zones) are indicated in the sections c 260–320 m, 615–630 m, 655–685 m and 725–780 m. These sections are mainly characterized by low resistivity anomalies and only partly decreased P-wave velocity. In Figure 5-21 below, diagrams showing estimated salinity, apparent porosity log (section 100–800 m), porosity measured on core samples, vertical temperature gradient and estimated fracture frequency of KLX03 are displayed. The rock porosity is generally low, also at several sections where the estimated fracture frequency is high, which may indicate that the suggested deformations zones are dominated by plastic deformation and/or alteration, and that open fractures are less common. One exception occurs along the section c 720–780 m where the apparent porosity is high and there are also several distinct anomalies in the vertical temperature gradient log that indicate the presence of water bearing fractures. There is a major increase in the salinity of the borehole fluid at the borehole length of c 750 m.

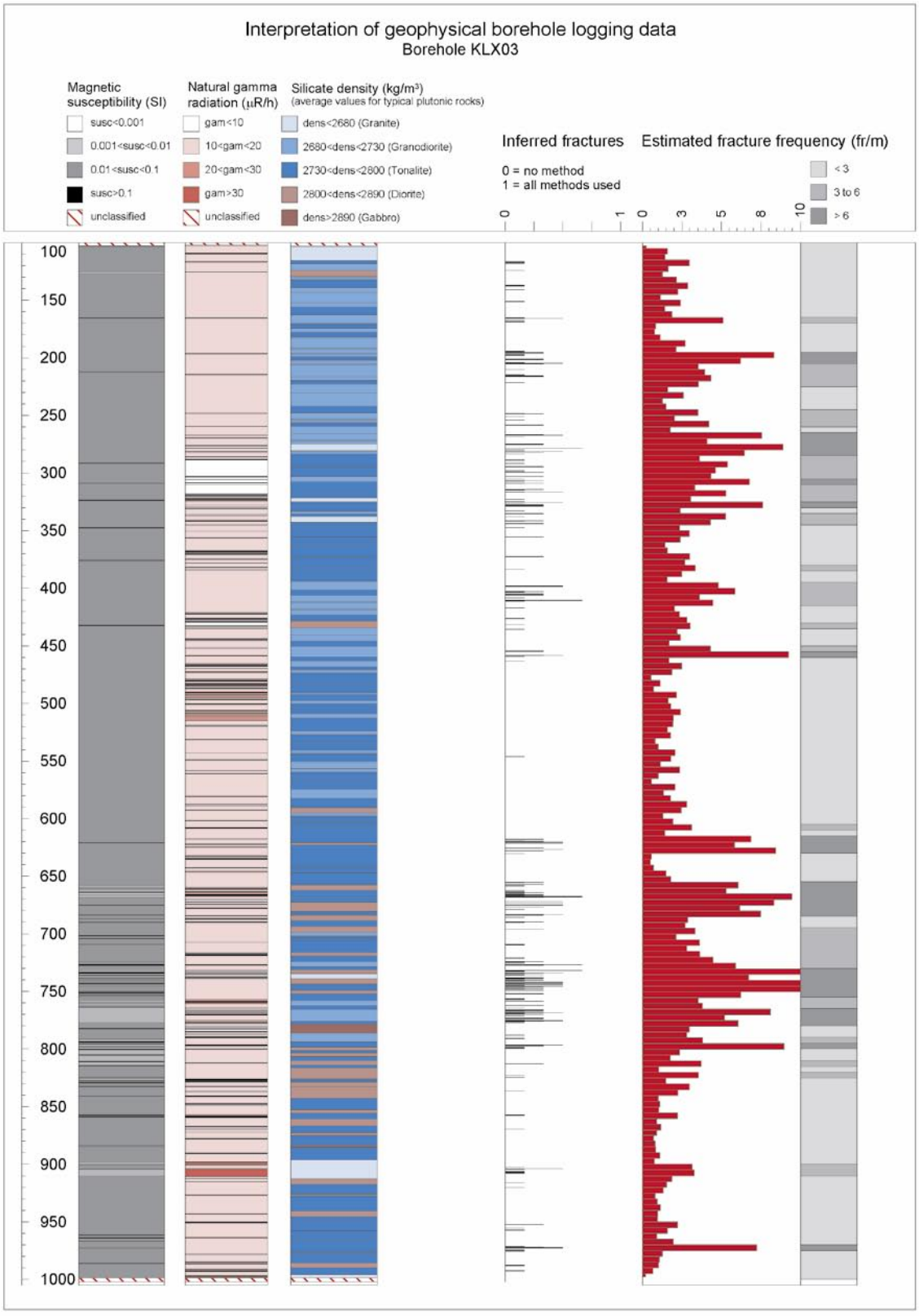

Figure 5-20. *Generalized geophysical logs of KLX03.*

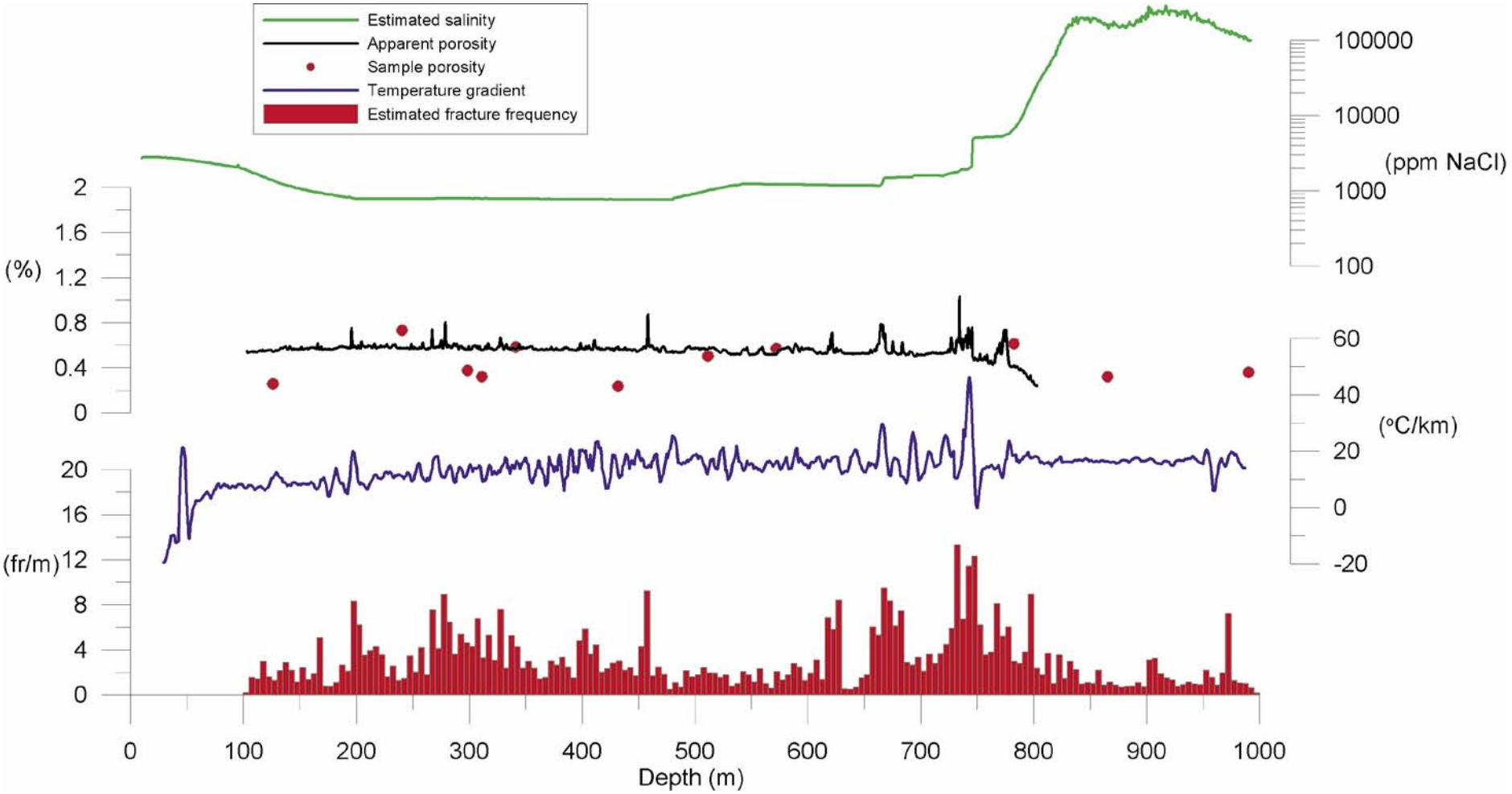

Figure 5-21. *Estimated salinity, apparent porosity, sample porosity, vertical temperature gradient and estimated fracture frequency of KLX03.*

Table 5-3. Distribution of silicate density classes with borehole length of KLX03.

Silicate density interval (kg/m^3)	Borehole length (m)	Relative borehole length (%)
dens < 2,680 (granite)	73	8
2,680 < dens < 2,730 (granodiorite)	268	30
2,730 < dens < 2,800 (tonalite)	415	46
2,800 < dens < 2,890 (diorite)	133	15
dens > 2,890 (gabbro)	7	1

5.4.3 Interpretation of KLX04

The results of the generalized logging data and fracture estimations of KLX04 are presented in Figure 5-22 below, and in a more detailed scale in Appendix 4.

As seen from Table 5-4 below the rocks in the vicinity of KLX04 are dominated by a silicate density in the interval 2,680–2,730 kg/m^3, corresponding to granodiorite mineral composition. The uppermost investigated section c 100–470 m is characterized by high natural gamma radiation and large fluctuations in the magnetic susceptibility. Along the following section, c 470–700 m, there is a general increase in the density and a corresponding decrease in the natural gamma radiation level, which indicates the occurrence of more mafic rocks compared to the uppermost section. Along this section the magnetic susceptibility keeps fairly constant at c 0.03–0.04 SI. The lowermost c 300 m of the borehole (section c 700–1,000 m) is dominated by silicate density in the interval 2,680–2,730 kg/m^3 that indicates a mineral composition corresponding to granodiorite rocks. The natural gamma radiation is low to moderate (< 20 μR/h) and the magnetic susceptibility is c 0.03–0.04 SI, except for the interval c 940–970 m which is dominated by low susceptibility (0.001–0.002 SI). Several positive natural gamma radiation anomalies occur along the entire borehole, and these correspond most likely to fine-grained granite or pegmatite dykes. Many of these occur close to high density anomalies, which suggests that felsic and mafic rocks often are related.

The fracture loggings indicate strongly increased fracturing along almost the entire section 100–450 m. Significant fracture anomalies occur in all geophysical logging methods along this section. A similar long section of strongly increased fracturing is identified at c 870–970 m borehole length. Minor sections (5–10 m) of increased fracturing also occur between 450 m and 870 m borehole length. The salinity log, apparent porosity log and the vertical temperature gradient log of KLX04 are shown together with the estimated fracture frequency in Figure 5-23. The general level of the porosity is most likely slightly overestimated but there are very distinct high porosity anomalies along the sections c 100–450 m and 870–980 m. The porosity anomalies coincide with a number of well defined anomalies in the vertical temperature gradient log, which suggests that several of the indicated fractures are water bearing.

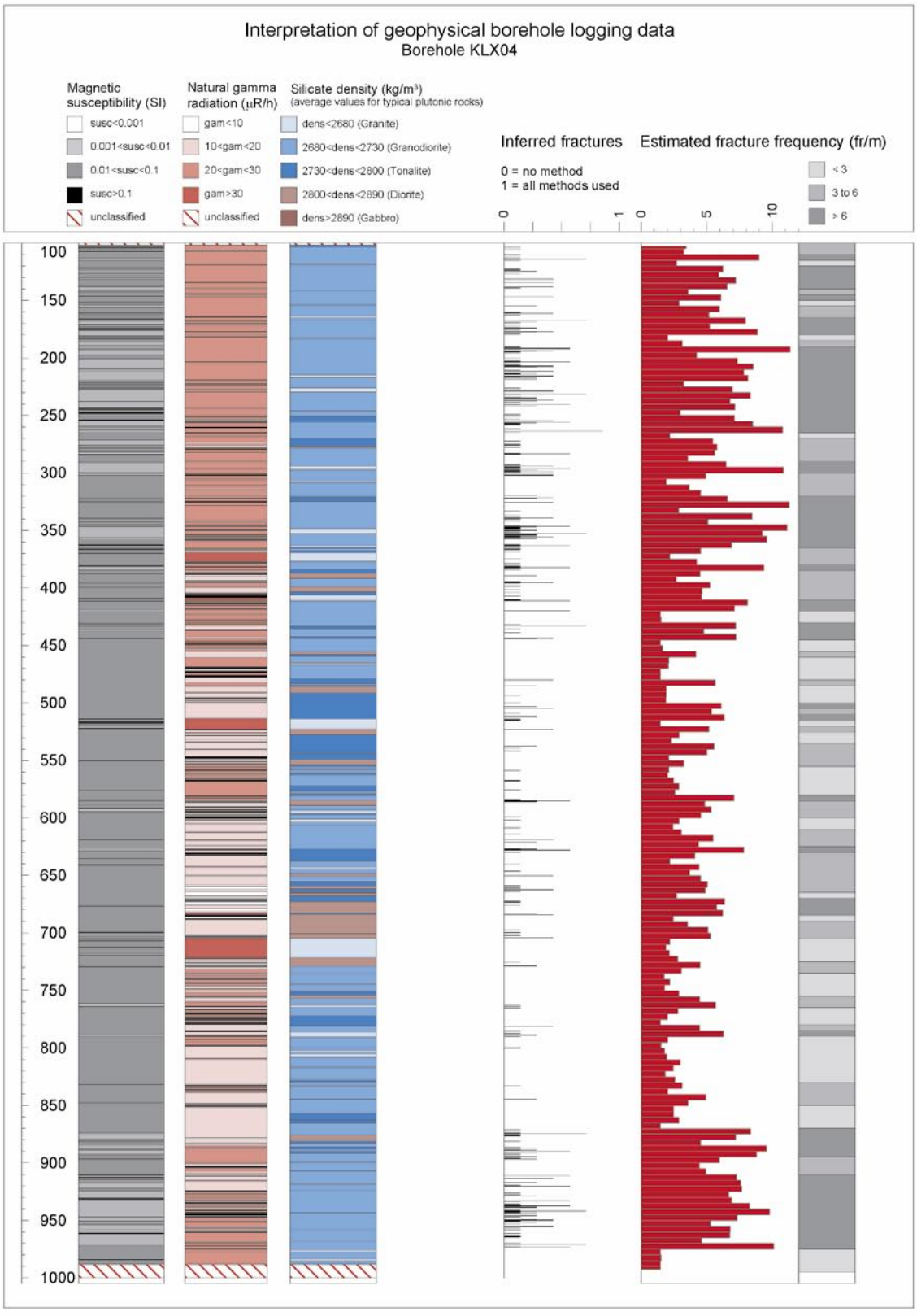

Figure 5-22. *Generalized geophysical logs of KLX04.*

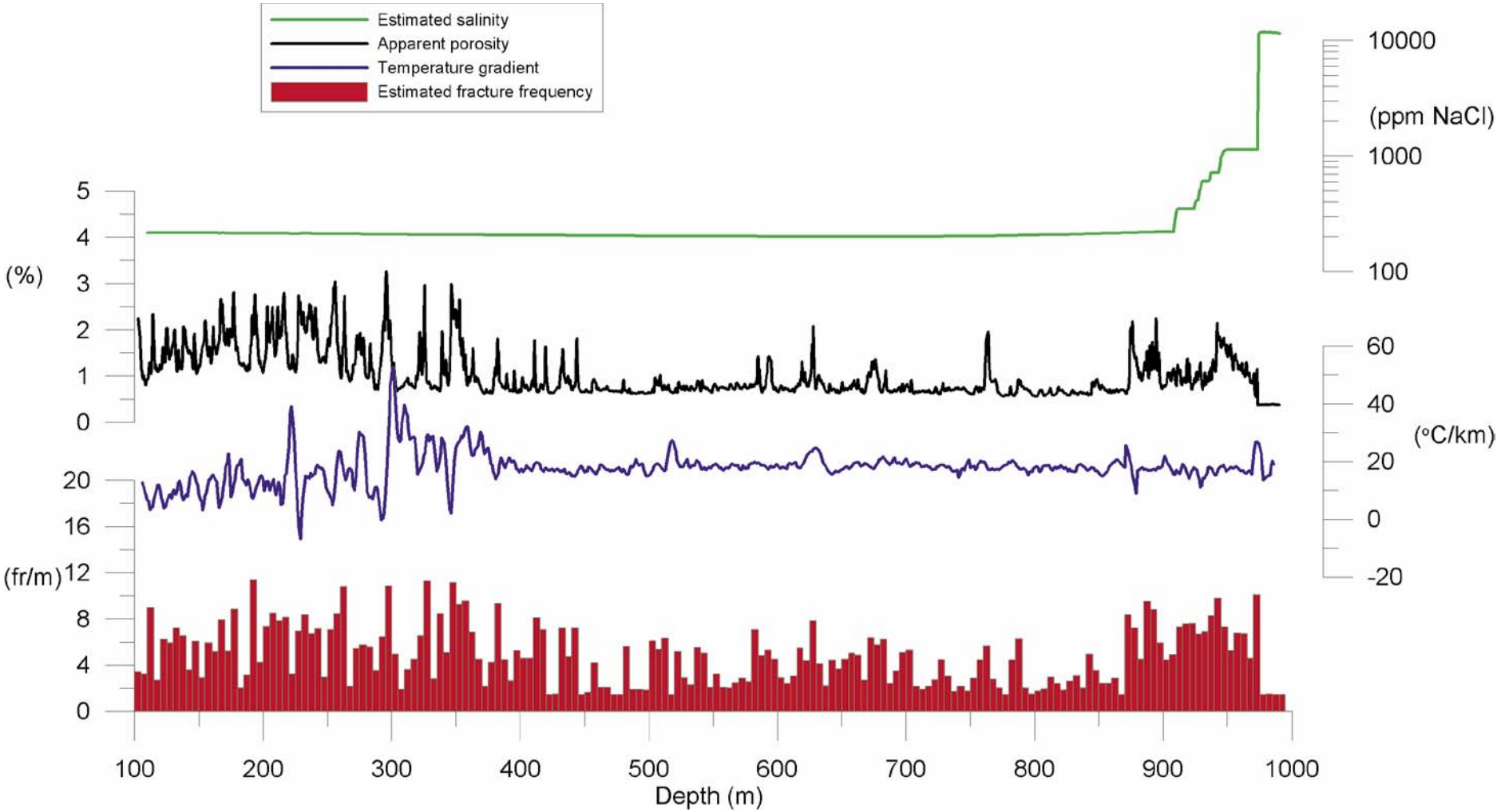

Figure 5-23. *Estimated salinity, apparent porosity, vertical temperature gradient and estimated fracture frequency of KLX04.*

Table 5-4. Distribution of silicate density classes with borehole length of KLX04.

Silicate density interval (kg/m³)	Borehole length (m)	Relative borehole length (%)
dens<2,680 (granite)	157	17.5
2,680<dens<2,730 (granodiorite)	478	54
2,730<dens<2,800 (tonalite)	174	20
2,800<dens<2,890 (diorite)	72	8
dens > 2,890 (gabbro)	4	0.5

5.4.4 Interpretation of HLX21

The results of the generalized logging data and fracture estimations of HLX21 are presented in Figure 5-24 below.

The rocks in the vicinity of HLX21 are dominated by silicate density < 2,680 kg/m^3, which indicates a mineral composition that corresponds to granite. A slight increase in the density occurs along the section c 55–80 m. The natural gamma radiation is fairly high in the entire borehole, and sometimes it is very high (> 35 μR/h). The short sections with very high natural gamma radiation most likely correspond to pegmatite or fine-grained granite. Along the upper c 10–110 m the magnetic susceptibility keeps at a low level, c 0.002 SI, and at c 110 m borehole length there is a sharp increase in the susceptibility level up to c 0.01 SI, which is kept through out the remaining part of the borehole.

The estimated fracture frequency is moderate to high along the section 10–110 m, and low from 110 m to 145 m. Possible deformation zones are indicated at the borehole sections c 10–30 m and 80–100 m. There are several large negative resistivity anomalies and major caliper anomalies along these two sections.

5.4.5 Interpretation of HLX22

The results of the generalized logging data and fracture estimations of HLX22 are presented in Figure 5-25 below.

The rocks in the vicinity of HLX22 are dominated by silicate density < 2,680 kg/m^3 (corresponding to granite composition) along the section c 10–100 m and 2,680–2,730 kg/m^3 (corresponding to granodiorite composition) along the lower 100–160 m of the borehole. The natural gamma radiation is moderate to high in the entire borehole, generally varying between 20 μR/h and 30 μR/h, and sometimes it is higher. The short sections with high natural gamma radiation most likely correspond to pegmatite or fine-grained granite. The magnetic susceptibility is low (< 0.002 SI) along the sections c 10–50 m and c 105–125 m. The section c 50–105 m is dominated by a magnetic susceptibility of c 0.01–0.02 SI.

The estimated fracture frequency is generally moderate or low. General decreasing resistivity levels occur at c 40–50 m and 100–120 m, but there are no major corresponding anomalies in the caliper or sonic data. These low resistivity section most likely indicate rock alteration and or plastic deformation zones.

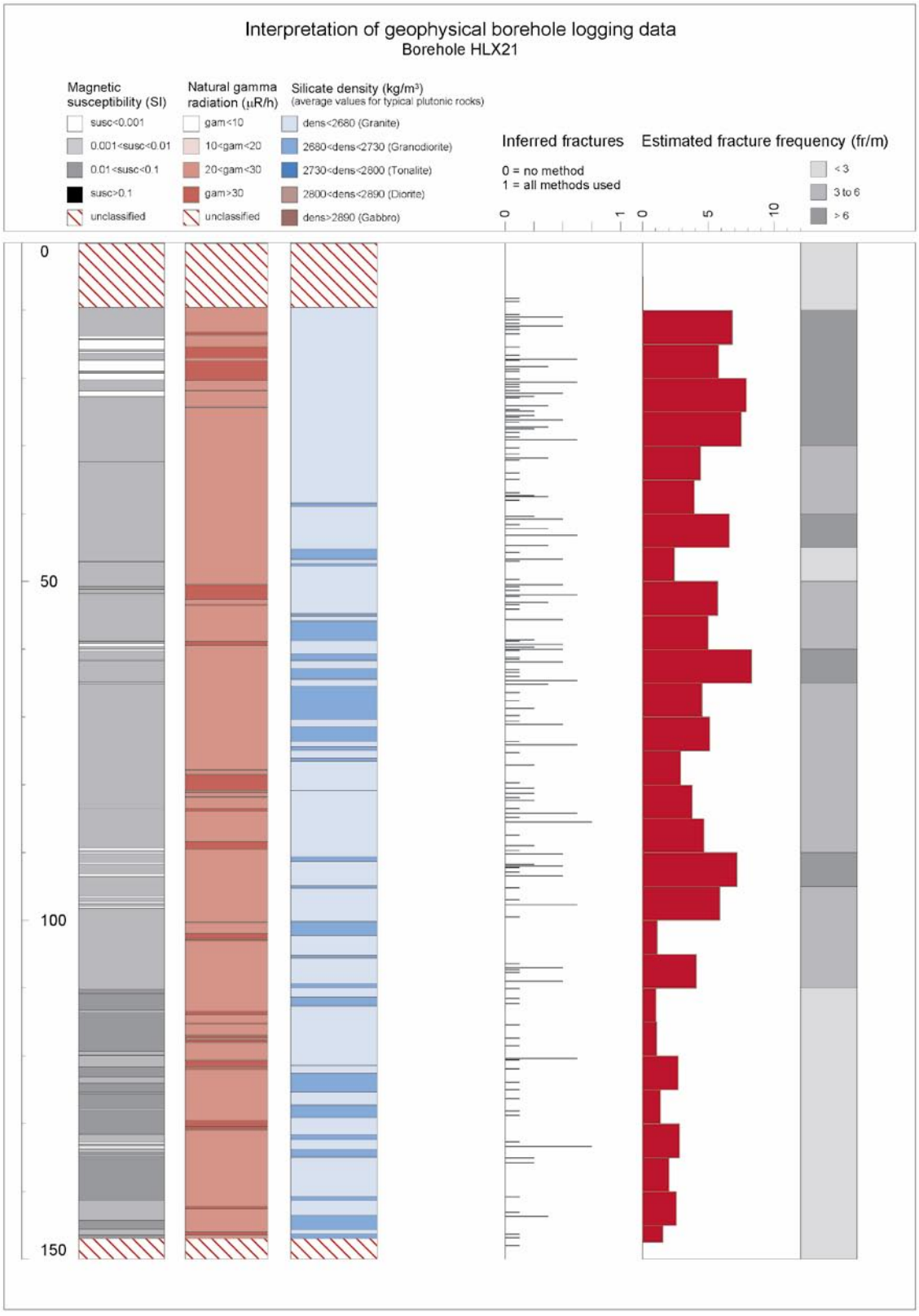

Figure 5-24. *Generalized geophysical logs of HLX21.*

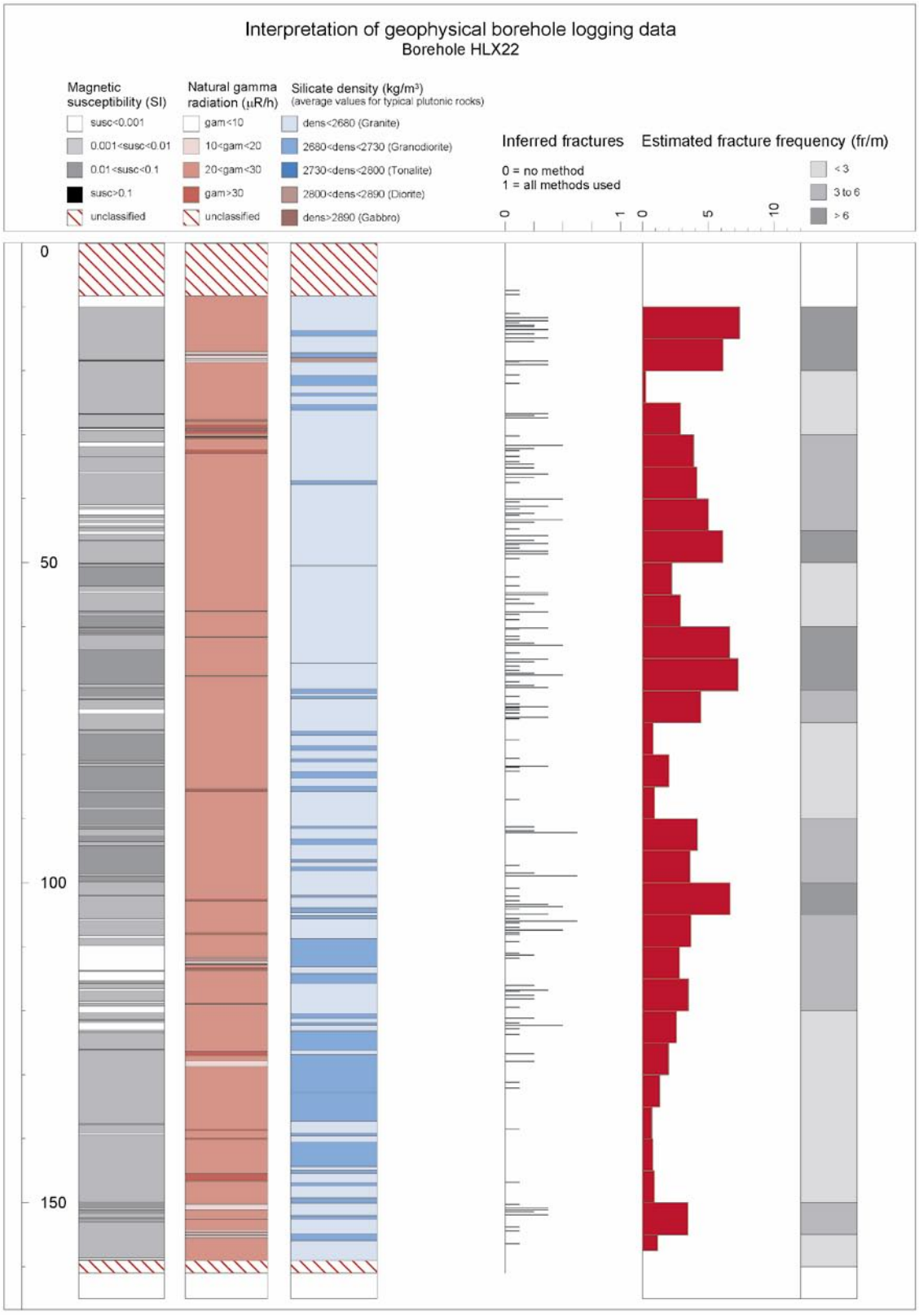

Figure 5-25. *Generalized geophysical logs of HLX22.*

5.4.6 Interpretation of HLX23

The results of the generalized logging data and fracture estimations of HLX23 are presented in Figure 5-26 below.

The rocks in the vicinity of HLX23 are completely dominated by silicate density < 2,680 kg/m^3, which indicates a mineral composition that corresponds to granite. Several short sections of higher density occur along the entire borehole. The natural gamma radiation is in general moderate to high, with a section of slightly lower radiation intensity at c 55–95 m. The magnetic susceptibility is mainly above 0.01 SI, apart from two low magnetic sections at c 10–35 m and 70–90 m.

The estimated fracture frequency is generally moderate or low. The section c 45–90 m has moderate to high estimated fracture frequency, indicated by numerous low resistivity, low sonic velocity and caliper anomalies. The data indicate a possible deformation zone. Note that this section broadly coincides with the low natural gamma radiation reported above.

5.4.7 Interpretation of HLX24

The results of the generalized logging data and fracture estimations of HLX24 are presented in Figure 5-27 below.

The rocks in the vicinity of HLX24 are dominated by silicate density < 2,680 kg/m^3, which indicates a mineral composition that corresponds to granite. Several short sections of slightly higher density occur along the entire borehole, and at two sections (53–56 m and 142–146.5 m) the density is significantly higher, most likely indicating the occurrence of diorite to gabbro rocks. Along both these sections the magnetic susceptibility and the natural gamma radiation levels are decreased. The natural gamma radiation is in general moderate to high, averaging at c 20 μR/h, and the magnetic susceptibility is low along the uppermost c 40 m of the borehole, and mainly moderate along the remaining part except for a large minimum at 139–146.5 m. At the lower end of the lower high density anomaly (borehole length c 146.5 m) there is a major positive natural gamma radiation anomaly, which indicates a spatial relation between the mafic and felsic rocks.

The estimated fracture frequency indicates increased fracturing and possible deformation zones along the sections c 24–42 m and c 53–80 m. These sections are characterized by numerous low resistivity, low sonic velocity and caliper anomalies.

Figure 5-26. *Generalized geophysical logs of HLX23.*

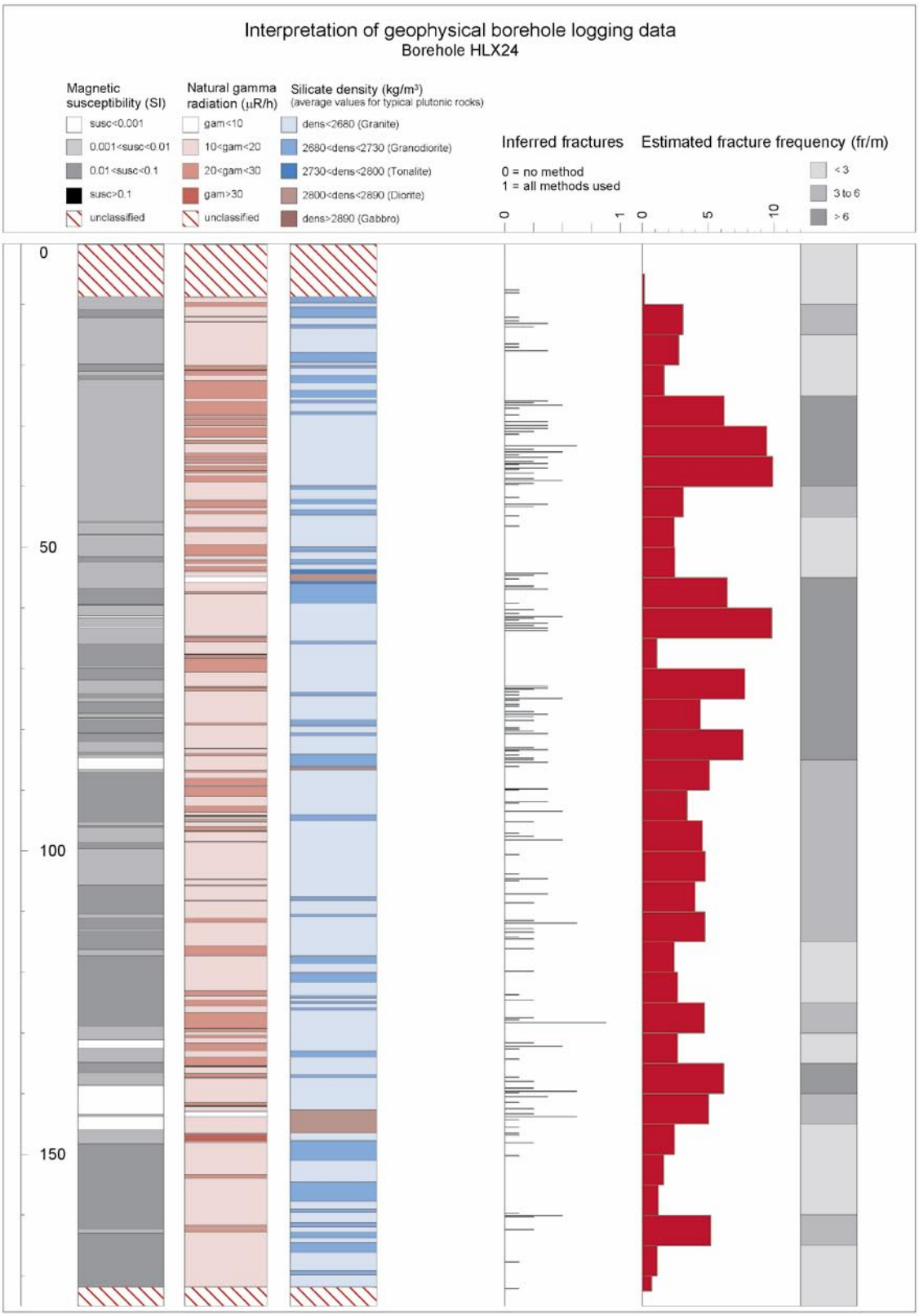

Figure 5-27. *Generalized geophysical logs of HLX24.*

5.4.8 Interpretation of HLX25

The results of the generalized logging data and fracture estimations of HLX25 are presented in Figure 5-28 below.

The rocks in the vicinity of the uppermost c 100 m of HLX25 (section 10–110 m) are characterized by silicate density < 2,680 kg/m^3, which indicates a mineral composition that corresponds to granite. Along this section the natural gamma radiation level is moderate, averaging at c 20 µR/h. A few short sections of slightly higher density occur along this part of the borehole. Along the lower 110–200 m the silicate density is significantly higher, indicating a large occurrence of diorite to gabbro rocks, and consequently the natural gamma radiation is significantly lower compared to the upper part. The magnetic susceptibility is generally low (0.001–0.004 SI) at the sections c 20–80 m and 145–180 m, and > 0.01 SI at c 80–145 m and c 180–200 m.

The estimated fracture frequency indicates increased fracturing and possible deformation zones along the sections c 40–50 m, c 65–75 m and c 165–185. These sections are characterized by several low resistivity, low sonic velocity and caliper anomalies.

5.4.9 Interpretation of HLX26

The results of the generalized logging data and fracture estimations of HLX26 are presented in Figure 5-29 below.

The rocks in the vicinity of HLX26 are characterized by silicate density in the interval of 2,730–2,800 kg/m^3, which indicates a mineral composition that corresponds to tonalite. Minor occurrences of low density rocks are also indicated in the borehole. The natural gamma radiation is mainly low (< 20 µR/h) but there are several narrow high radiation anomalies along the entire borehole length, and these most likely indicate the presence of pegmatite and/or fine-grained granite. The magnetic susceptibility is generally moderate to high (0.01–0.02 SI). Significant low magnetization occurs along the section c 13–22 m and minor decrease in the magnetic susceptibility is seen along the section c 48–100 m.

The estimated fracture frequency indicates increased fracturing and a possible deformation zone along the sections c 30–70 m. The section is characterized by several low resistivity, low P-wave velocity and caliper anomalies.

5.4.10 Interpretation of HLX27

The results of the generalized logging data and fracture estimations of HLX27 are presented in Figure 5-30 below.

The rocks in the vicinity of HLX27 are characterized by silicate density in the interval of 2,730–2,800 kg/m^3, which indicates a mineral composition that corresponds to tonalite. Minor occurrences of lower and higher densities also occur in the borehole. The natural gamma radiation is mainly low (< 10 µR/h) but there are several narrow high radiation anomalies along the entire borehole length, and these most likely indicate the presence of pegmatite and/or fine-grained granite. The magnetic susceptibility is moderate to high (0.01–0.02 SI) along the section c 6–115 m, and low magnetization (< 0.001 SI) occurs along large parts of the section c 115–160 m.

The estimated fracture frequency indicates low or moderate fracturing, and no possible deformation zone is identified.

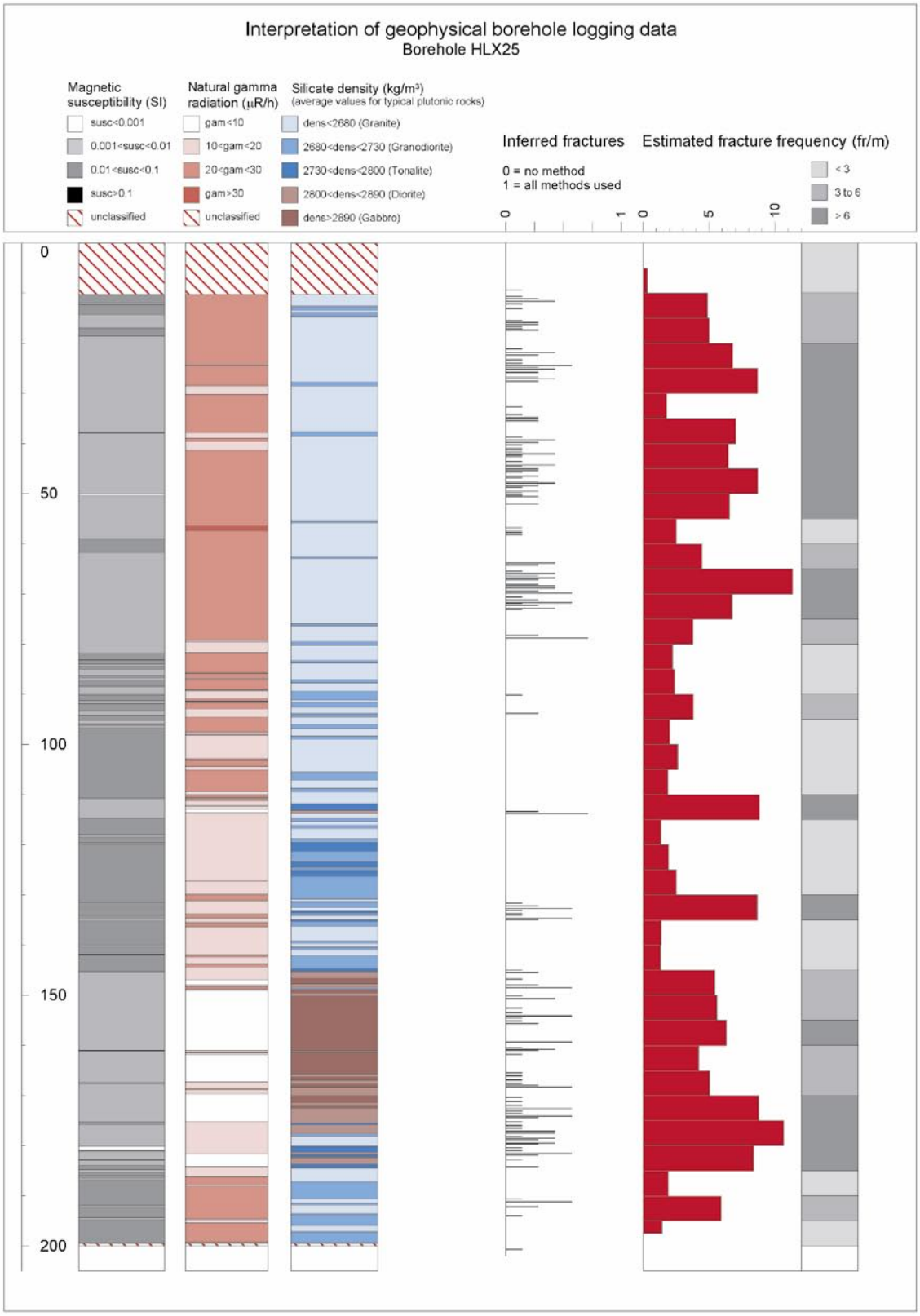

Figure 5-28. *Generalized geophysical logs of HLX25.*

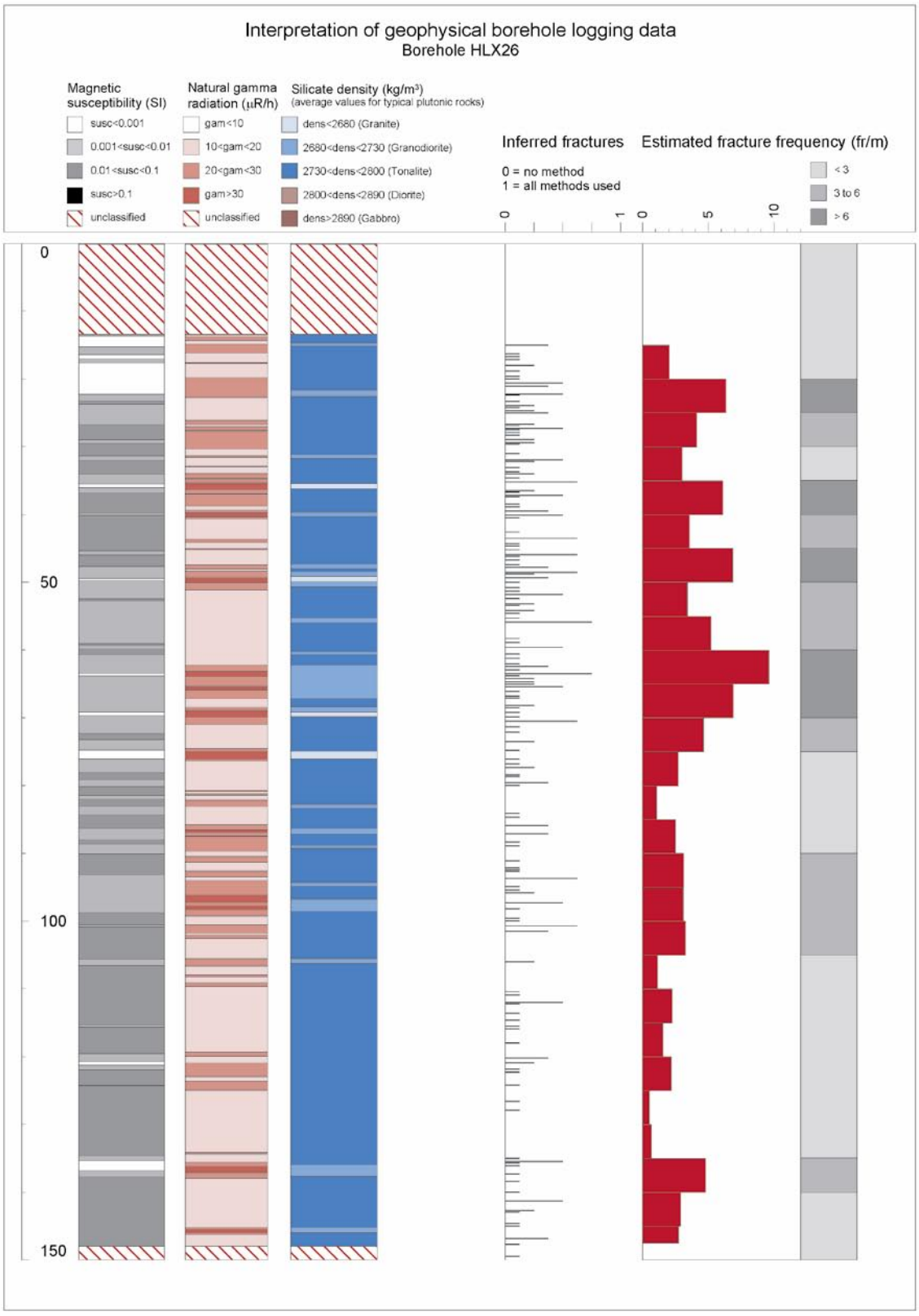

Figure 5-29. *Generalized geophysical logs of HLX26.*

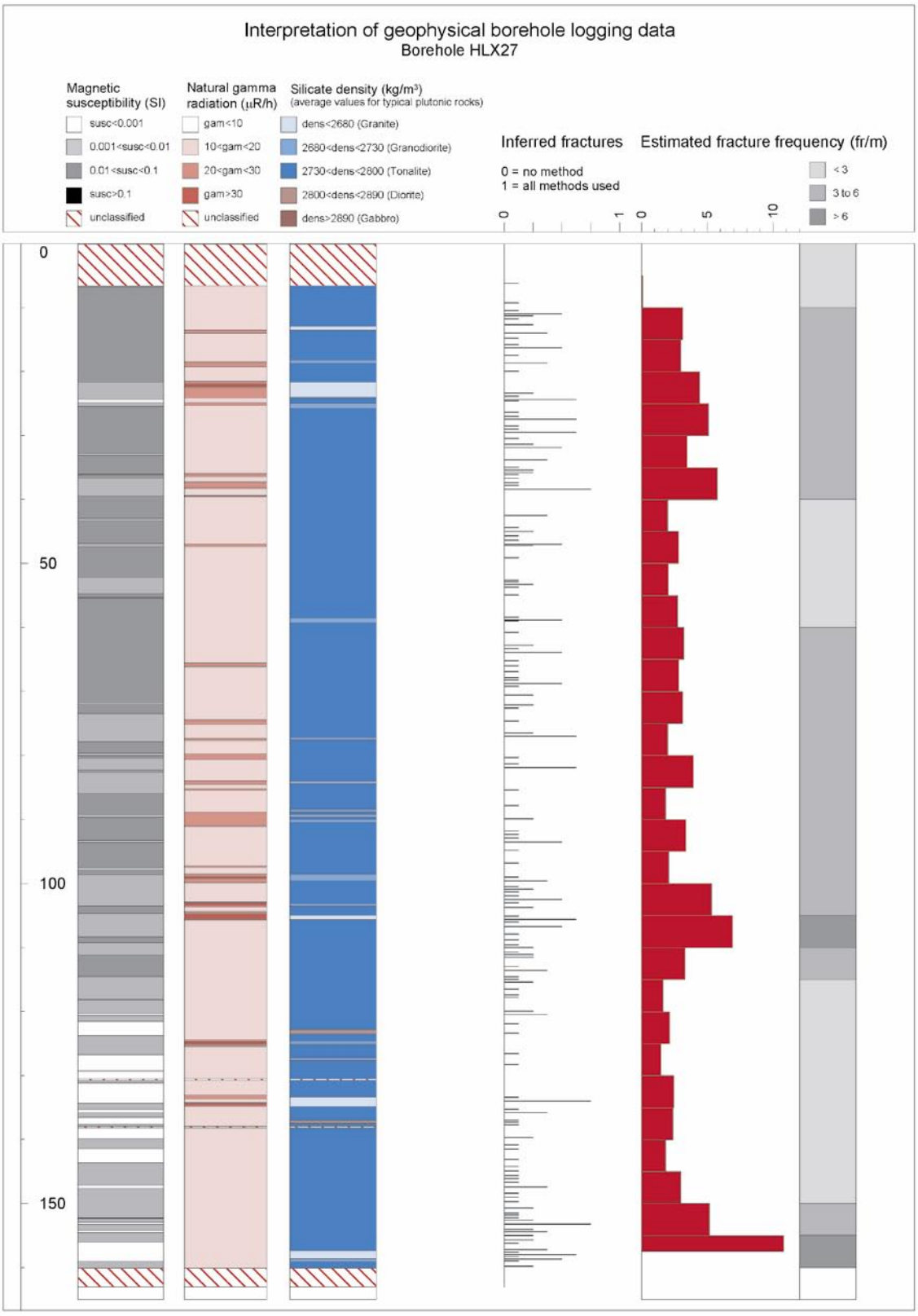

Figure 5-30. *Generalized geophysical logs of HLX27.*

5.4.11 Interpretation of HLX28

The results of the generalized logging data and fracture estimations of HLX28 are presented in Figure 5-31 below.

The rocks in the vicinity of HLX28 are characterized by silicate density in the interval of 2,730–2,800 kg/m^3, which indicates a mineral composition that corresponds to tonalite. Minor occurrences of lower and higher densities also occur in the borehole. The natural gamma radiation is mainly moderate or low (< 20 μR/h) but there are several narrow high radiation (and corresponding low magnetic) anomalies along the entire borehole length, and these most likely indicate the presence of pegmatite and/or fine-grained granite. The magnetic susceptibility is generally moderate to high (0.01–0.02 SI) along the entire borehole.

The estimated fracture frequency indicates moderate fracturing. A possible deformation zone is distinctly indicated along the section c 77–88 m. The section is characterized by several low resistivity, low P-wave velocity and caliper anomalies.

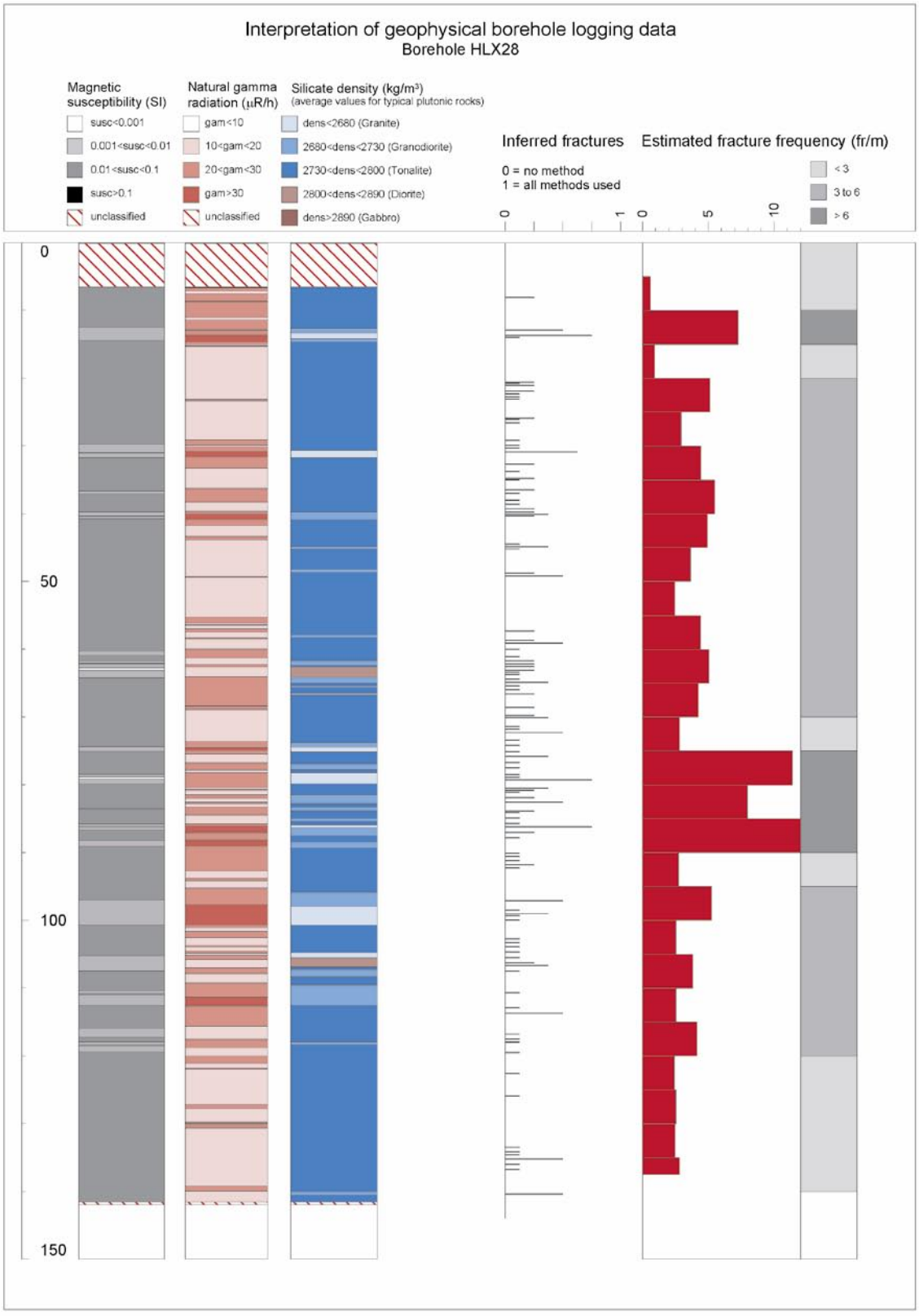

Figure 5-31. *Generalized geophysical logs of HLX28.*

6 Summary and discussions

This investigation of physical properties of the rocks in the vicinities of the cored boreholes KLX01, KLX03 and KLX04 (Figure 6-1), and the percussion drilled boreholes HLX21–28, shows that there are dominant occurrences of rocks with silicate density that indicates a mineral composition corresponding to that of tonalite in KLX03 and in HLX26–28. These four boreholes are located in, or close to, the large quartz monzodiorite rock unit in the southern part of the Laxemar area. In the boreholes KLX01, KLX04 and HLX21–25, in the central part of the Laxemar area, there is a clear dominance of more low density rocks. The silicate density of the rocks in the vicinity of KLX01 and KLX04 mainly indicates a mineral composition corresponding to granodiorite (Figure 6-2), and in HLX21–25 there is a clear dominance of even lower densities, mainly indicating granitic mineral composition. Silicate densities indicating diorite to gabbro rocks are evenly distributed in the three cored boreholes, and they constitute c 10–15% of the total borehole length (Figure 6-2). Such high densities are rare in the percussion drilled boreholes, except for a c 30 m long section of HLX25.

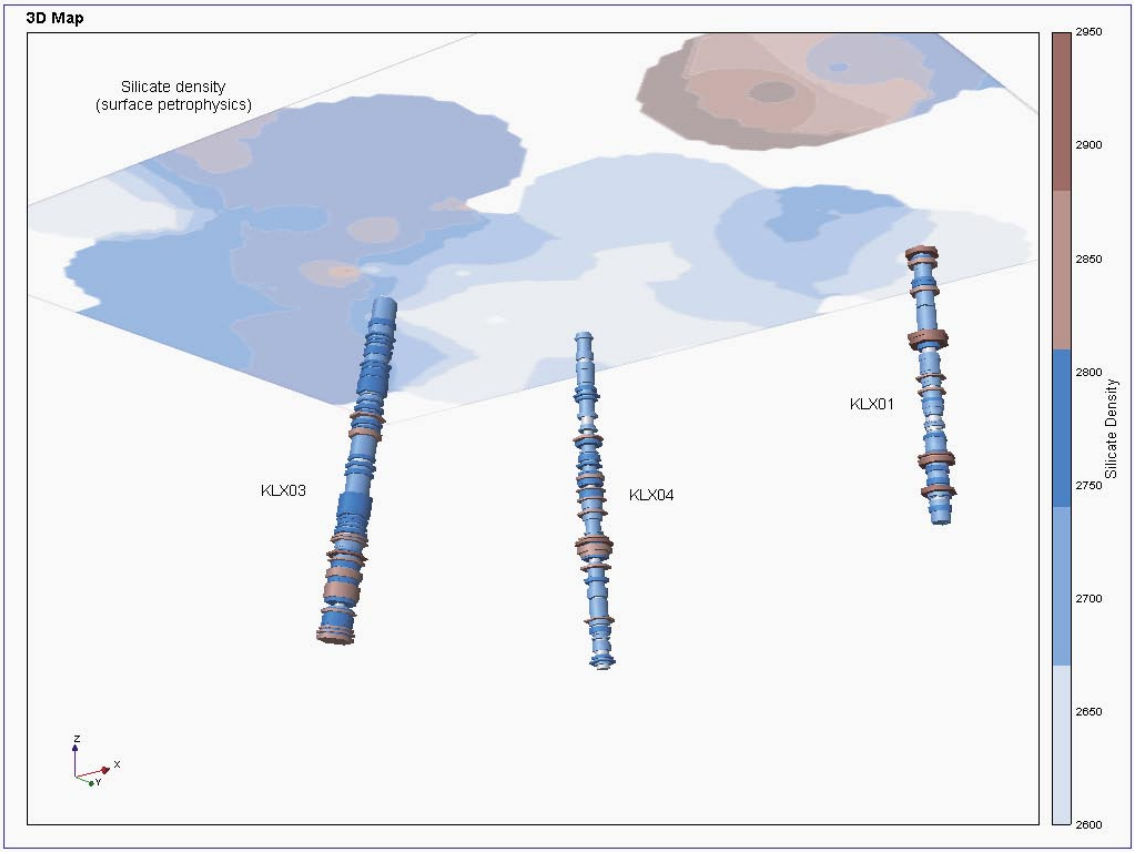

Figure 6-1. *3D visualisation of the silicate density distribution in KLX01, KLX03 and KLX04 (view from southeast). The top surface displays the silicate density distribution from petrophysical surface measurements from samples taken from bedrock outcrops.*

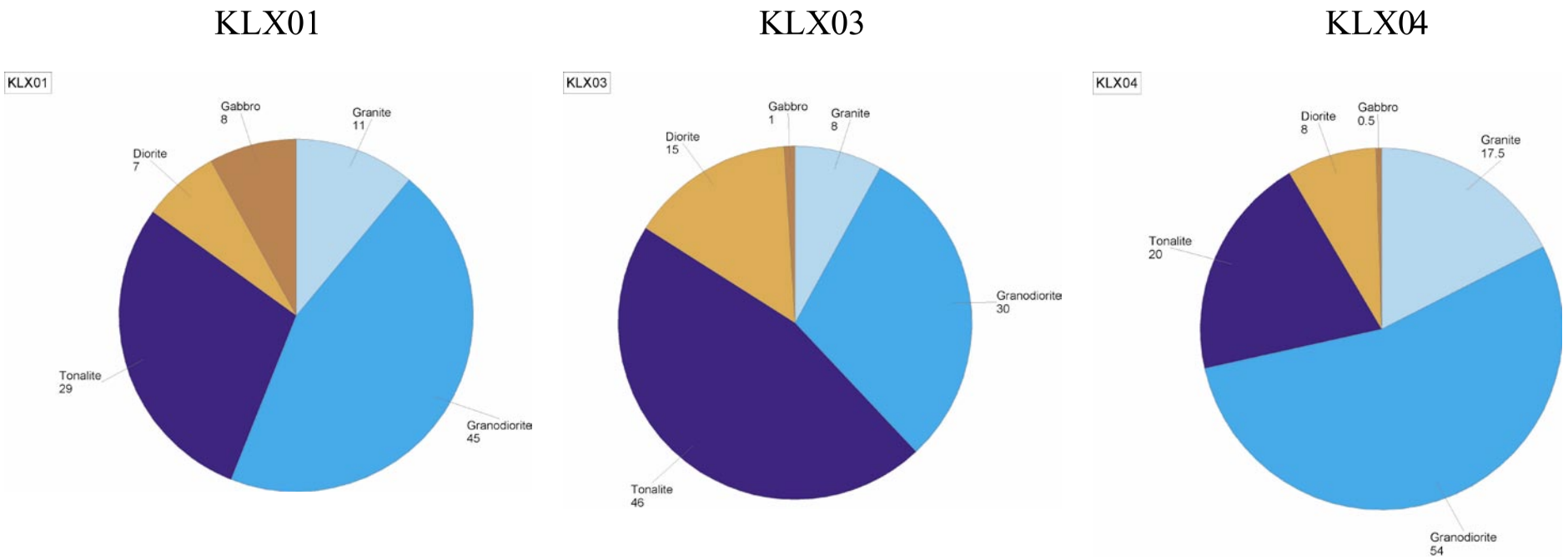

Figure 6-2. *Pie diagrams showing distribution in percent of the entire borehole length of rock types as indicated by silicate density logging data from the three cored boreholes KLX01, KLX03 and KLX04. The indicated rock types originate from /8/.*

The natural gamma radiation in KLX04 is significantly higher along the section c 100–400 m compared to the corresponding sections in KLX01 and KLX03 (the three cored boreholes dip fairly steep so the borehole length is fairly close to the actual depth). Along the section c 400–700 m the radiation levels in KLX01 and KLX04 are comparable and slightly higher than along the corresponding section of KLX03. In the interval 700–1,000 m the radiation level is clearly higher in KLX04 compared to that of KLX03 (there are no logging data below 700 m section length in KLX01). Low, or moderate, natural gamma radiation levels (< 25 μR/h) are also found in HLX26–28 (located in the vicinity of KLX03), whereas the natural gamma radiation levels of HLX21–23 and HLX25 are mainly moderate to high (> 25 μR/h). The natural gamma radiation in HLX24 is mainly low. Short sections of very high natural gamma radiation, generally with corresponding low density, occur in all boreholes, though least commonly in KLX03. The anomalies most likely indicate occurrences of fine-grained granite dykes. Many of the high natural gamma radiation anomalies in KLX01 and KLX04 have adjacent high density anomalies (and low gamma radiation), which suggests that felsic and mafic rocks (probably dykes or enclaves) often are spatially related.

The highest magnetisations in the cored boreholes are found in KLX03, but the general susceptibility level of supposedly fresh rock in KLX01 and KLX04 (0.02–0.05 SI) is comparable to that of KLX03 (0.04 SI). However, the magnetic susceptibility of the rocks along sections that have suffered from deformation and/or alteration, e.g. c 100–350 m of KLX04, is significantly lower. The percussion drilled boreholes are most often directed through a possible deformation zone, and this reflects the magnetisation level in these boreholes. The magnetic susceptibility of HLX21–28 broadly varies between 0.005 SI and 0.015 SI, which in average is about 3–4 times lower than the susceptibility in the cored boreholes.

The estimated fracture frequency of KLX01 is generally low, and partly moderate. However, there are four fairly large and distinct fracture anomalies that coincide with increased porosity and they also occur close to major anomalies in the fluid temperature gradient log, which suggest that they are water bearing.

In KLX03 increased fracture frequencies (possible deformation zones) are indicated in the sections c 260–320 m, 615–630 m, 655–685 m and 725–780 m. However, the sections are mainly characterized by low resistivity anomalies and only partly decreased P-wave velocity, which may indicate that the suggested deformations zones are dominated by plastic deformation and/or alteration, and that open fractures are less common. One exception occurs along the section c 720–780 m where the apparent porosity is high and there are also several distinct anomalies in the vertical temperature gradient log that indicate the presence of water bearing fractures. This interpretation of the geophysical fracture frequency is supported when comparing it to the fracture mapping reported from the Boremap investigations (Figure 6-3). The open fracture frequency of KLX03 is generally low in the entire borehole, whereas the sealed fracture frequency varies, and it is fairly high along certain sections (Figure 6-3a). The diagrams in the figure clearly show that there is a good co-variation between the mapped fracture frequency (open + sealed) and the geophysical estimation. It is also evident that the geophysical estimation is heavily influenced by sealed fractures, most likely since sealed fractures are filled with clay minerals (e.g. chlorite) and often coincide with zones of mineral oxidation, which is often associated with a lowering of the electric resistivity of the rock. The underestimation of the geophysical fracture frequency along

a)

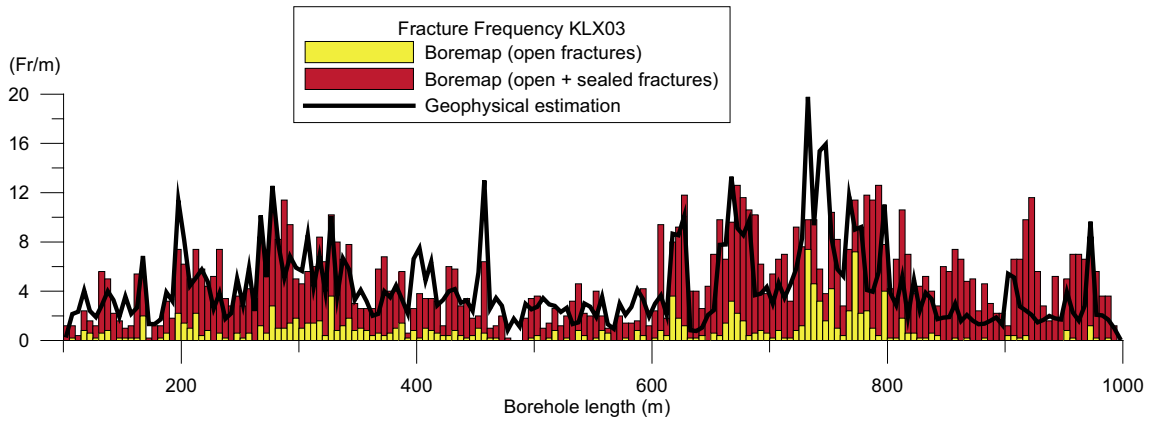

b)

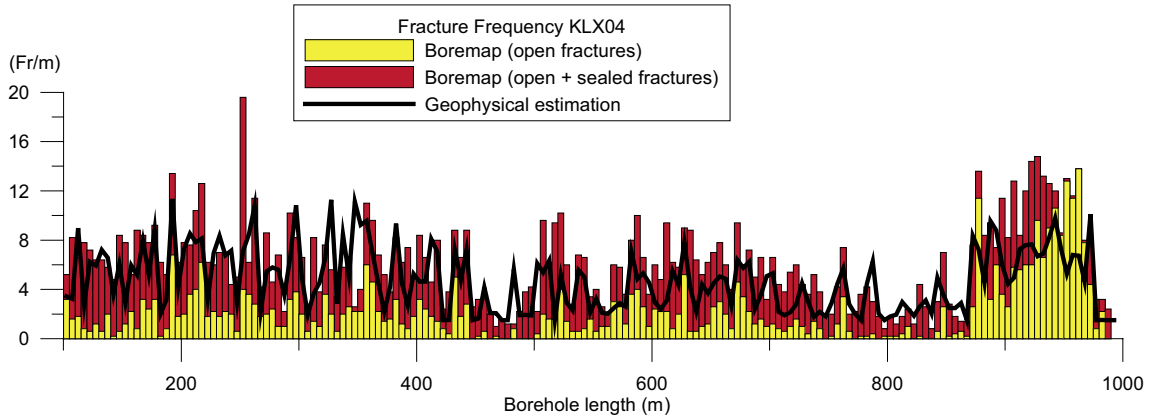

Figure 6-3. *Fracture frequency estimated from geophysical loggings compared to geological mapping data for a) KLX03 and b) KLX04.*

745–1,000 m borehole length is caused by a major increase in the borehole fluid salinity at 745 m section coordinate, most likely related to a water bearing fracture as indicated by the fluid temperature data. The salinity increase decreases the amplitude variations in the resistivity logs from 745 m to 1,000 m, which has a significant effect on the geophysical fracture estimation.

Large sections of the rocks in the vicinity of KLX04 seem to have been affected by deformation. The geophysical fracture loggings indicate strongly increased fracturing along major parts of the section 100–450 m. Significant fracture anomalies occur in all geophysical logging methods along this section (including the sonic and caliper logs). A similar long section of strongly increased fracturing is indicated at c 870–970 m borehole length. There are distinct high porosity anomalies along the sections c 100–450 m and 870–980 m and they coincide with a number of well defined anomalies in the vertical temperature gradient log, which suggests that several of the indicated fractures are water bearing. The geophysical fracture estimation of KLX04 generally agrees well with the mapped fracture frequency (open + sealed fractures), even though there is a slight underestimation in the geophysical estimation of the deformation zone in the bottom of the borehole (Figure 6-3b).

Since percussion drilled boreholes are generally located close to lineaments in geophysical or topographical data, possible deformation zones are often identified in these boreholes. In general, one or two possible deformation zones are indicated in each of the investigated boreholes HLX21–28, apart from HLX27 in which there are only minor indications of increased fracturing.

The petrophysical data compiled from KLX01 and KLX03 generally agrees well with corresponding data from samples collected on bedrock outcrops on the surface. The average density of fresh Ävrö granite in KLX01 is 2,740 ± 37 kg/m^3 (44 samples) and in KLX03 it is 2,756 ± 16 kg/m^3 (6 samples). These average values are high compared to the average density of the Ävrö granite on the surface, which is 2,690 ± 24 kg/m^3, and this is a clear indication that the mineral composition of the Ävrö granite in the vicinity of KLX01 and KLX03 differs from the general distribution on the surface. One quartz monzodiorite sample in KLX03 (depth = 782.47 m) has a density of 2,941 kg/m^3 and appears to have been incorrectly classified. The rock sample should most likely belong to the diorite to gabbro rock type group. AMS (magnetc fabric) measurements on the samples from KLX03 show that degree of anisotropy is moderate or low for a majority of the samples, which suggests that these rocks are primary or only slightly deformed. There is a clear negative correlation between the degree of anisotropy and the dip of the magnetic foliation and this indicates that the rock fabric rotates from subvertical to subhorizontal with increasing degree of strain.

In conclusion, the investigation presented in this report shows that there are large variations in several physical properties of the rocks in KLX03 (incl. HLX26–28) compared to KLX01 and KLX04 (incl. HLX21–25), especially regarding the rock type Ävrö granite. In Figure 6-4 below histograms of silicate density, natural gamma radiation and magnetic susceptibility are displayed, covering c 500 m section length (or c 5,000 measurement points) classified as Ävrö granite, from each of KLX03 and KLX04. The corresponding average values are presented in Table 6-1. The results clearly indicate major compositional variations in the Ävrö granite.

Table 6-1. Average value and corresponding standard deviation of silicate density, natural gamma radiation and magnetic susceptibility for the rock type Ävrö granite in KLX03 and KLX04.

Property	Ävrö granite KLX03	Ävrö granite KLX04
Silicate density (kg/m^3)	2,729 ± 39	2,702 ± 27
Natural gamma radiation (μR/h)	14 ± 4	22 ± 5
Magnetic susceptibility (log 10^{-5} SI)	3.62 ± 0.13	3.19 ± 0.44

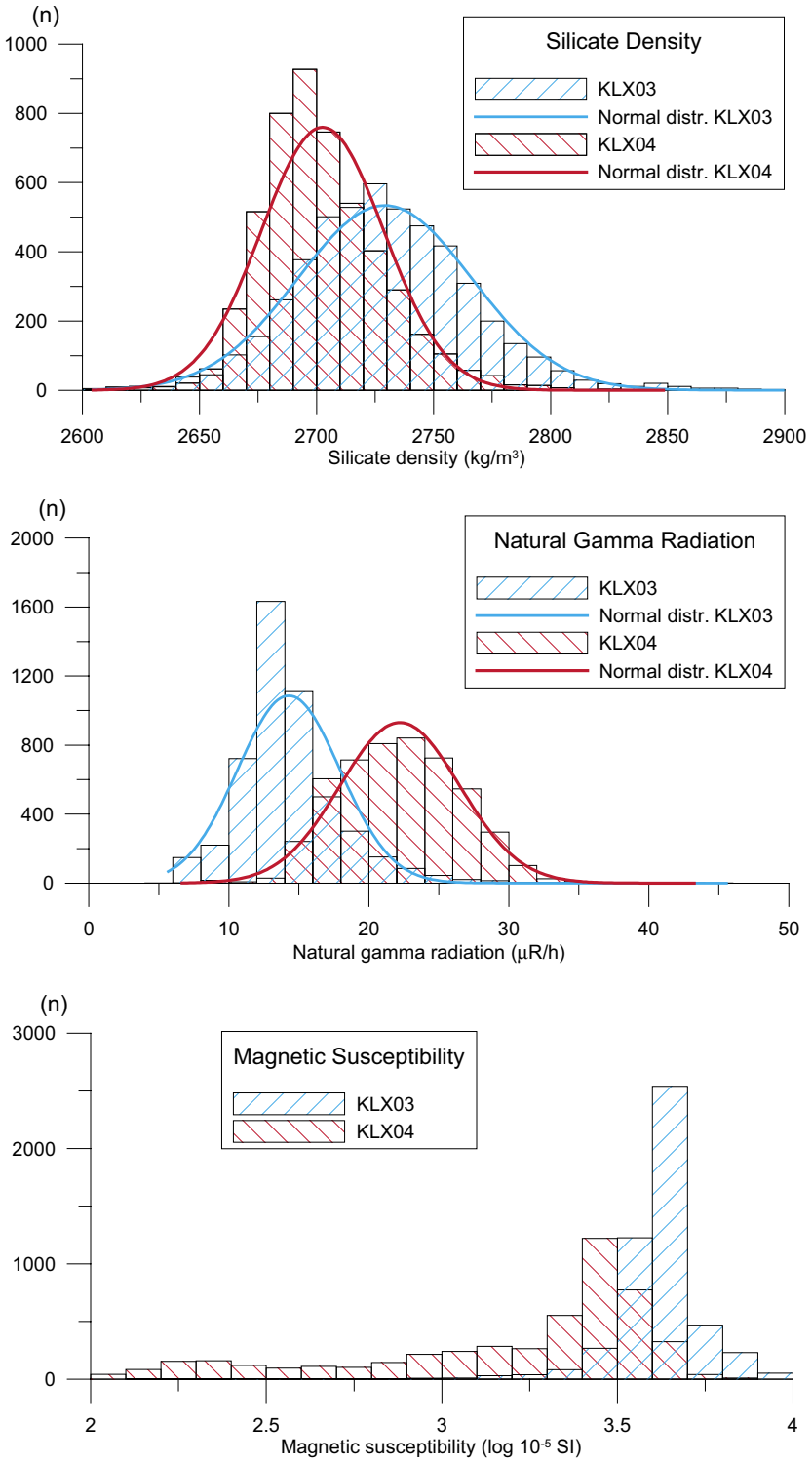

Figure 6-4. *Histograms of silicate density, natural gamma radiation and magnetic susceptibility for sections classified as Ävrö granite in KLX03 and KLX04.*

References

/1/ **Nisca D H, 1988.** Geophysical laboratory measurements on core samples from KLX01, Laxemar and KAS02, Äspö. SKB Progress report 25-88-06, Svensk Kärnbränslehantering AB.

/2/ **Mattsson H, Thunehed H, 2003.** Measurements of petrophysical parameters on rock samples during autumn 2002. SKB P-03-19, Svensk Kärnbränslehantering AB.

/3/ **Mattsson H, Thunehed H, 2004.** Interpretation of geophysical borehole data from KSH01A, KSH01B, KSH02 (0–100 m), HSH01, HSH02 and HSH03, and compilation of petrophysical data from KSH01A and KSH01B. SKB P-04-28, Svensk Kärnbränslehantering AB.

/4/ **Mattsson H, Thunehed H, 2004.** Interpretation of geophysical borehole data and compilation of petrophysical data from KSH02 (80–1,000 m) and KAV01. SKB P-04-77, Svensk Kärnbränslehantering AB.

/5/ **Mattsson H, 2004.** Interpretation of geophysical borehole data and compilation of petrophysical data from KSH03A (100–1000 m), KSH03B, HAV09, HAV10 and KLX02 (200–1,000 m). SKB P-04-214, Svensk Kärnbränslehantering AB.

/6/ **Mattsson H, 2004.** Interpretation of geophysical borehole data and compilation of petrophysical data from KAV04A (100–1000 m), KAV04B, HLX13 and HLX14. SKB P-04-217, Svensk Kärnbränslehantering AB.

/7/ **Henkel H, 1991.** Petrophysical properties (density and magnetization) of rock from the northern part of the Baltic Shield. Tectonophysics 192, 1–19.

/8/ **Puranen R, 1989.** Susceptibilities, iron and magnetite content of precambrian rocks in Finland. Geological survey of Finland, Report of investigations 90, 45 pp.

/9/ **Archie G E, 1942.** The electrical resistivity log as an aid in determining some reservoir characteristics: Trans. Am. Inst. Min., Metallurg., Petr.Eng., 146, 54–62.

/10/ **Sehlstedt S, 1988.** Description of geophysical data on the SKB data base GEOTAB. SKB TR 88-05, Svensk Kärnbränslehantering AB.

/11/ **Tarling D H, Hrouda F, 1993.** The magnetic anisotropy of rocks, Chapman and Hall, London, United Kingdom. 217 pp.

/12/ **Keller G V, Frischknecht F C, 1966.** Electrical methods in geophysical prospecting. Pergamon Press.

/13/ **Mattsson H, Thunehed H, Triumf C-A, 2005.** Compilation of petrophysical data from rock samples and in situ gamma-ray spectrometry measurements Stage2 – 2004 (including 2002). SKB P-04-294, Svensk Kärnbränslehantering AB.

Appendix 1

Samples for petrophysical analyses in KLX01 with updated rock type nomenclature

Borehole length (m)	Old rocktype	Updated rocktype	Comment
11.88	VB	Fine-grained diorite to gabbro	
17.98	VB	Fine-grained diorite to gabbro	
20.45	VB	Fine-grained diorite to gabbro	
28.48	VB	Fine-grained diorite to gabbro	
33.13	PSE	Ävrö granite	
40.01	PSE	Ävrö granite	oxidized, red
47.92	VB	Fine-grained diorite to gabbro	
51.03	VB	Fine-grained diorite to gabbro	
57.85	PSE	Ävrö granite	
69.45	HSC	Fine-grained granite	red-brown
79.95	PSE	Ävrö granite	augen-bearing
83.2	VB	Fine-grained diorite to gabbro	
90.07	PSE	Ävrö granite	augen-bearing
105.03	PSE	Ävrö granite	augen-bearing
107.34	PSE	Ävrö granite	with remnants of volcanics
112.74	PSE	Ävrö granite	augen-bearing
120.45	VB	Fine-grained diorite to gabbro	
132.58	PSE	Ävrö granite	tectonized, altered
137.91	PSE	Ävrö granite	augen-bearing
147.97	PSE	Ävrö granite	augen-bearing
150.58	PSE	Ävrö granite	oxidized, red
155.83	PSE	Ävrö granite	augen-bearing
160.16	PSE	Ävrö granite	tectonized, altered
169.94	PSE	Ävrö granite	augen-bearing
178.8	PSE	Ävrö granite	augen-bearing
179.84	PSE	Ävrö granite	augen-bearing
186.43	PSE	Ävrö granite	oxidized, red
193.04	PSE	Ävrö granite	oxidized, red
200.17	PSE	Ävrö granite	
211.13	PSE	Ävrö granite	augen-bearing
220.45	HSC	Fine-grained granite	red-brown
221.1	HSC	Fine-grained granite	red-brown
226.14	PSE	Ävrö granite	augen-bearing
232.15	VB	Diorite to gabbro	
246.87	VB	Diorite to gabbro	
256.11	PSE	Ävrö granite	augen-bearing
265.96	HSC	Fine-grained granite	red-brown
277.28	PSE	Ävrö granite	augen-bearing
280.05	PSE	Ävrö granite	augen-bearing
289.95	PSE	Ävrö granite	augen-bearing
296	PSE	Ävrö granite	augen-bearing
306.06	HSC	Fine-grained granite	red-brown

Borehole length (m)	Old rocktype	Updated rocktype	Comment
315.03	PSE	Ävrö granite	augen-bearing
327.95	HSC	Fine-grained granite	red-brown
335.83	VB	Fine-grained diorite to gabbro	
346.92	PSE	Ävrö granite	augen-bearing
357.02	VB	Fine-grained diorite to gabbro	
360.99	VB	Fine-grained diorite to gabbro	
373.07	PSE	Ävrö granite	augen-bearing
382.86	PSE	Ävrö granite	oxidized, red
389.88	PSE	Ävrö granite	augen-bearing
401.53	PSE	Ävrö granite	augen-bearing
411.75	PSE	Ävrö granite	augen-bearing
417.86	PSE	Ävrö granite	augen-bearing
427.89	PSE	Ävrö granite	oxidized, red
440.16	PSE	Ävrö granite	oxidized, red
444.2	PSE	Ävrö granite	
454.98	PSE	Ävrö granite	augen-bearing
465.91	HSC	Fine-grained granite	red-brown
476.69	PSE	Ävrö granite	augen-bearing
488.05	PSE	Ävrö granite	augen-bearing
494.81	PSE	Ävrö granite	augen-bearing
504.08	PSE	Ävrö granite	augen-bearing
514.23	PSE	Ävrö granite	augen-bearing
521.19	PSE	Ävrö granite	augen-bearing
531.04	VB	Diorite to gabbro	
532.9	VB	Diorite to gabbro	
534.35	VB	Diorite to gabbro	
535.2	HSC	Fine-grained granite	
542.52	VB	Diorite to gabbro	
552.01	PSE	Ävrö granite	oxidized, red
556.81	VB	Fine-grained diorite to gabbro	
565.33	PSE	Ävrö granite	augen-bearing
574.63	PSE	Ävrö granite	augen-bearing
582.08	PSE	Ävrö granite	oxidized, red
584.03	PSE	Ävrö granite	oxidized, red
586.86	PSE	Ävrö granite	tectonized, altered
590.06	PSE	Ävrö granite	
600.88	HSC	Fine-grained granite	red-brown
607.71	PSE	Ävrö granite	oxidized, red
619.71	PSE	Ävrö granite	oxidized, red
622.56	PSE	Ävrö granite	oxidized, red
635.3	HSC	Fine-grained granite	red-brown
637.84	HSC	Fine-grained granite	red-brown
640.6	PSE	Ävrö granite	augen-bearing
650.56	PSE	Ävrö granite	augen-bearing
664.41	PSE	Ävrö granite	augen-bearing
674.01	PSE	Ävrö granite	augen-bearing
683.92	PSE	Ävrö granite	augen-bearing
694.62	PSE	Ävrö granite	augen-bearing

Appendix 2

Generalized geophysical loggings of KLX01

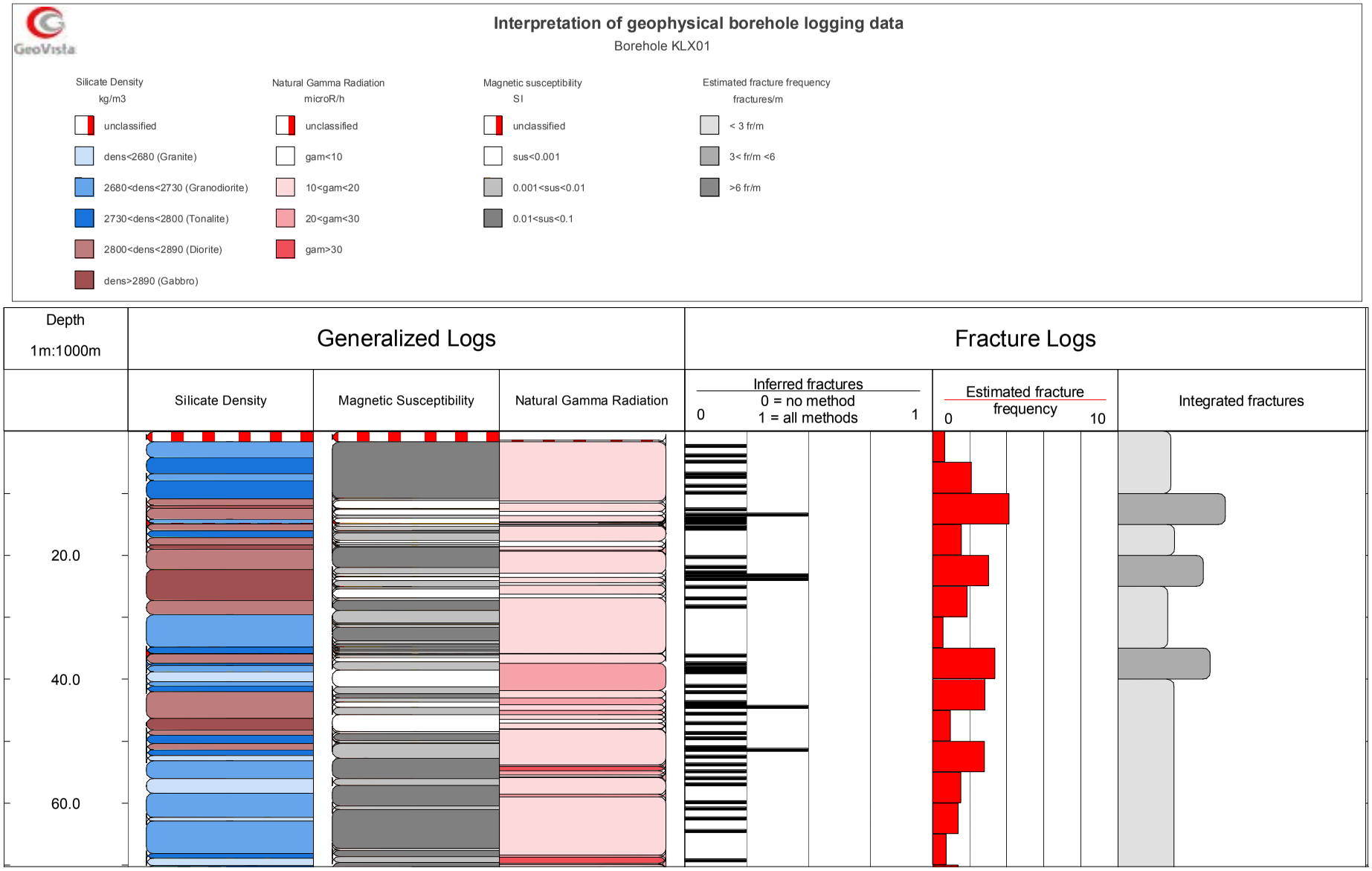
Interpretation of geophysical borehole logging data
Borehole KLX01
GeoVista
Silicate Density
kg/m3
unclassified
dens<2680 (Granite)
2680<dens<2730 (Granodiorite)
2730<dens<2800 (Tonalite)
2800<dens<2890 (Diorite)
dens>2890 (Gabbro)
Natural Gamma Radiation
microR/h
unclassified
gam<10
10<gam<20
20<gam<30
gam>30
Magnetic susceptibility
SI
unclassified
sus<0.001
0.001<sus<0.01
0.01<sus<0.1
Estimated fracture frequency
fractures/m
< 3 fr/m
3< fr/m <6
>6 fr/m
Depth
1m:1000m
Generalized Logs
Fracture Logs
Silicate Density
Magnetic Susceptibility
Natural Gamma Radiation
Inferred fractures
0 = no method
1 = all methods
0
1
Estimated fracture frequency
0
10
Integrated fractures
20.0
40.0
60.0

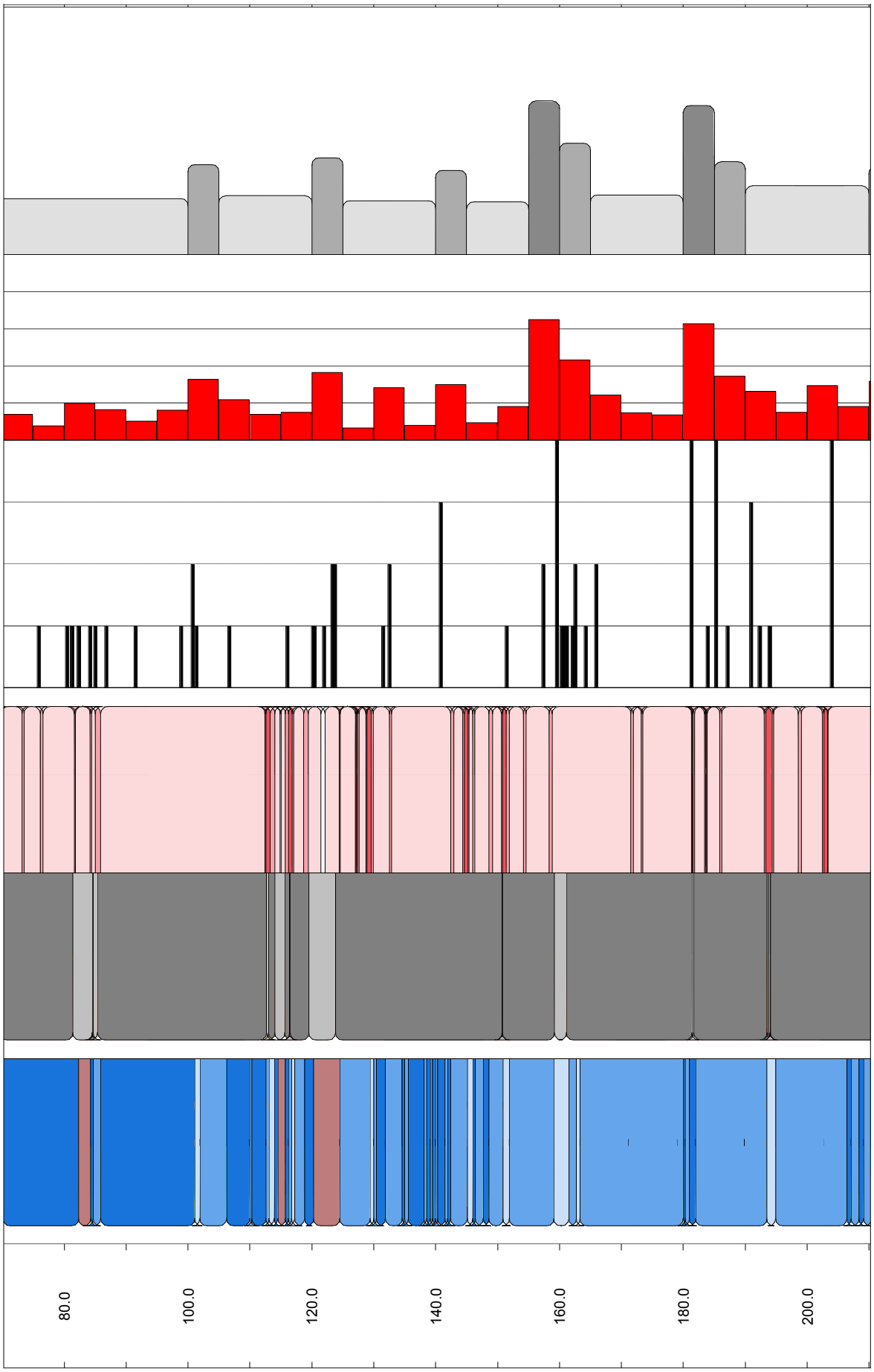
80.0
100.0
120.0
140.0
160.0
180.0
200.0

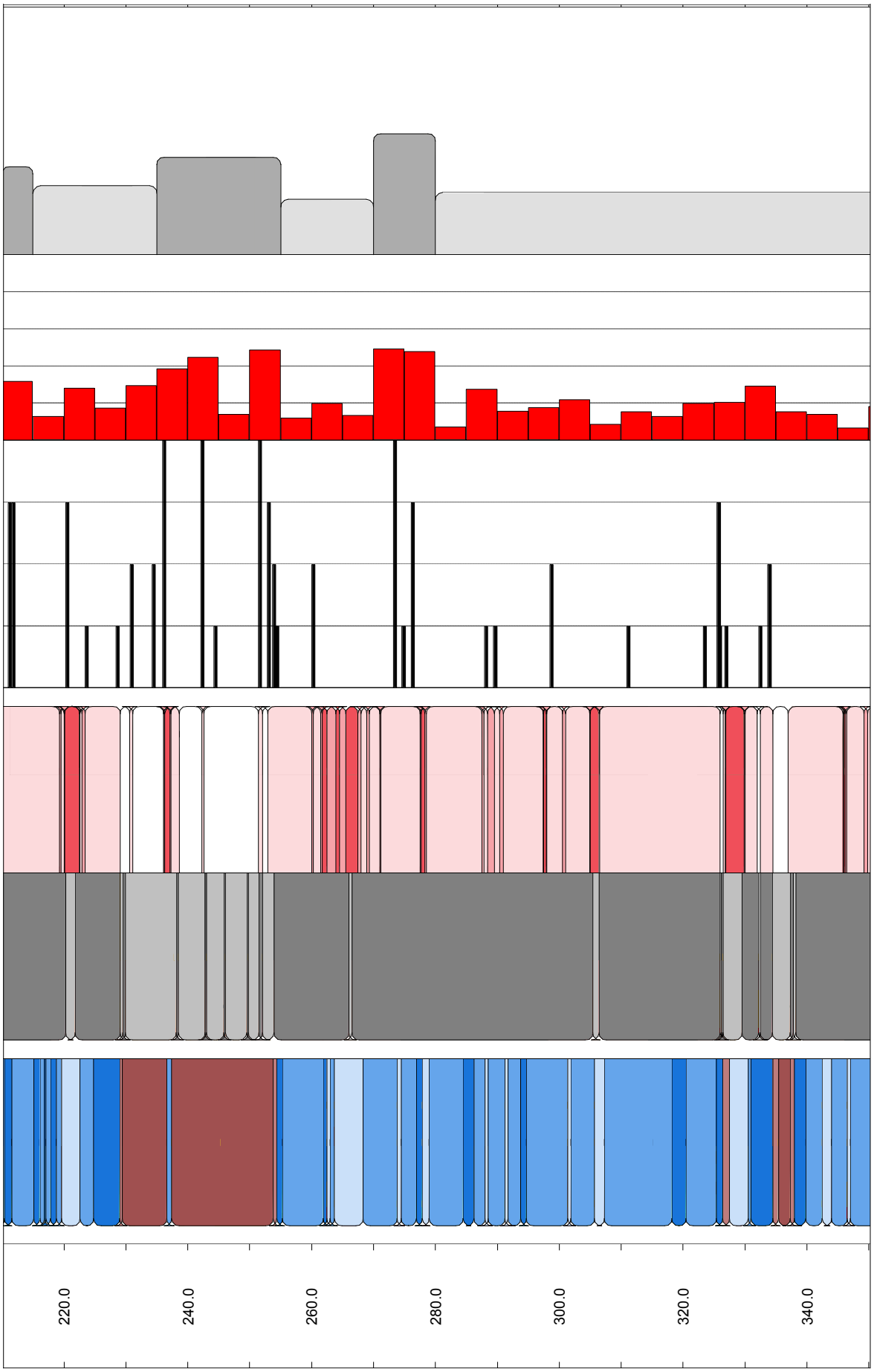
220.0
240.0
260.0
280.0
300.0
320.0
340.0

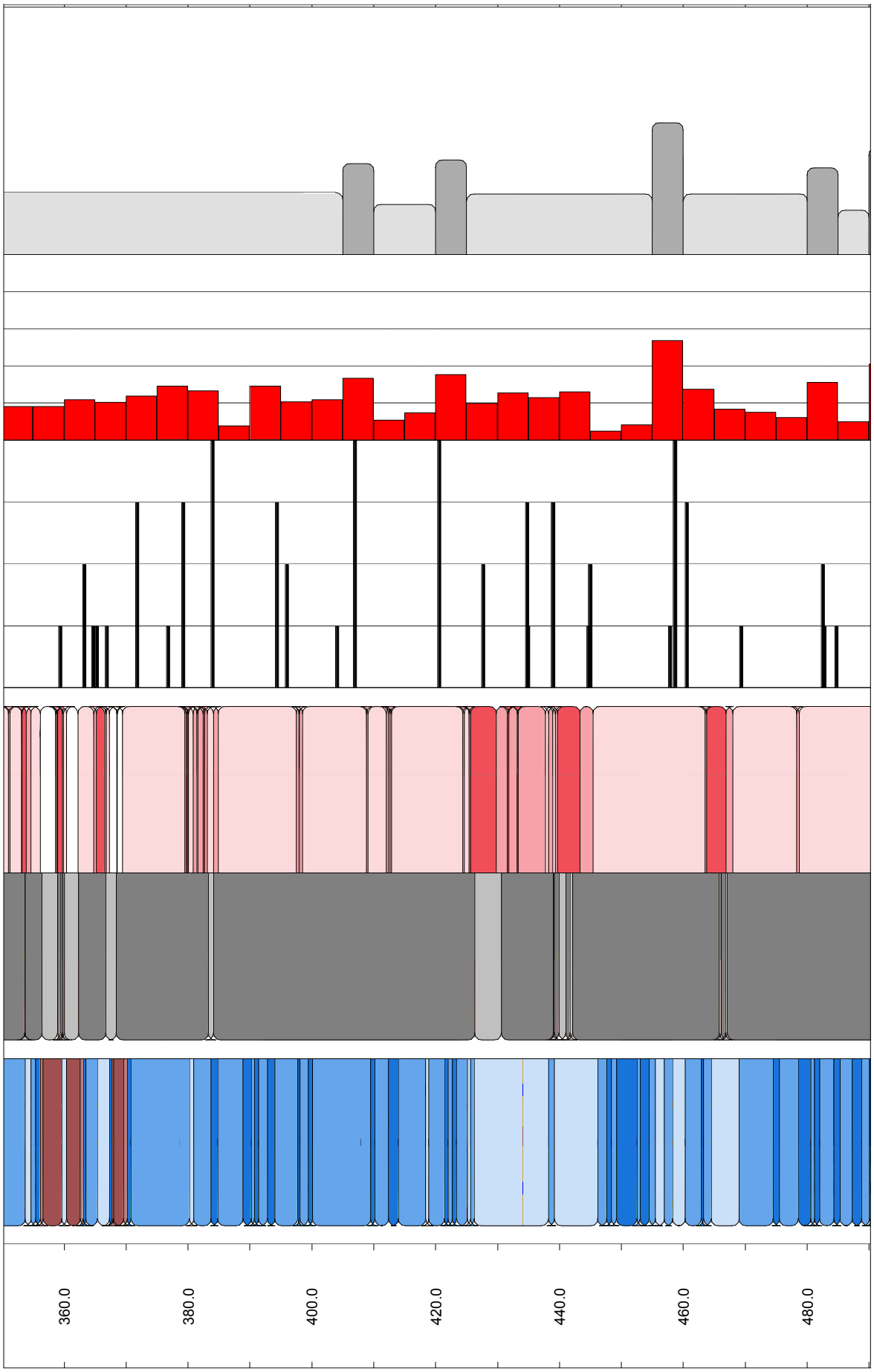
360.0
380.0
400.0
420.0
440.0
460.0
480.0

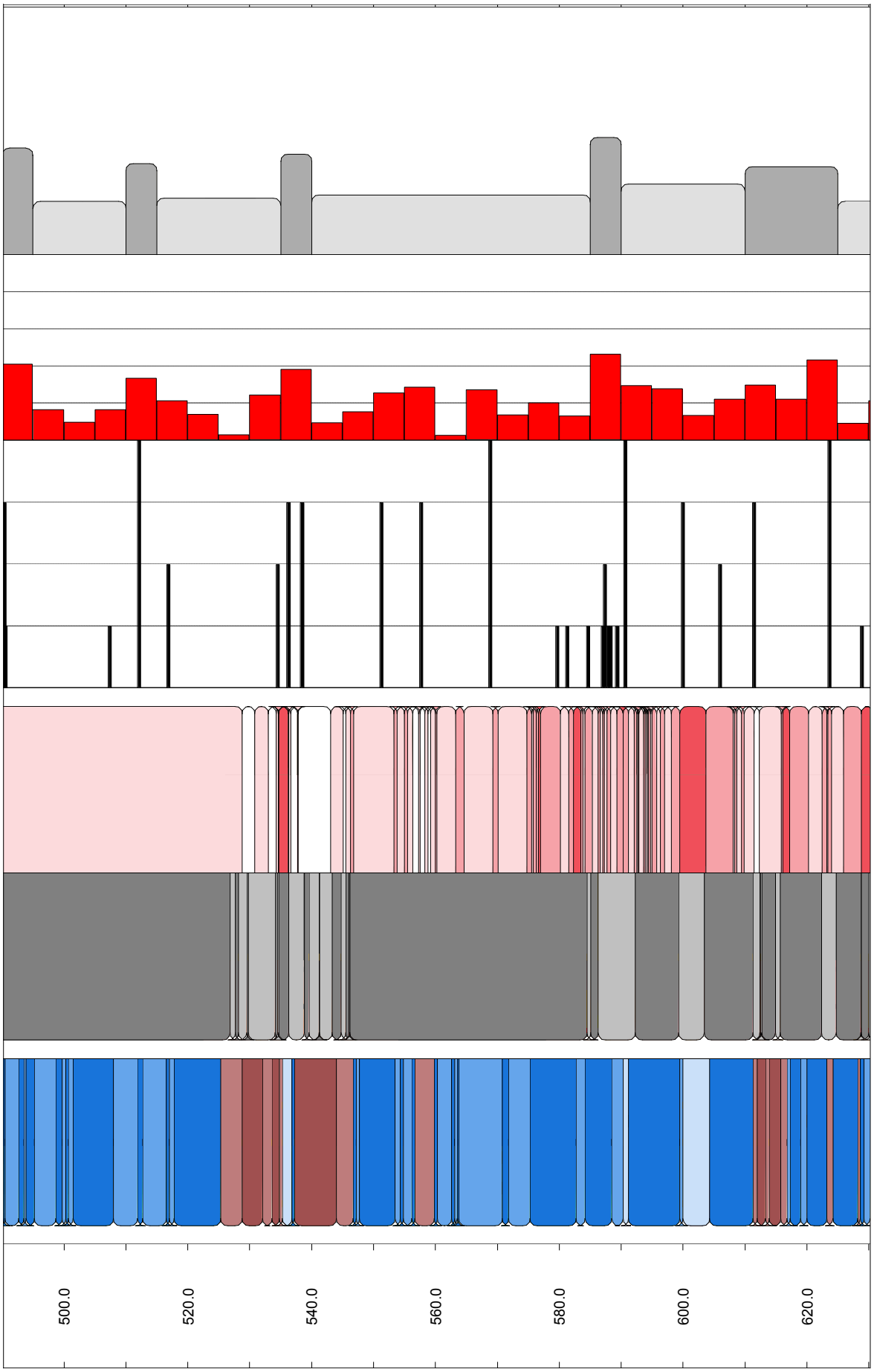
500.0
520.0
540.0
560.0
580.0
600.0
620.0

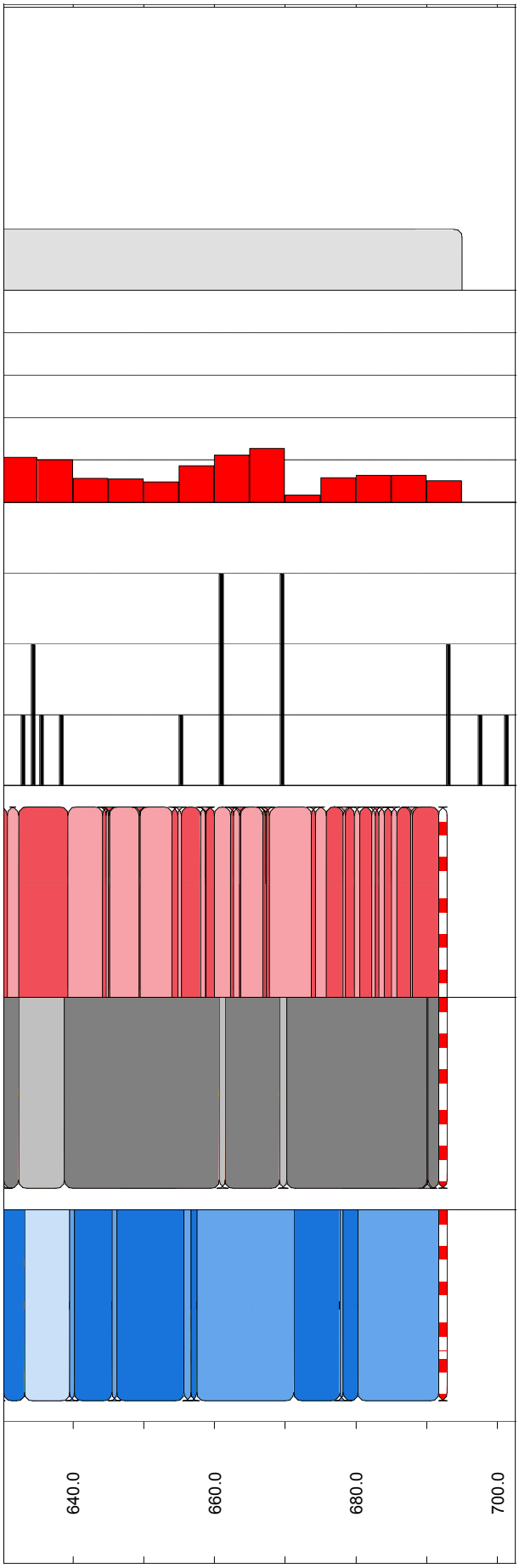
640.0
660.0
680.0
700.0

Appendix 3

Generalized geophysical loggings of KLX03

Interpretation of geophysical borehole logging data

Borehole KLX03

Silicate Density
kg/m3
- unclassified
- dens<2680 (Granite)
- 2680<dens<2730 (Granodiorite)
- 2730<dens<2800 (Tonalite)
- 2800<dens<2890 (Diorite)
- dens>2890 (Gabbro)

Natural Gamma Radiation
microR/h
- unclassified
- gam<10
- 10<gam<20
- 20<gam<30
- gam>30

Magnetic susceptibility
SI
- unclassified
- sus<0.001
- 0.001<sus<0.01
- 0.01<sus<0.1
- sus>0.1

Estimated fracture frequency
fractures/m
- < 3 fr/m
- 3< fr/m <6
- >6 fr/m

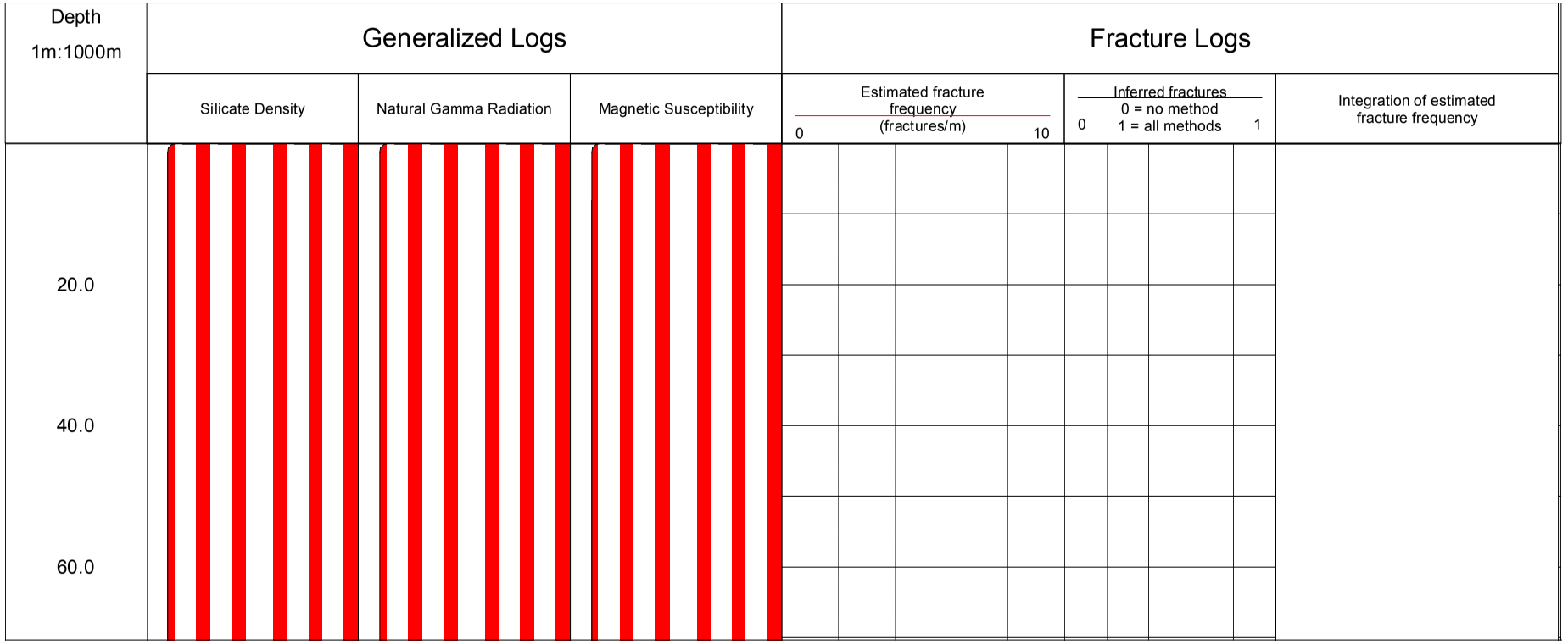

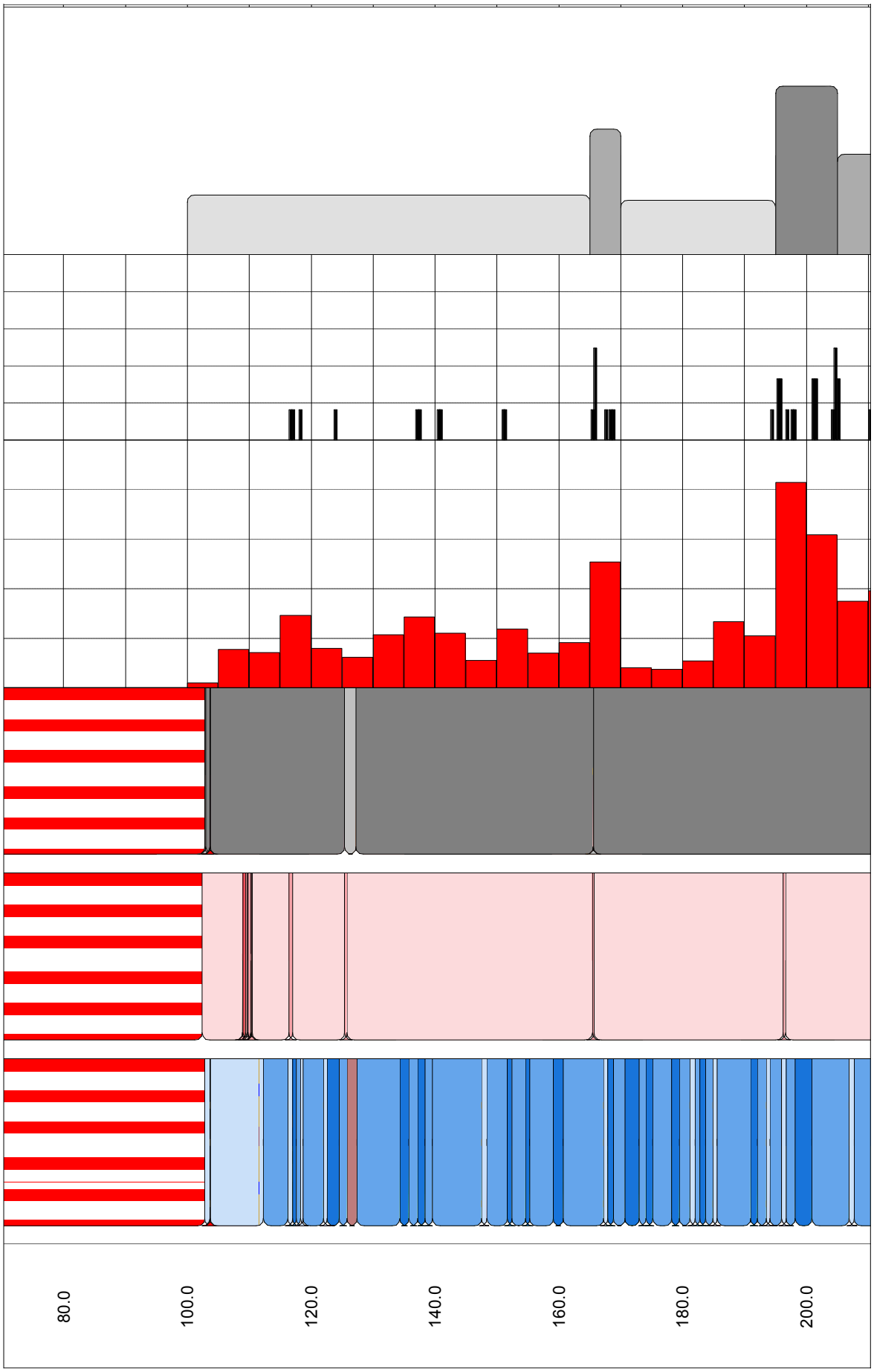
80.0
100.0
120.0
140.0
160.0
180.0
200.0

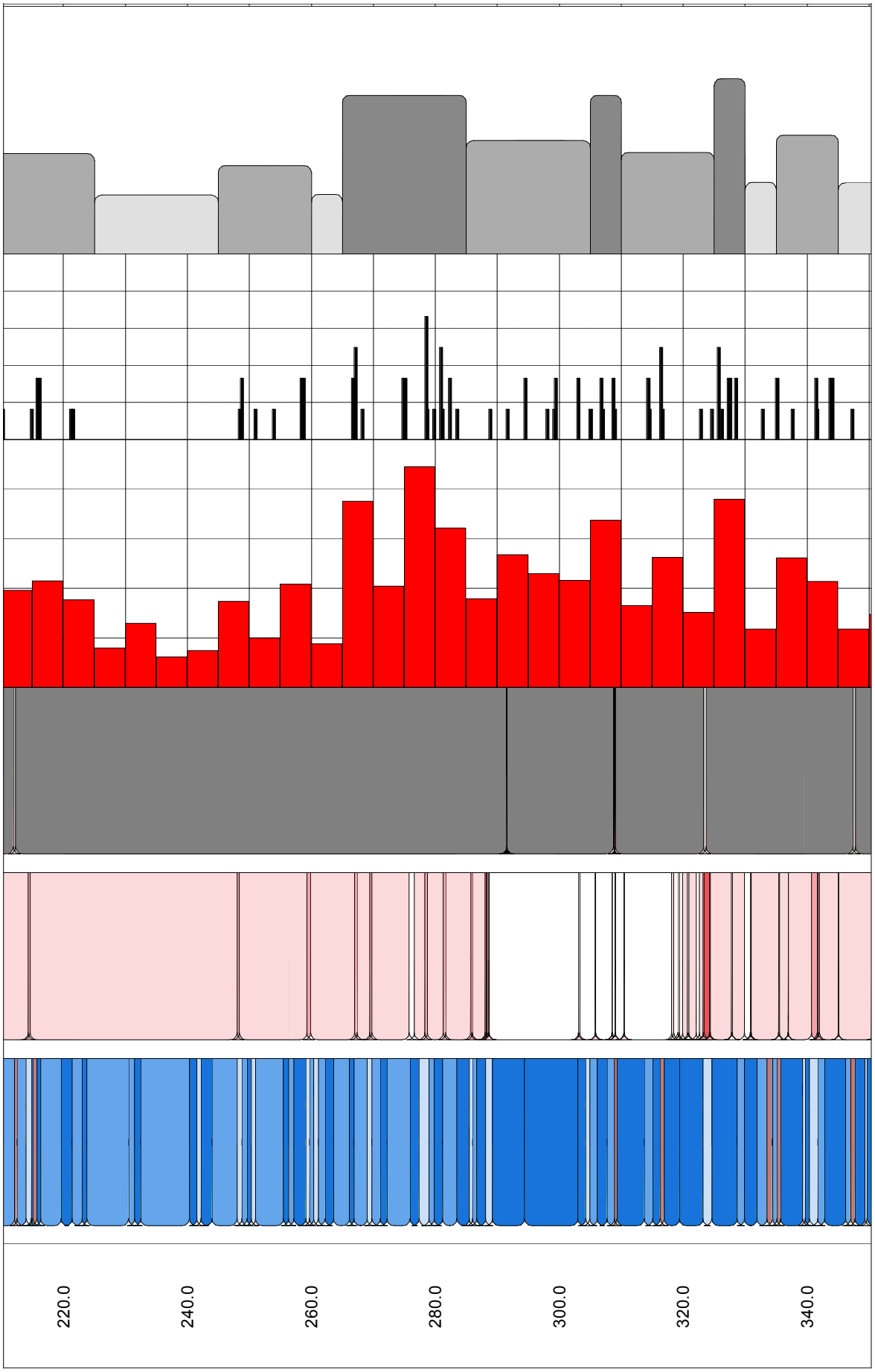
220.0
240.0
260.0
280.0
300.0
320.0
340.0

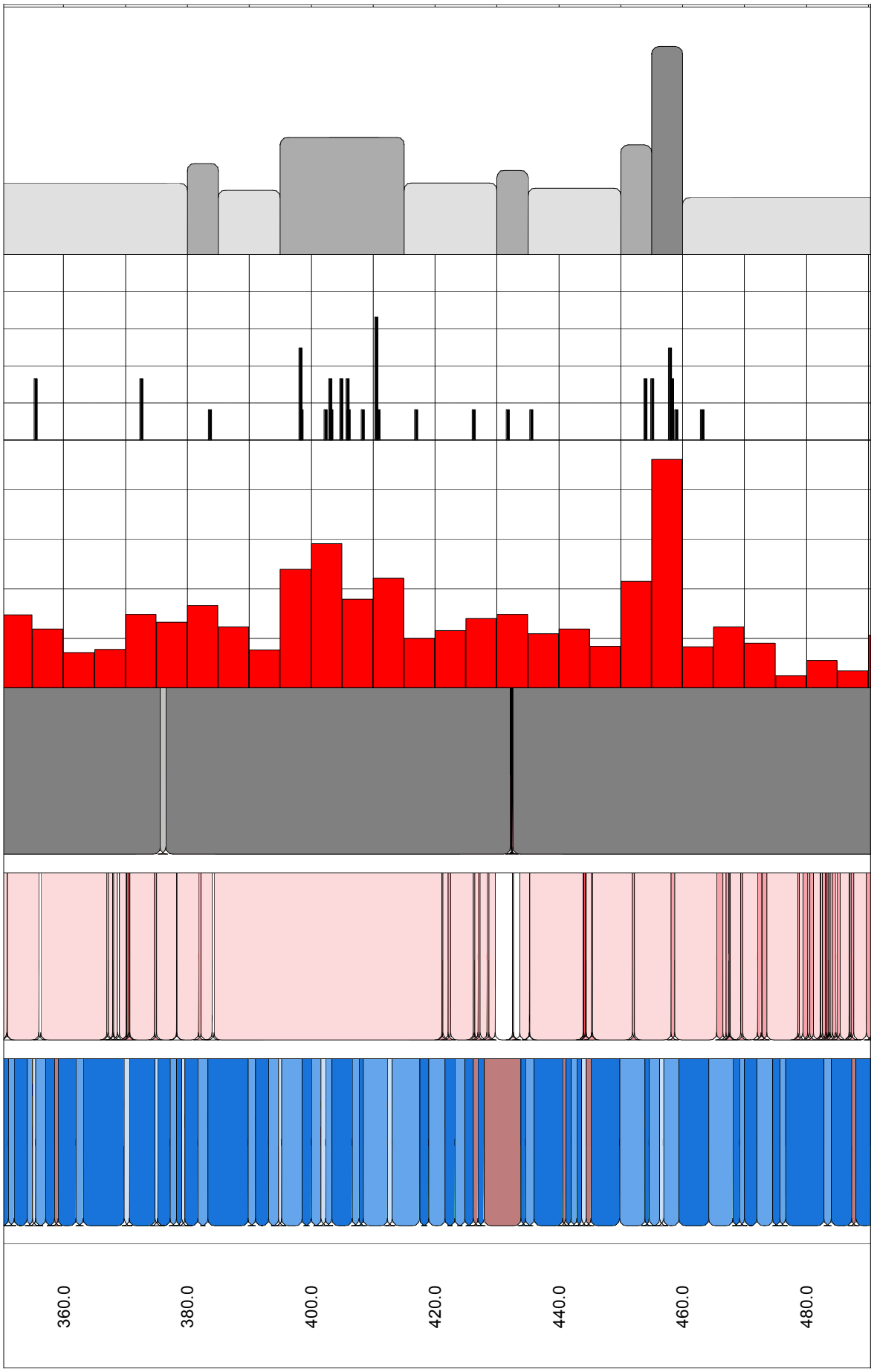
360.0
380.0
400.0
420.0
440.0
460.0
480.0

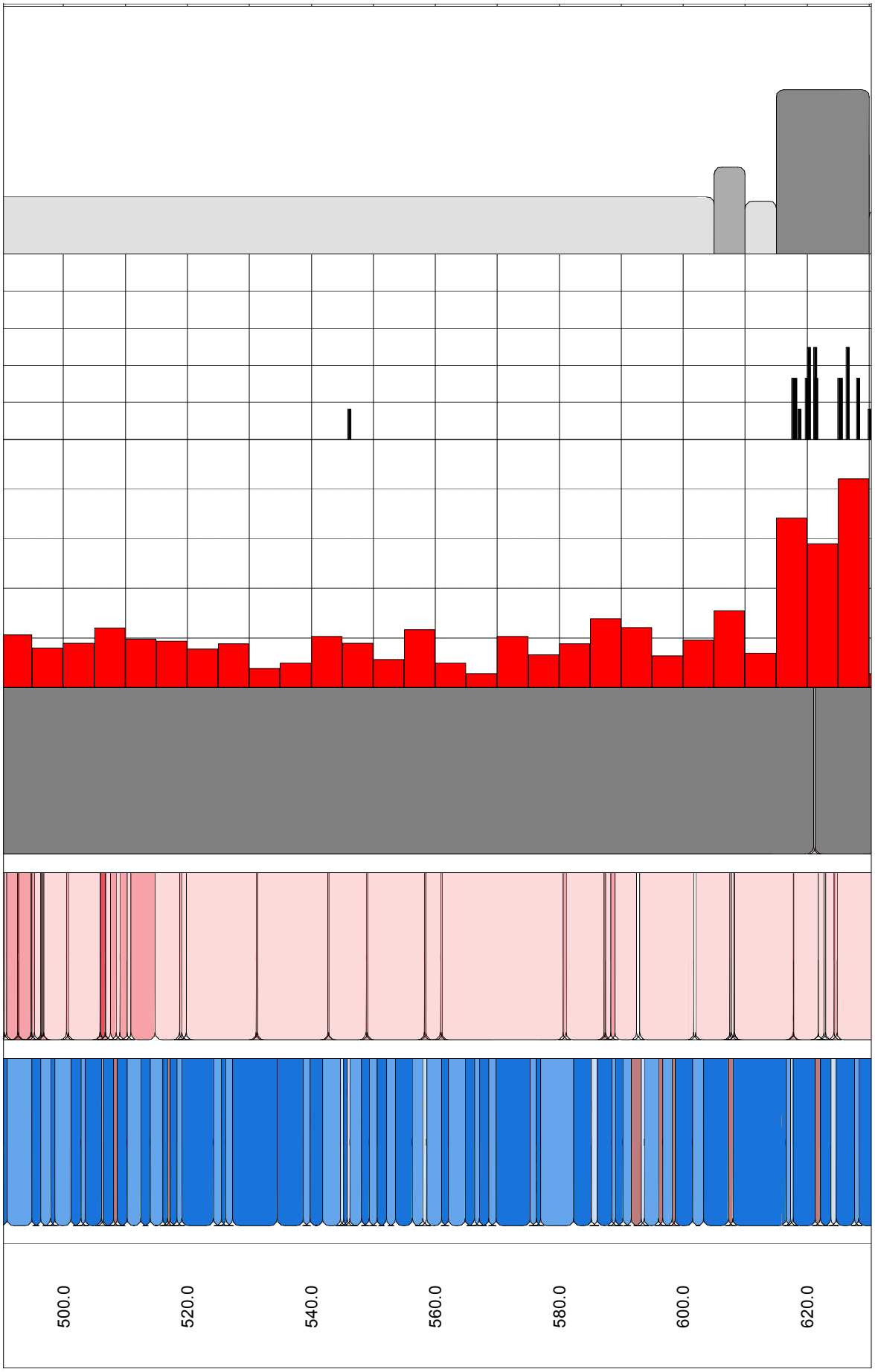
500.0
520.0
540.0
560.0
580.0
600.0
620.0

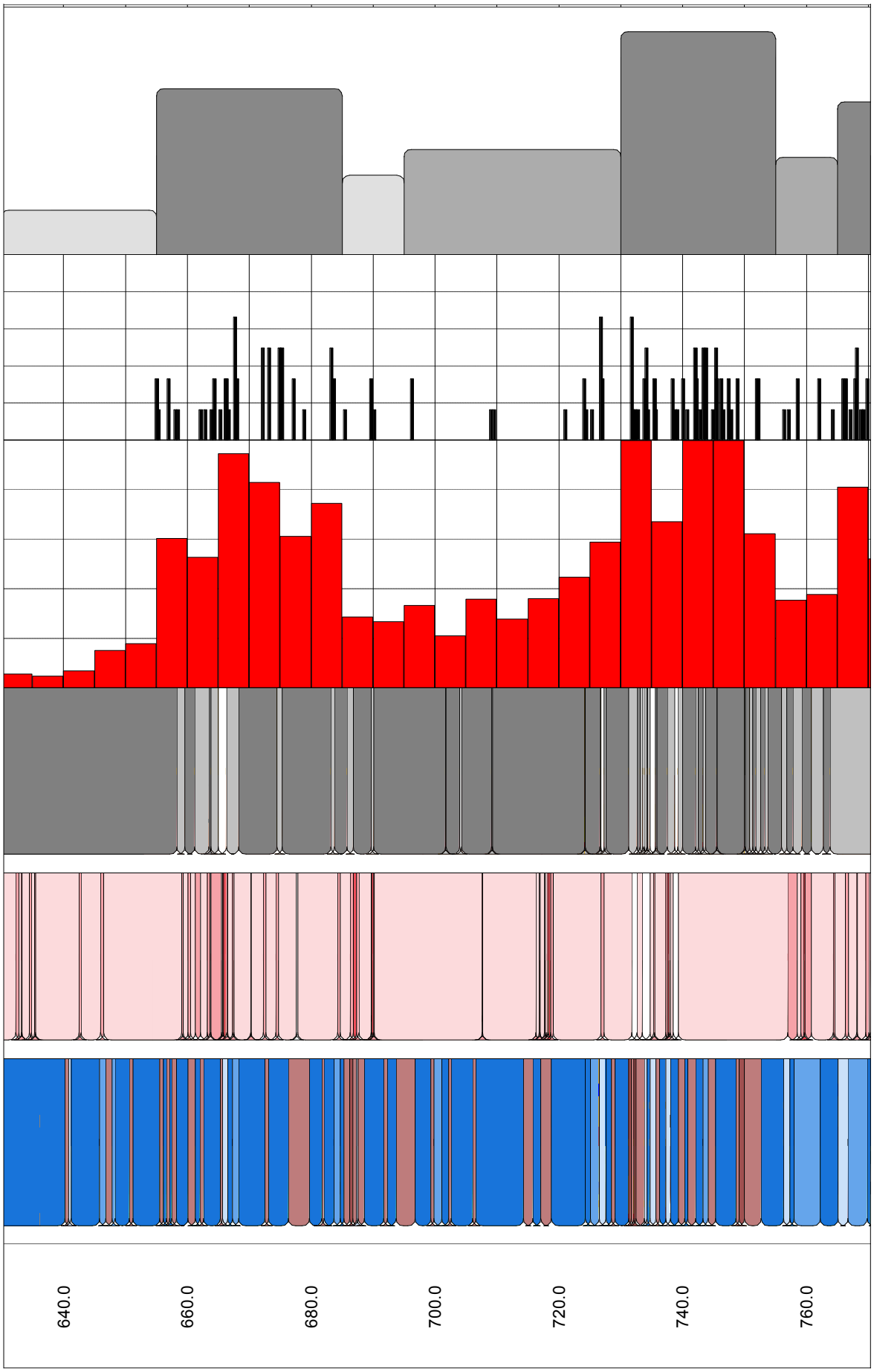
640.0
660.0
680.0
700.0
720.0
740.0
760.0

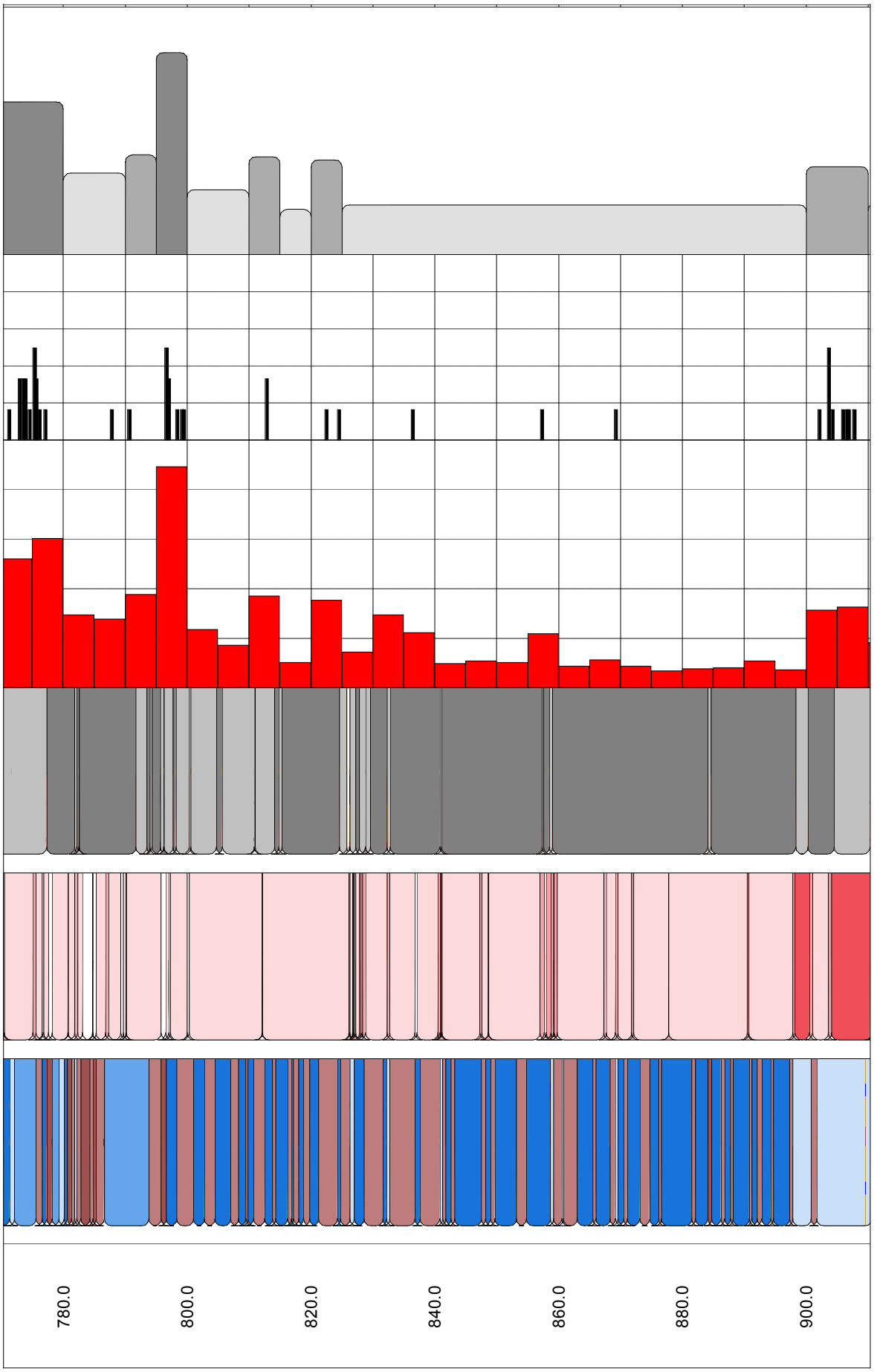
780.0
800.0
820.0
840.0
860.0
880.0
900.0

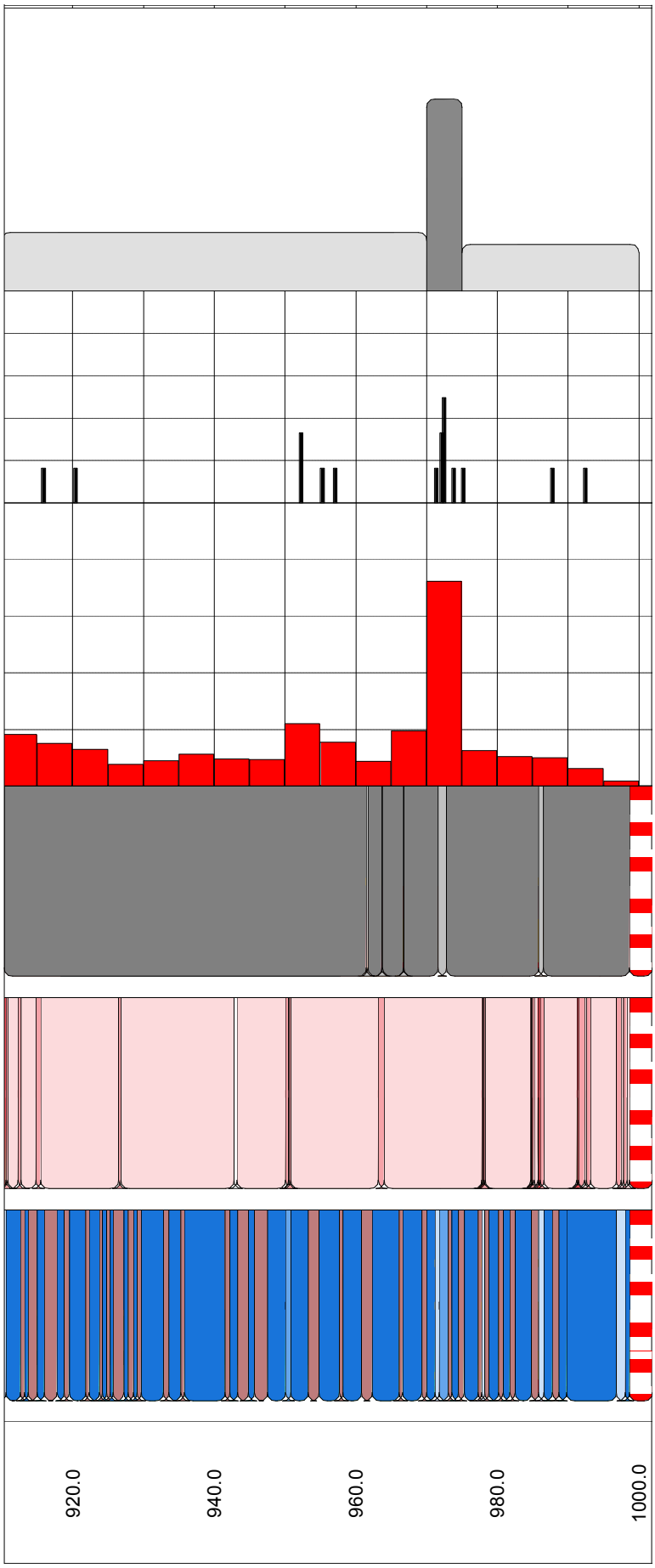
920.0
940.0
960.0
980.0
1000.0

Appendix 4

Generalized geophysical loggings of KLX04

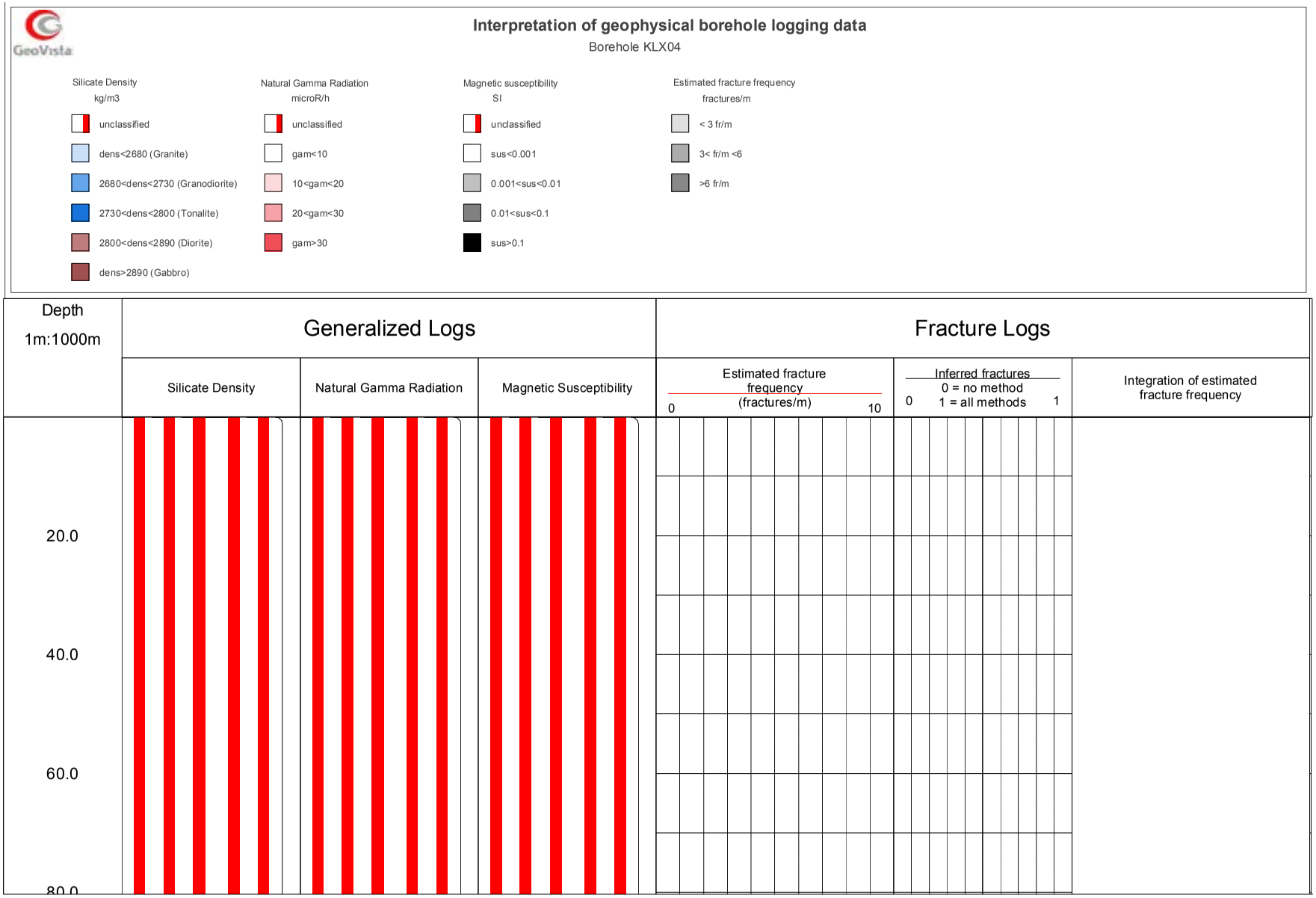
GeoVista
Interpretation of geophysical borehole logging data
Borehole KLX04
Silicate Density
kg/m3
unclassified
dens<2680 (Granite)
2680<dens<2730 (Granodiorite)
2730<dens<2800 (Tonalite)
2800<dens<2890 (Diorite)
dens>2890 (Gabbro)
Natural Gamma Radiation
microR/h
unclassified
gam<10
10<gam<20
20<gam<30
gam>30
Magnetic susceptibility
SI
unclassified
sus<0.001
0.001<sus<0.01
0.01<sus<0.1
sus>0.1
Estimated fracture frequency
fractures/m
< 3 fr/m
3< fr/m <6
>6 fr/m
Depth
1m:1000m
Generalized Logs
Silicate Density
Natural Gamma Radiation
Magnetic Susceptibility
Fracture Logs
Estimated fracture frequency
(fractures/m)
0
10
Inferred fractures
0 = no method
1 = all methods
0
1
Integration of estimated fracture frequency
20.0
40.0
60.0
80.0

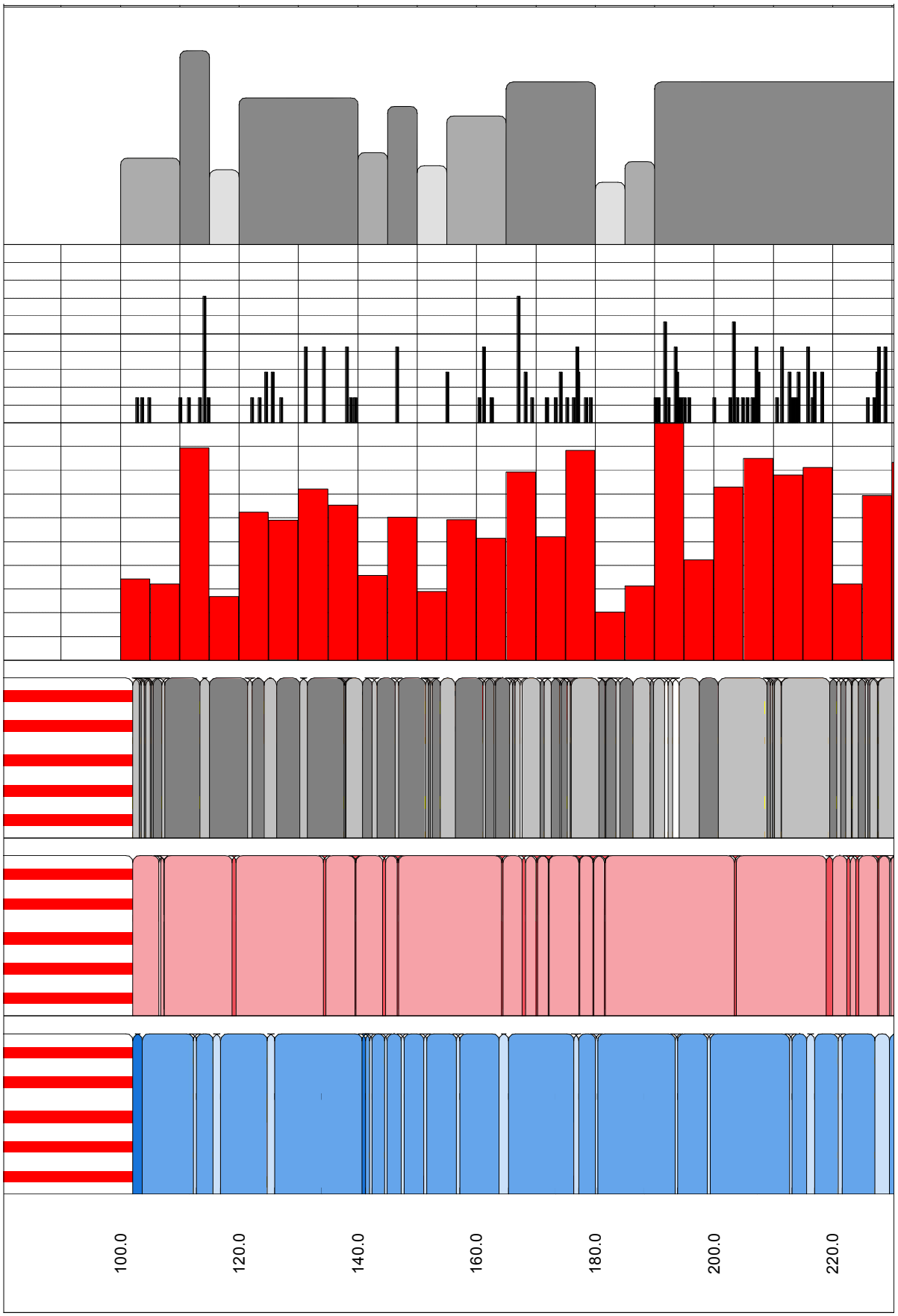
100.0
120.0
140.0
160.0
180.0
200.0
220.0

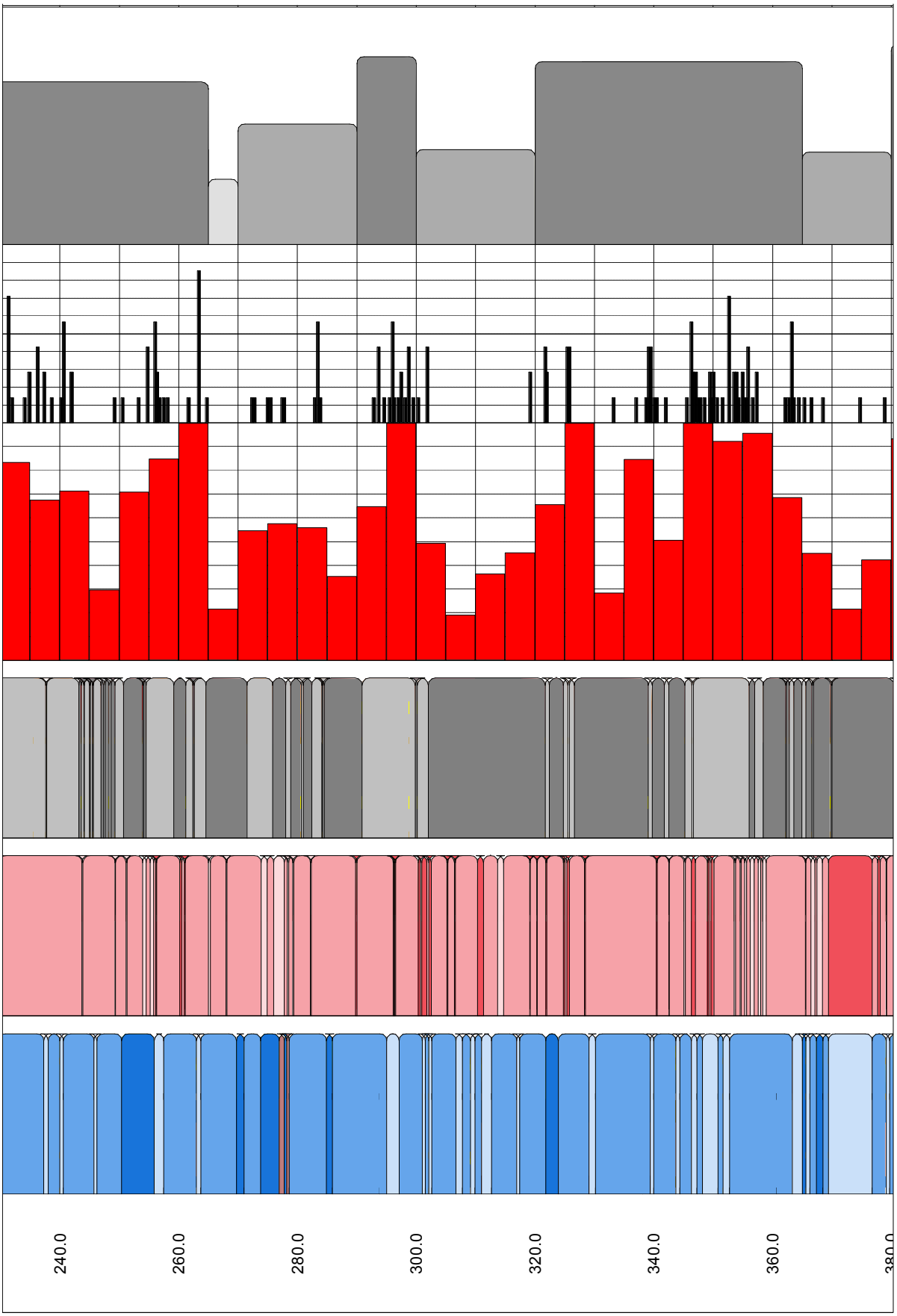
240.0
260.0
280.0
300.0
320.0
340.0
360.0

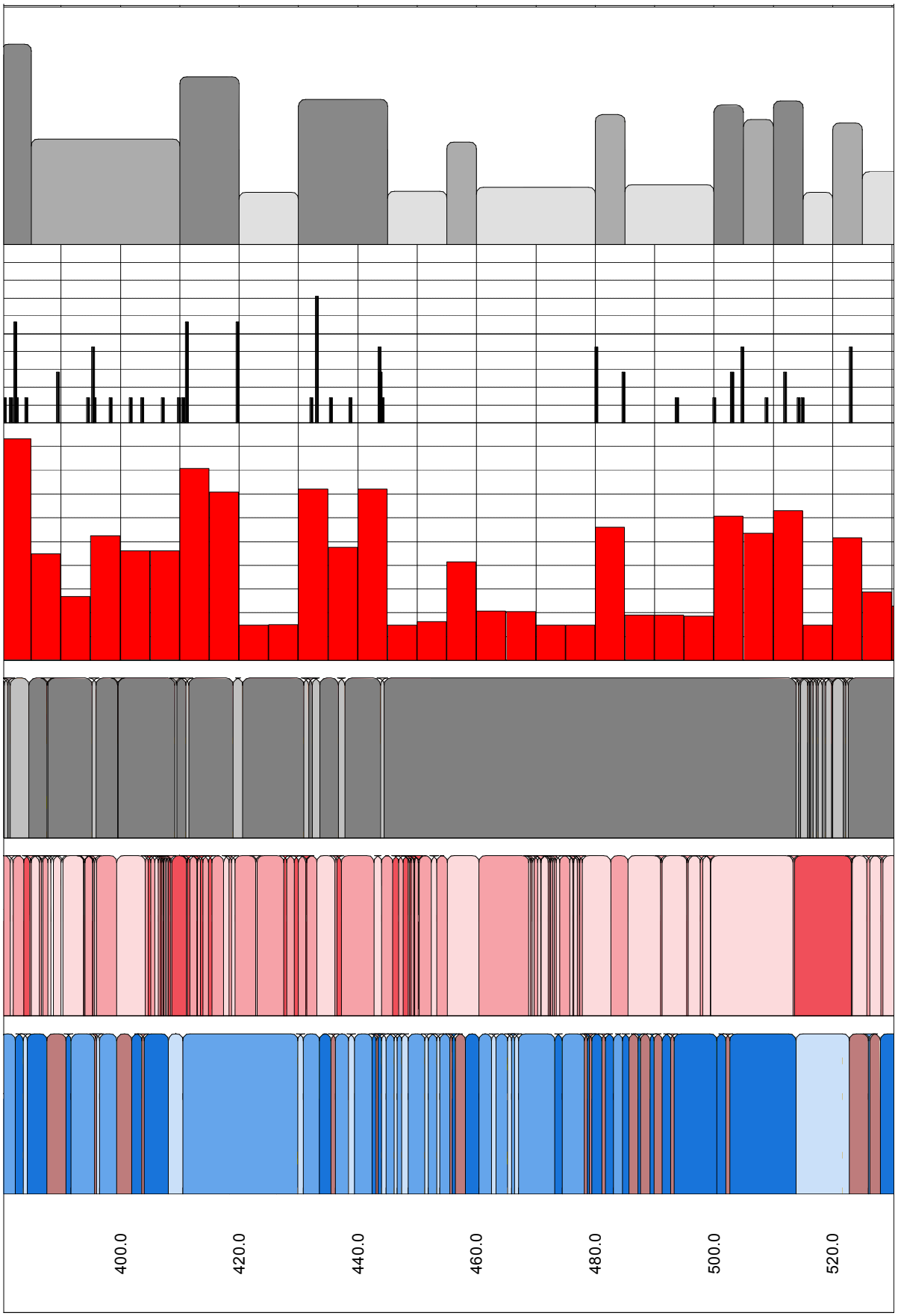
400.0
420.0
440.0
460.0
480.0
500.0
520.0

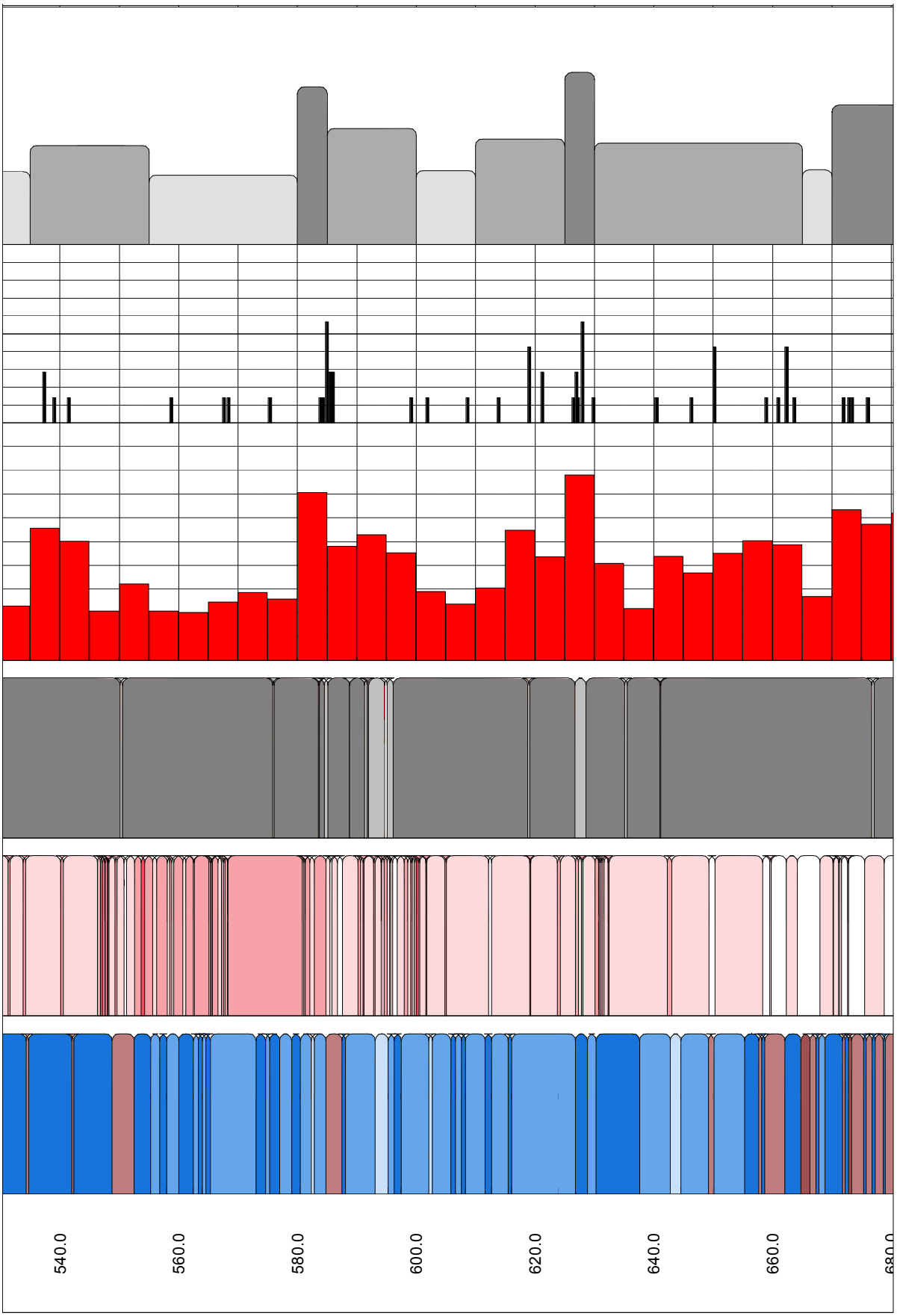
540.0
560.0
580.0
600.0
620.0
640.0
660.0

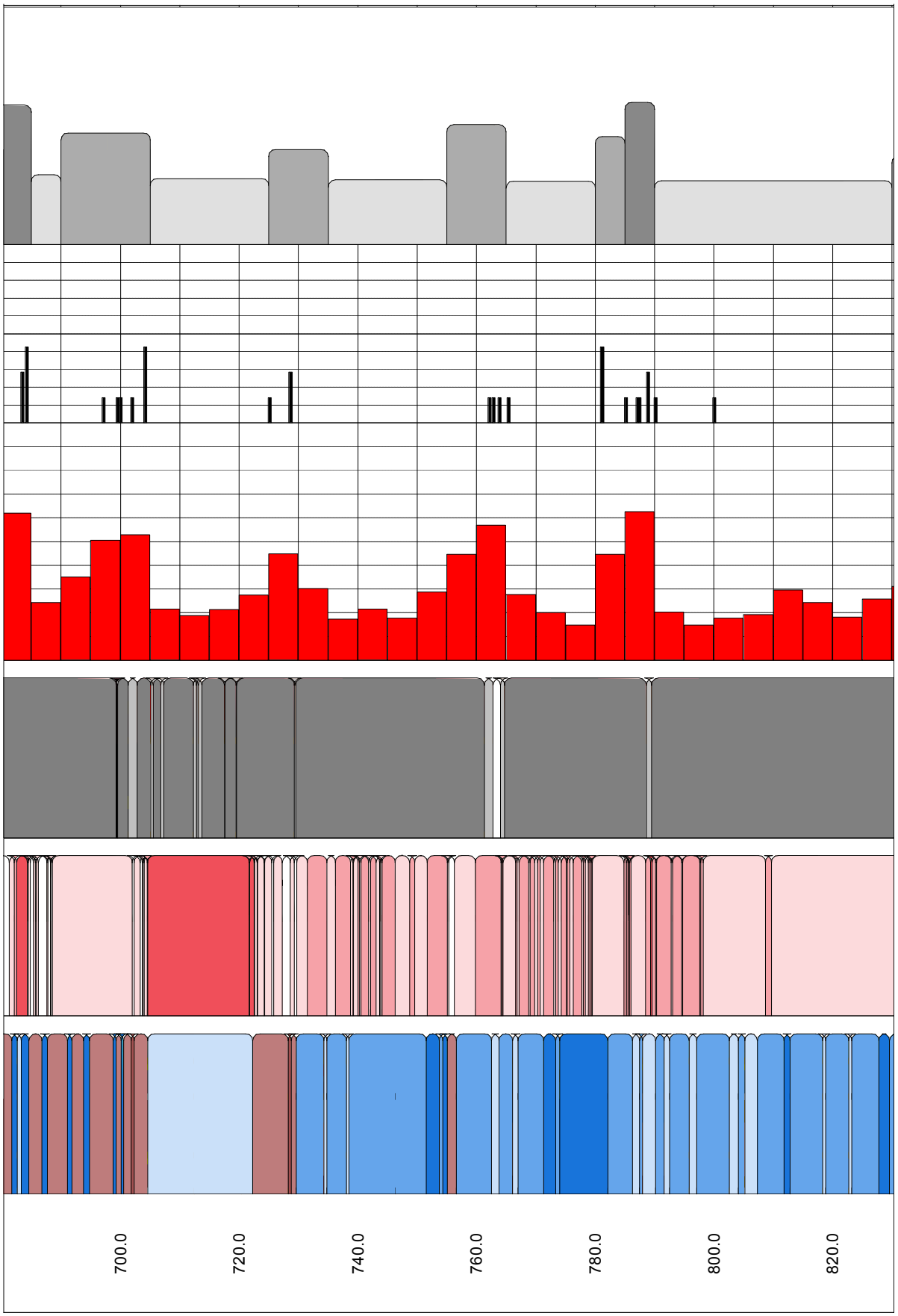
700.0
720.0
740.0
760.0
780.0
800.0
820.0

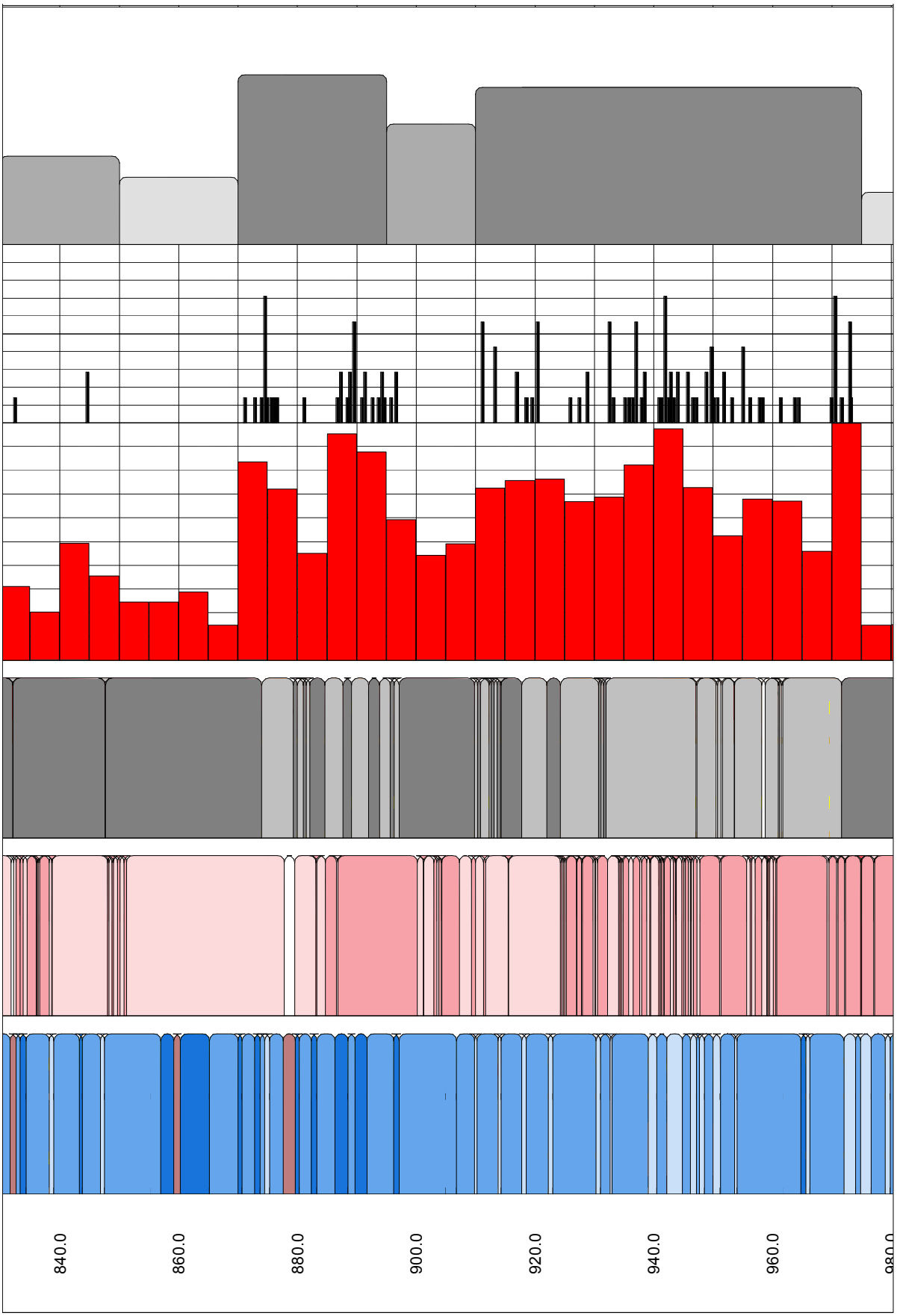
840.0
860.0
880.0
900.0
920.0
940.0
960.0